Potassium chloride cotransporter KCC2

in the rodent auditory brain stem:

development and effects in knock-out animals

Dissertation

zur Erlangung des Doktorgrades der

Naturwissenschaften

Fachbereich Biologie
Technische Universität Kaiserslautern

vorgelegt von
Ekaterina Doncheva
Oktober 2004

Vorsitzender: Prof. Dr. Ekkehard Neuhaus

Betreuer: Prof. Dr. Eckhard Friauf

Korreferent: Prof. Dr. Joachim W. Deitmer

Tag der Disputation: 19th November 2004

I, Ekaterina Doncheva, do hereby declare that this submission is my own work and that, to the best of my knowledge and belief, it contains no material previously published by another person, nor material which to a substantial extent has been accepted for the award of any other degree or diploma of a university or other institute of higher learning.

Kaiserslautern, 15th October 2004.

Table of contents

1 General introduction

1.1 The central auditory system

1.1.1 An overview of the mammalian ascending pathway

The fundamental function of the central auditory system is to transform signals from the acoustic environment in order to extract new information. For the animals, including humans, this information has a vital importance for their life experience, orientation, and survival. The acoustic signals travel through the air, enter the pinna and continue to the cochlea, passing the outer and the middle ear. In the cochlea, the air-borne sound is transformed into a neuronal signal with the help of the auditory receptor cells, (i.e. the hair cells). These cells form synapses on the spiral ganglion neurons (the first-order neurons of the auditory system) whose cell bodies are located within the modiolus. Afferents from the spiral ganglion enter the brain stem via the auditory nerve (cranial nerve VIII) **(Fig. 1.1)**. At the level of the medulla, each axon branches so that it projects onto neurons in the dorsal and ventral cochlear nucleus (VCN). Cells in the VCN send out axons into the ventral acoustic stria that project to the superior olivary complex (SOC) on both sides of the brain stem. The neurons from these nuclei, in turn, project to both the ipsi- and contralateral inferior colliculi in the midbrain via a collection of axons termed the lateral lemniscus. Although there are other routes from the cochlear nuclei to the inferior colliculus, with additional intermediate relays, all ascending auditory
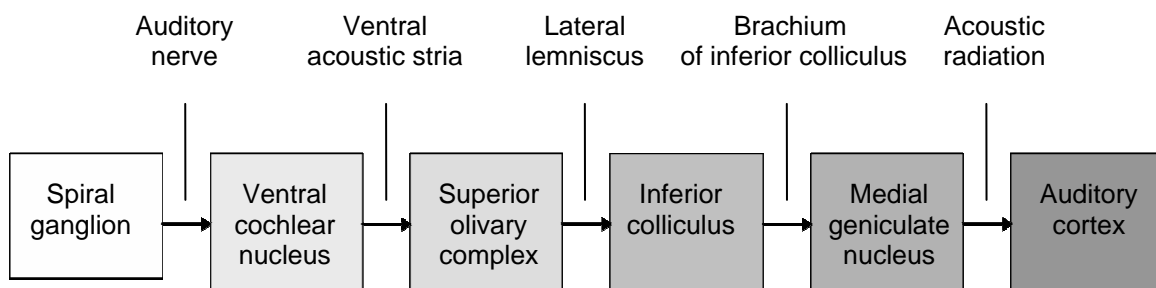
Figure 1.1: The main auditory pathway

There are numerous of paths by which neuronal signals can travel from the spiral ganglion to the auditory cortex. Here, a primary ascending pathway is shown schematically.

2.4   Summary of chapter 2

1.   It was demonstrated that in the rat auditory brain stem nuclei, the KCC2 protein is present already at birth.

2.   A difference appeared in the KCC2 immunofluorescent intensity between the nuclei during development; the MNTB remained weakly labelled throughout the investigated period. In my opinion, this is due to a delay in the development of the inhibitory machinery in the MNTB in comparison to the other brain stem nuclei.

3.   KCC2 was localized in the region of the plasma membrane already at birth (P0) and its expression in the rat auditory brain stem developed via an increase of the immunofluorescent signal intensity between P0-P12. However, this change is with a moderate magnitude. I conclude that it is only of minor importance and does not explain the change in KCC2 functionality.

4.   The transient (at P8 and at P12) appearance of KCC2 immunofluorescent puncta in the soma surface of the MNTB neurons is consistent with: 1) weaker KCC2 labelling in this nucleus throughout the investigated period and a delay in the development of an inhibitory machinery in comparison to MSO, LSO, and SPN; 2) an initial period of missing or less powerful inhibition and colocalization of KCC2 with immature inhibitory synapses. I speculate that transient puncta in the soma surface of the other nuclei may be present prenatally, in correlation with the earlier maturation of inhibitory synapses.

5.   The main developmental reorganization (in qualitative as well as in quantitative aspects) of KCC2 immunoreactivity in the brain stem auditory nuclei was observed in the neuropil. I suppose that, at least in part, the decrease in the signal intensity can be explained by an age-related reduction of dendritic branches via the pruning mechanism and with the absence of an abnormal Cl^- load via extrasynaptic $GABA_A$ receptors. This is consistent with the proposed additional role of KCC2, namely to maintain the cellular ionic homeostasis and to prevent dendritic swelling (Gulyás et al., 2001).

6.   Neither the increase in the KCC2 soma surface signal intensity, nor the reorganization in the neuropil, can be strictly related to the developmental switch in GABA/glycine signalling and the onset of KCC2 function, although some correlation (the appearance of a specific membrane-confined *dendritic* pattern) between structure and function was found. Further implication of different molecular methods, regarding the proposed posttranslational modification of KCC2, will shed light upon the question of what leads to the functional activation of the cotransporter.

pathways converge onto the inferior colliculus. The neurons in the colliculus send out axons via the brachium, mainly to the medial geniculate nucleus of the thalamus, which in turn projects to the auditory cortex, via the acoustic radiation. The described primary ascending pathway, which connects the spiral ganglion and the auditory cortex, is schematically shown in Figure 1.1. For detailed descriptions of the neuroanatomy of the auditory pathways, see Irvine (1986; 1992), Webster et al. (1992), Cant (1997), and Oliver (2000).

1.1.2   The superior olivary complex

The SOC is the first station where the information from both ears converges (review: Illing et al., 2000). It consists of several nuclei, and the main ones are the medial nucleus of the trapezoid body (MNTB), the medial superior olive (MSO), the lateral superior olive (LSO), and the superior paraolivary nucleus (SPN) **(Fig. 1.2)**.

The MNTB is one of the most prominent structures in the mammalian SOC. The nucleus is situated medially to the other nuclei from the complex and it is penetrated by many fibers of passage. Its principle cells are large with globular somata and relatively few dendrites (Sommer et al., 1993). The MNTB neurons receive monaural excitatory input from the contralateral cochlear nucleus (CN) via one of the most powerful presynaptic terminals in the central nervous system, i.e., the calyx of Held (Held, 1893; Friauf and Ostwald, 1988; Smith et al., 1998). MNTB neurons themselves are inhibitory (Wenthold, 1991) and their main task is to convert the excitatory input from the contralateral ear into a fast and well-timed inhibitory input on neurons from the other main nuclei in the ipsilateral SOC to which the MNTB neurons send afferents (Thompson and Schofield, 2000).

The MSO is situated in the region between the MNTB and the LSO. Its principle neurons are bipolar, arranged like a pile of coins, with dendrites extending both medially and laterally (Ramon y Cajal, 1907). The majority of the MSO principle neurons receive binaural excitatory input from the CN (Glendenning et al., 1985; Joris et al., 1998). The MSO has been considered as the primary site for processing interaural time differences (ITDs) in mammals by coincidence detection of incoming bilateral synaptic excitation, making possible the localization of sound at low frequencies (Goldberg and Brown, 1969; Caird and Klinke, 1983; Joris et al., 1998).
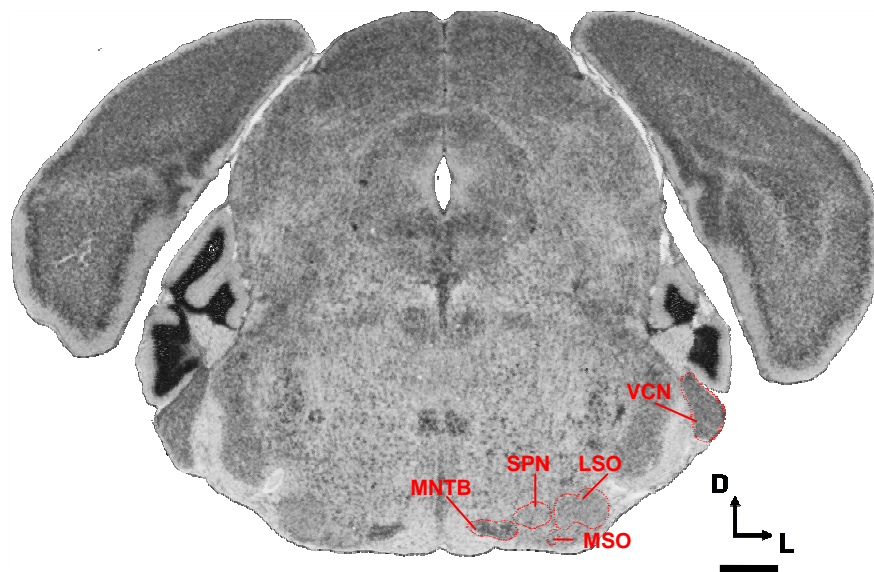
Figure 1.2: Nissl-stained coronal section from the mouse brain (P12) at the level of the superior olivary complex (SOC) and the ventral cochlear nucleus (VCN)

The major nuclei of the SOC are outlined, namely, the lateral superior olive (LSO), the medial superior olive (MSO), the medial nucleus of the trapezoid body (MNTB), and the superior paraolivary nucleus (SPN). D, dorsal; L, lateral. Scale bar is 500 µm.
(Modified from The Mouse Brain Library http://www.mbl.org/mbl_main/atlas.html)

The LSO, clearly detected by its "S"-shape in rodents and carnivores (Schwarz, 1992), occupies the most lateral part in the SOC. Like the MSO, this nucleus is involved in binaural hearing. Due to differences in sound level between the two ears, the LSO is the initial site for processing interaural intensity differences (IIDs), the main cue for localizing high frequency sounds (for review see Irvine, 1992). To fulfil this function, the great majority of the LSO neurons receive excitatory and inhibitory input originating from the ipsi- and the contralateral ear, respectively (for review see Irvine, 1986). The principal cells in the LSO are bipolar and multipolar neurons, although five other classes, occurring less frequently, have been described (Rietzel and Friauf, 1998): small multipolar neurons, banana-like neurons, bushy neurons, unipolar neurons and marginal neurons.

The SPN is another prominent structure located between the LSO and the MNTB, but dorsally to the MSO (Ollo and Schwartz, 1979). Typical SPN neurons are medium to large multipolar cells with long, scarcely branched and smooth dendrites that extend

over long distances within a nearly parasagittal plane (Saldana and Berrebi, 2000). They receive excitatory inputs from the ipsi- and the contralateral CN (Behrend et al., 2002; Dehmel et al., 2002; Kulesza et al., 2003). Despite recent interest in the structure and connectivity of the SPN, little is known concerning the physiological response properties of this nucleus or its functional role in auditory processing. Behrend and co-workers (2002) hypothesized that the SPN, or at least a significant proportion of its neurons, is directly involved in sound localization; another postulate from the same authors states that SPN neurons are involved in processing temporal aspects of sounds, independent of putative interaural time difference sensitivity.

1.2   Inhibition in the Central Nervous System (CNS)

Nowadays, a lot of data is available regarding the excitation of the brain and the development of the excitatory connections in the CNS. The past several decades succeeded to reveal the general rules, the cellular and molecular mechanisms regarding the developmental refinement of the excitatory synaptic circuits, mainly glutamatergic and cholinergic (for review see Goodman and Shatz, 1993; Shatz, 1996; Zhang and Poo, 2001). However, the mechanisms and events that govern the organisation of the inhibitory circuits remain elusive.

The appropriate electrical activity in the brain is obtained through a delicate balance between excitation and inhibition. Both inhibitory and excitatory afferents contribute to the maturation of postsynaptic neurons as well as to the maturation of the neuronal network. Moreover, many diseases (e.g. epilepsy, concussion, and ischemia) are related to disturbances in the inhibitory system, excitotoxic cellular damage and death. Thus, the inhibitory synapses, being around 40% of all synapses in the CNS (Sanes and Friauf, 2000), prevent the spread of excitatory activity.

The inhibitory synaptic transmission is also known to play an important role during maturation of the central auditory pathways (for reviews see Sanes and Friauf, 2000; Kandler, 2004). The well-timed inhibition has been hypothesized to be involved in auditory processing (Brand et al., 2002; Pollak et al., 2002; Grothe, 2003; Needham and Paolini, 2003). It has been shown that the inhibition can sharpen the tuning curves and modulate discharge properties of auditory neurons, and it is crucial to the ability to localize high-frequency sounds (Yang et al., 1992; Caspary et al., 1994; Klug et al.,

1995; Koch and Grothe, 1998). Therefore, it is not surprising that a broad amount of investigations are concentrated to shed light on the processes regarding the inhibition of the brain and especially in the central auditory system.

1.2.1   Inhibitory projections in the SOC

The central auditory system has a large number of inhibitory projections. Regarding the inhibition in the brain stem, in Figure 1.3 a schematic drawing of the main SOC nuclei is shown, together with the source of their main excitatory and inhibitory input.

It is known that the source of excitation in the MNTB are the globular bushy cells in the contralateral anteroventral cochlear nucleus (AVCN) (Friauf and Ostwald, 1988; Smith et al., 1998; for review see Thompson and Schofield, 2000). The MNTB is very often described as a relay station, providing inhibitory input from the contralateral CN to the ipsilateral MSO, LSO, and SPN (Sommer et al., 1993; for review see Thompson and Schofield, 2000) and the presence of inhibition onto MNTB neurons was often omitted. Only recently, it was proposed that excitatory transmission in the MNTB might be subject to inhibition, strong enough to offset the massive excitatory input from the calyx of Held (Kopp-Scheinpflug et al., 2003). The primary inhibitory input, which MNTB neurons receive, comes from recurrent collaterals of their own axons (Guinan and Li, 1990; Kuwabara and Zook 1991; Sommer et al., 1993; Smith et al., 1998; review: Thompson and Schofield, 2000). Additionally, the MNTB receives inhibitory input from neurons in the ventral nucleus of the trapezoid body (Ostapoff et al. 1997) and the SPN (Helfert et al. 1989). Therefore, since the MNTB provides well-timed inhibition to the other main nuclei in the SOC, the glycinergic modulation of MNTB activity could have profound consequences. For example, Kopp-Scheinpflug et al. (2003) suggested that "side-band" inhibition could block calyceal transmission postsynaptically. Together, with the presynaptic mechanisms known to modulate glutamate release from the calyx (Trussell, 2002), the effect can be enhanced or diminished excitatory transmission to the LSO, the MSO, and the SPN.

The MSO receives excitatory input from both ipsi- and contralateral CN and the origin of these projections are the spherical bushy cells located in the AVCN (Harrison and Irving, 1966; Smith et al., 1993; Grothe, 2000). Additionally, it receives inhibitory
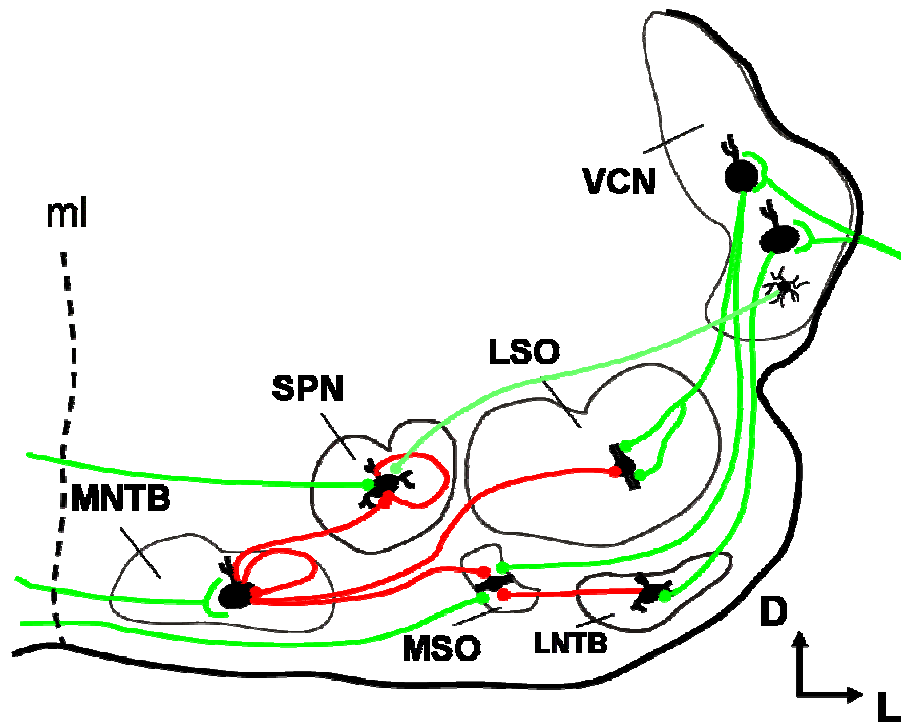
Figure 1.3: Excitatory and inhibitory inputs to the main auditory brain stem nuclei

The MSO and the SPN receive excitatory inputs from both ears, whereas the LSO and the MNTB have monaural excitatory inputs from the ipsilateral and the contralateral CN, respectively. The MNTB converts the excitatory input from the contralateral ear into an inhibitory one on neurons from the other three main nuclei in the ipsilateral SOC. For the LSO this projection is the predominant source for inhibition. The MNTB neurons, themselves, are also the target of an inhibitory projection that comes from the recurrent collaterals of their own axons. Additional to the MNTB inhibition, the SPN receives inhibitory input from its axons that collateralize before leaving the nucleus and contact other SPN neurons. The MSO is the only nucleus which is inhibited from the contralateral side via the MNTB and from the ipsilateral side via the LNTB.
LSO, lateral superior olive; LNTB, lateral nucleus of trapezoid body; MNTB, medial nucleus of trapezoid body; MSO, medial superior olive; SPN, superior paraolivary nucleus; VCN, ventral cochlear nucleus; ml, midline; D, dorsal; L, lateral

input from the ipsilateral MNTB and lateral nucleus of trapezoid body (Cant and Hyson, 1992; Kuwabara and Zook, 1992; Grothe and Sanes, 1993; Smith et al., 2000). Considering the MSO as the primary site for processing ITDs in low-frequency hearing mammals, the contribution of the inhibitory inputs to the classical model proposed by Jeffress (1948) was unknown. Brand and co-workers (2002) proposed that in low-frequency hearing mammals, that rely heavily on ITDs for sound localization (gerbils, cats), the precisely timed glycine-controlled inhibition is a critical part of the mechanism

by which the physiologically meaningful ITDs are encoded in the MSO in the microsecond range (for review see Grothe, 2003).

The LSO receives direct excitatory input from the ipsilateral CN, and the most afferents arise from spherical bushy cells in the AVCN (Sanes and Rubel, 1988; Smith et al., 1993). The LSO gets the predominant inhibitory input from globular bushy cells in the contralateral CN via the ipsilateral MNTB (Warr, 1972; Kuwabara and Zook, 1992; Sommer et al., 1993). This pattern of innervation to LSO cells is fundamental for processing IIDs (Wu and Kelly, 1992a; Sanes, 1993). However, despite its relative homogeneity, IID sensitivity varies substantially from cell to cell (Grothe and Park, 2000). In other words, the particular IID that results in a criterion degree of inhibition varies among cells over the range of IIDs (Sanes and Rubel, 1988).

In contrast to the other brain stem nuclei, the SPN does not appear to receive excitation from globular/spherical bushy cells in the CN (Warr, 1966; Friauf and Ostwald, 1988). Friauf and Ostwald (1988) showed that the excitatory input from the ipsi- and the contralateral side originates from multipolar/stellate cells and multipolar/octopus cells in the posteroventral cochlear nucleus, respectively. Therefore, in the SPN these excitatory inputs, having different physiological characteristics than the bushy cells, can create a variety of response patterns (Kulesza and Berrebi, 2000). It is also supposed that these excitatory influences in the SPN are balanced by finely tuned glycine-mediated inhibition arising from the MNTB (Banks and Smith, 1992; Kuwabara and Zook, 1991, 1992; Sommer et al., 1993) and also by its own collateral innervation (Kulesza et al., 2000; Kulesza and Berrebi, 2000).

The VCN is also the object of inhibition (projections not shown in Fig. 1.3). In vitro recordings and immunocytochemical labelling have shown that neurons in the VCN also receive a variety of inhibitory inputs (Gleich and Vater, 1998). In fact, more than half of axosomatic endings on bushy cells in the VCN are non-cochlear, contradicting the commonly held view that these cells are largely relay neurons (Shore, 1998). Shore claimed that the large proportion of the synapses on bushy cells has either flattened or pleomorphic vesicles. These vesicles are usually associated with synaptic inhibition and contain either glycine or γ-amino-butyric acid (GABA) and, in some cases, both. Large numbers of these putative inhibitory synapses are strategically placed on cell bodies and axon hillocks of bushy and stellate cells to affect the output of their projection. Other studies have shown that there is a significant intrinsic inhibitory circuit to the bushy cells

in the VCN from vertical cells in the dorsal cochlear nucleus (Wu and Oertel, 1986; Wickesberg and Oertel, 1988, 1990; Kolston et al., 1992; Ferragamo et al., 1998), and also an extrinsic inhibition via a descending pathway from the SOC [from the MNTB and the SPN (Schofield, 1991, 1994); from the lateral and the ventral nucleus of the trapezoid body (Covey et al., 1984; Warr and Beck, 1996)] and the contralateral CN (Shore et al., 1991).

Taken together, the knowledge about how well-defined inhibitory projections in the auditory system develop and how inhibitory synaptic transmission appears to influence neuronal maturation will help to understand the basic and specific characteristics of the brain during maturation.

1.2.2   Inhibition and inhibitory circuit development

An important feature of the inhibitory pathways is that they develop through excitation. Although GABA is one of the main inhibitory neurotransmitters in the adult nervous system, GABAergic synapses develop early and GABA produces most of the excitatory drive in the immature brain, even before the glutamatergic transmission is functional (Ben-Ari et al., 1997). Further on, only during the first two postnatal weeks in rodents, GABA becomes inhibitory (hippocampus: Ben-Ari et al., 1989; neocortex: Luhmann and Prince, 1991; retina: Huang and Redburn, 1996). The glycinergic system follows a similar maturation pattern (brain stem: Kandler and Friauf, 1995; Singer et al., 1998; Ehrlich et al., 1999). Hence, the GABA/glycine responses undergo a developmental shift from depolarization to hyperpolarization, and this phenomenon has been attributed to the decrease in the intracellular Cl^- concentration in neurons with age (Owens et al., 1996; DeFazio et al., 2000; Balakrishnan et al., 2003).

1.3   Chloride regulation in neurons and the role of potassium chloride cotransporter KCC2

Nowadays, it is well established that Cl^- plays a vital role in cell physiology. Most animal cells exhibit a non-equilibrium distribution of Cl^- across their plasma membranes. By this, Cl^- serves as a key player in a variety of cellular functions such as intracellular pH regulation (Russell and Boron, 1976), cell volume regulation (Basavappa, 1996),

transepithelial salt transport (Mount and Gamba, 2001), synaptic signalling (for review see Reimer et al., 2001), neuronal growth, migration and targeting (Kriegstein and Owens, 2001; Payne et al., 2003), and K^+ scavenging (Payne, 1997). It is also known that Cl^- is actively transported and tightly regulated in virtually all cells via Cl^- cotransporters and exchangers (for review see Mount et al., 1998; Alvarez-Leefmans, 2001; Payne et al., 2003).

In various regions in the CNS, it was shown that the intracellular Cl^- concentration in adults is regulated at the inhibitory synapses by the outward-directed potassium chloride cotransporter (KCC2) (cultured midbrain neurons: Jarolimek et al., 1999; neocortex: DeFazio et. al., 2000; hippocampus: Ganguly et al. 2001; brain stem: Ehrlich et al., 1999, Balakrishnan et al., 2003). KCC2 is the neuron-specific isoform (Payne et al., 1996; Williams et al., 1999) within a family comprising four electroneutral K^+-Cl^- cotransporters (KCC1–KCC4) (for review, see Alvarez-Leefmans, 2001; Delpire and Mount, 2002). It is present in the plasma membrane of the soma and the dendrites of various neuronal types (Lu et al., 1999; Gulyás et al., 2001; Hübner et al., 2001; Blaesse et al., 2004). Under normal physiological conditions, KCC2 actively extrudes Cl^- from the nerve cells using the outward-directed K^+ electrochemical gradient maintained by the Na^+-K^+ pump. This drives Cl^- uphill against its chemical gradient and keeps the Cl^- reversal potential more negative than the resting membrane potential making possible the hyperpolarizing action of inhibitory transmitters like GABA and glycine in the adult CNS. Hence, KCC2 plays a major role in Cl^- homeostasis in mature
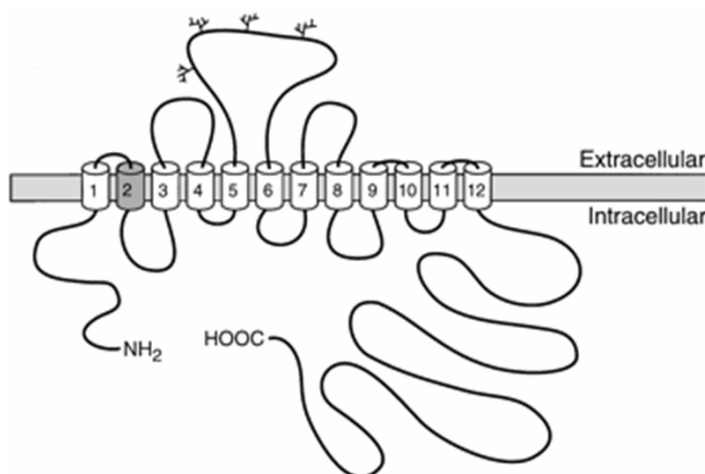
Figure 1.4: A model of KCC2

Based on analysis of the primary structure, 12 transmembrane segments bounded by N- and C-terminal cytoplasmic regions were predicted for the KCC2. On the extracellular intermembrane loop between putative transmembrane segments 5 and 6, there are four sites for N-linked glycosylation. Also, the KCC2 protein contains five consensus phosphorylation sites for protein kinase C, as well as one consensus tyrosine protein kinase phosphorylation site located within the hydrophilic domains at the N or C terminus of the protein. (Modified from Payne, 1997)

neurons and seems to be crucial for the mechanism of postsynaptic inhibition in the adult brain. During early postnatal development, despite the continuous expression of KCC2 in the brain stem, electrophysiological data showed that the cotransporter is not functional, i.e. the KCC2 is present in the brain stem during both depolarizing and hyperpolarizing period (Balakrishnan et al., 2003). In contrast, in the higher brain regions (hippocampus, cerebellum, and cortex), the KCC2 expression is developmentally up-regulated and this correlates with GABA/glycine signalling being depolarizing early in development and hyperpolarizing later on (Rivera et al., 1999; Lu et al., 1999, DeFazio et al., 2000; Vu et al., 2000, Balakrishnan et al., 2003). In this context, it appears that there is a notable difference in the Cl^- regulation mechanisms among the different brain regions.

As it was mentioned above, there is no simple causality between the presence of KCC2 mRNA and/or expression of the protein and its functionality in the brain stem. A recent study from out lab proposed a subcellular redistribution of KCC2 during development and subsequent functional activation (Balakrishnan et al., 2003). However, an immunohistochemical study in the rat LSO revealed that the expression of KCC2 during the first 2 postnatal weeks is not retained within the biosynthetic secretory pathway; KCC2 does not colocalize with markers for endoplasmatic reticulum and Golgi, vesicle and cytosolic/dendritic marker, neither at postnatal day (P) 4 nor at P12 (Blaesse et al., 2004). Moreover, optical imaging with voltage-sensitive dyes and electrophysiological data showed a differential maturation of inhibitory synapses in the SOC, namely that the change in the polarity of glycine responses occurs at different times during development in the various auditory nuclei (Oberhofer, unpublished results; Srinivasan et al., 2004a).

The precise role of the KCC2 in CNS function is still not completely understood. The importance of the KCC2 has been established by the characterization of mice with targeted deletions of the KCC2 gene (Hübner et al., 2001; Woo et al., 2002). The animals with trace amounts of KCC2 protein (Woo et al., 2002) demonstrate handling-induced seizure behaviour, likely to be responsible for their short life span (P17). Electrophysiology data from these animals showed the depolarizing effect after the glycine application in the LSO during the investigated period (at P3 and at P12) (Balakrishnan et al., 2003). Moreover, during normal development, the depolarizing action of GABA and glycine early on provides a trophic signal for increasing the motility

of migrating cells (Barker et al., 1998), regulating the rate of neurogenesis (Maric et al., 2001), facilitating the synapse formation (Ben-Ari et al., 1997; Cherubini et al., 1998; Kirsch and Betz, 1998) and promoting morphological differentiation (Ben-Ari et al., 1994; Marty et al., 1996; Kullmann et al., 2002). Therefore, it is likely that KCC2 actively participates in the development of inhibitory GABA/glycine responses and that in loss-of-function KCC2 animals, the immature state is imitated. In addition, KCC2 may actively regulate ion gradients during synaptic activity. Absence of KCC2 could then lead to the inability to conserve Cl^- and/or K^+ gradients, especially during high rates of synaptic activity. In general, the early function of KCC2 might be critical during brain development and the formation of brain circuit.

The advantage of KCC2 knock-out animals made it possible, via manipulating the duration of the depolarizing phase of GABA/glycine transmission, to analyse the effect of disturbed Cl^- regulation and, thus, the effect of disturbed GABA and glycine neurotransmission (lack of inhibition).

1.4   Aims of this thesis

In my thesis, two main aims were addressed:

First (Chapter 2), to analyse the KCC2 expression during maturation in various auditory brain stem nuclei (the MNTB, the MSO, the LSO, and the SPN) in rats and to find out whether a specific cellular expression pattern correlates with the time of change in GABA/glycine polarity. Immunohistochemistry and confocal microscopy were used to address these issues.

Second (Chapter 3), to investigate the importance of Cl^- homeostasis in the central auditory system to maintain general and specific aspects of brain development. Brain stem slices from KCC2 knock-out (-/-) and wild type (+/+) mice were stained for Nissl substance and the analyses were performed with the help of basic morphometrical and stereological methods.

2   Immunohistochemical analysis of the potassium chloride cotransporter KCC2 in the developing auditory brainstem

2.1   Materials and Methods

2.1.1   Animals

The experiments were performed using Sprague-Dawley rats at five different ages: P0, P4, P8, P12 and P60. In each age-group, two animals were used. All protocols were in compliance with the current German Animal Protection Law and were approved by the local animal care and use committee.

2.1.2   Perfusion and fixation

Before perfusion, the body weight of the animals was obtained. Thereafter, they were anaesthetized with chloral hydrate (70 mg/100 g body weight i.p.) and perfused through the left ventricle with 0.1 M PBS (phosphate buffer saline, pH 7.4) for 5 minutes, followed by 4% paraformaldehyde (PFA) for 7-15 minutes. The fixation procedure was done using a pulsatory forcing pump. After perfusion, the brain was removed from the skull and cryoprotected/postfixed for about 36 hours in 30% sucrose/PFA solution. Coronal slices (30 µm thickness) were cut with a freezing microtome. Three to six serials were collected in 15% sucrose in PBS. Thereafter, all serials were washed three times in PBS (5 to 10 min) and they were used for the immunohistochemical protocol described below (see 2.1.4 Immunohistochemistry) or stored at 4°C until further usage.

In a previous series of experiments, Zamboni's fixative (4% PFA and 15% saturated picrinic acid in PBS; pH=7.4) was used. This fixative is recommended because the addition of picrinic acid enhances antigenicity that can be decreased by the fixative (de Martino and Zamboni, 1967; Somogyi and Takagi, 1982). Photomicrographs were obtained with a high-resolution digital camera (C4742-95-12NR, 1280x1024 pixels; Hamamatsu, Japan) from animals perfused with the two different fixation protocols **(Figs. 2.1, 2.2)**. As an example, the MNTB at P4 and P12 is used. The KCC2 immunofluorescent signal in the auditory brainstem nuclei was compared in order to address which of the two fixatives provided better results (see Page 15 for the results).

2.1.3 Primary antibodies

Initially, two kinds of polyclonal primary KCC2 antibodies were used and the immunofluorescent signal between them was compared in order to check whether they yield differences **(Figs. 2.1, 2.2).** The first primary antibody was a generous gift from Dr. Eric Delpire (Nashville, TN) (Lu et al., 1999). Briefly, a 104-amino-acid peptide (residues 931–1034) located in the carboxyl-terminus of the rat KCC2 (Payne et al., 1996) had been fused to maltose binding protein (New England Biolabs, Beverly, MA). The fusion protein had been grown in *Escherichia coli*, purified with an amylase resin column, and it had been injected subcutaneously into rabbits to generate polyclonal antisera (Covance; Antisera Division, Denver, PA). The specificity of the antibody had been demonstrated previously by Lu et al. (1999). A Western blot from a rat brain had demonstrated the absence of signal (protein doublet at 130-140 kDa) in which the affinity-purified KCC2 antibody had been preabsorbed with the KCC2 fusion protein.
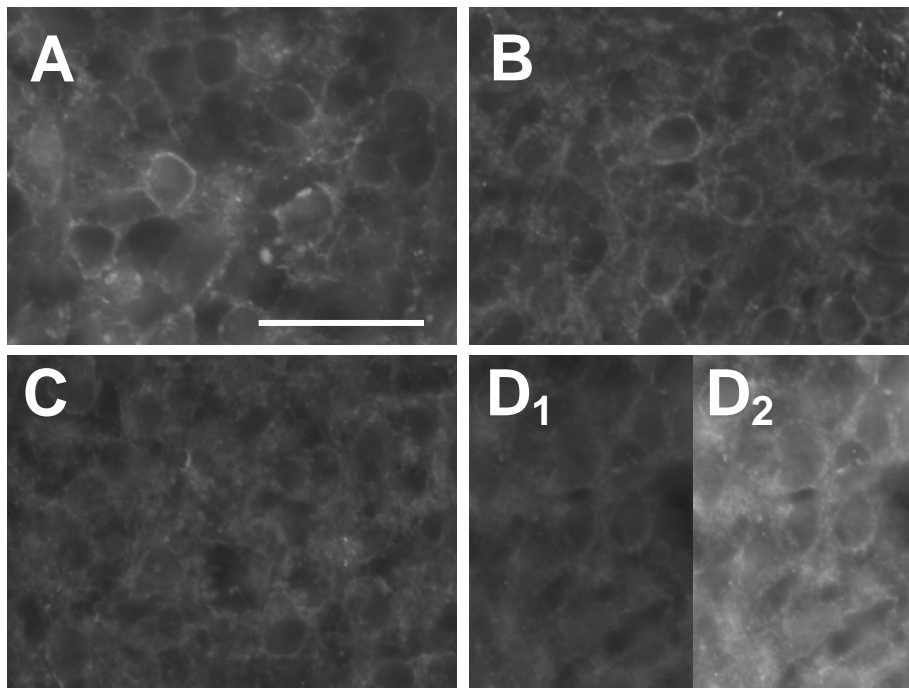
Figure 2.1: Comparison of KCC2 immunofluorescence obtained with two different brain fixation protocols and two different primary antibodies. Slices are from the MNTB at P4

(A) and (B) show application of picrinic acid and PFA fixation protocol, respectively, with antibody from Dr. Delpire (Lu et al., 1999).

(C) and (D) show application of picrinic acid and PFA fixation protocol, respectively, with Upstate Biotechnology antibody (Payne, 1997; Williams et al., 1999; Rivera et al., 1999).

Note that (D$_2$) picture is overexposed when it is taken with the same exposure time (440 ms) as (A), (B) and (C); (D$_1$) is taken with 220 ms exposure time. Hence, PFA fixation protocol and Upstate Group, Inc antibody yielded the best results. Scale bar, 50 µm in all photomicrographs.

The second primary antibody was purchased from Upstate Biotechnology, USA (Payne, 1997; Williams et al., 1999; Rivera et al., 1999). Briefly, a KCC2 fusion protein (termed B22) had been prepared, containing a 112-amino acid segment of the carboxyl terminus of rat KCC2 (amino acids 932–1043). The fusion protein had been produced in *Escherichia coli* and it had been purified using metal chelation chromatography, following the manufacturer's instructions (His-Bind Resin; Novagen, Madison, WI). Purified B22 fusion protein had been injected subcutaneously into rabbits to generate polyclonal antisera (Animal Resource Service of the School of Veterinary Medicine, University of California, Davis). Western blots from rat brain membranes and from various HEK-293 cell lines with protein band ~140-kDa, representing KCC2 protein, and subsequent immunoadsorption experiments demonstrated the specificity of this antibody (Williams et al., 1999).
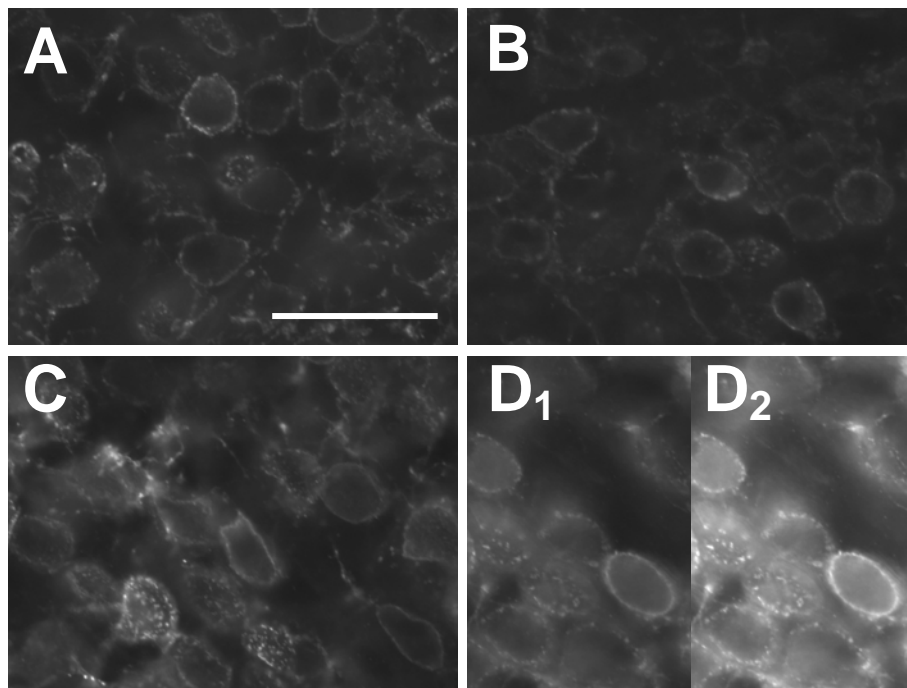
Figure 2.2: Comparison of KCC2 immunofluorescence obtained with two different brain fixation protocols and two different primary antibodies. Sections are from the MNTB at P12

(A) and (B) show application of picrinic acid and PFA fixation protocol, respectively, with antibody from Dr. Delpire (Lu et al., 1999).

(C) and (D) show application of picrinic acid and PFA fixation protocol, respectively, with Upstate Biotechnology antibody (Payne, 1997; Williams et al., 1999; Rivera et al., 1999).

Note that panel D_2 is overexposed when it is taken with the same exposure time (440 ms) as (A), (B) and (C); (D_1) is taken with 220 ms exposure time. Hence, PFA fixation protocol and Upstate antibody yielded the results. Scale bar, 50 µm in all photomicrographs.

Comparison between the two different antibodies and perfusion with Zamboni's fixative or PFA revealed that the brightest image at both ages (P4 and P12) was obtained from the PFA perfused animals stained with Upstate primary antibody **(Figs. 2.1D$_2$, 2.2D$_2$)**. Therefore, I continued with the Upstate antibody and the PFA protocol in subsequent experiments. It should also be mentioned that this primary antibody is commercially available, which presents another advantage over the one from Dr. Delpire.

2.1.4 Immunohistochemistry

The free-floating technique was used to visualize the KCC2 protein. The permeabilisation step was considered very important for the penetration of the antibody into the relatively thick slices (30 μm). At first, the slices were treated with 1% sodium dodecyl sulfate (SDS) and 8% ß-mercaptoethanol in PBS (Lu et al., 1999; also recommended by Dr. Erdem Güresir, University of Frankfurt). However, this treatment damaged the slices from P0 and P4 animals, even when they were kept in the solution for only 1 minute. Therefore, a less harmful permeabilisation step was used subsequently. To do so, slices were incubated for 1 hour at 4°C on the shaker in blocking solution (1.5% (v/v), normal goat serum and 1% (w/v) bovine serum albumin in PBS to which 0.3% Triton X-100 was added to permeabilise the tissue and to allow the antibodies' access to the structures (Friauf et al., 1999).

The two permeabilisation protocols were investigated before the Upstate antibody was chosen as superior to the one from Dr. Delpire. The comparison using the latter antibody is shown in Figures 2.3 and 2.4. No difference in the signal intensity in P4 animals treated with SDS **(Fig. 2.3A)** and triton **(Fig. 2.4A)** was shown. However, in P12 animals treated with SDS **(Fig. 2.3C)**, the intensity of the signal was higher than in P12 animals treated with triton **(Fig. 2.4C)**. Still, the argument was in favour of the triton treatment because the slices from P4 were well preserved. When triton slices were stained with Upstate primary antibody **(Fig. 2.5)**, it appeared that at both ages, P4 **(Fig. 2.5A)** and P12 **(Fig. 2.5C)**, the signal intensity was higher than in the case with Dr. Delpire's antibody **(Figs. 2.3A,C; 2.4A,C)**. Another, not less important, advantage of the triton treatment should be taken into consideration: the slices can be stored for about 2 months and then photographed without fade out problems. Compare panels A and C
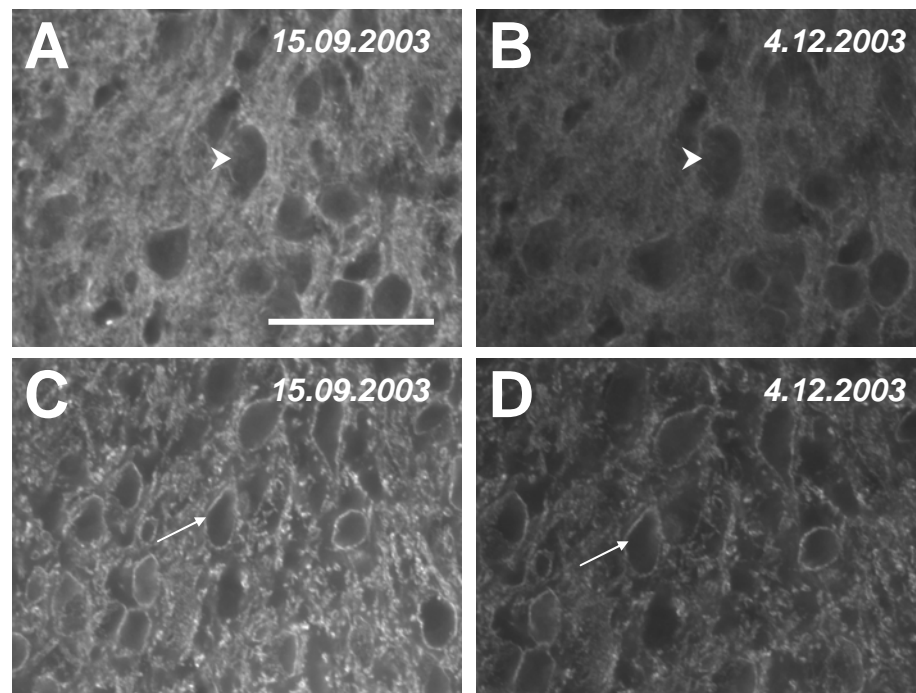
Figure 2.3: Comparison of the fluorescent signal in P4 (A and B) and P12 (C and D) animals after brain fixation with PFA, SDS permeabilisation step and immunostaining protocol with KCC2 primary antibody from Dr. Delpire

At both ages the comparison shows lower intensity of the fluorescent signal after 2 months. This result indicates that the applied protocol was not in favour of the storage of the slices. This could be due to the sodium dodecyl sulfate (SDS) step or to the quality of the antibody and the extended storage time. In order to show that the same area has been photographed twice, the same cell body is marked with arrowheads (P4, panels A and B) or arrows (P12, panels C and D). Scale bar, 50 µm in all photomicrographs.

(immediate pictures) with panels B and D (the same slice photographed 2 months later) in Figures 2.3-2.5.

After incubation in the blocking solution (see above), the primary KCC2 antibody (1:300 dilution) was added, and the incubation was continued overnight at 4°C. After several rinses in PBS (5 to 10 min each), slices were treated with the secondary antibody (Alexa Fluor 488 goat anti–rabbit immunoglobulin G (IgG) antibody, 1:1000 dilution; Molecular Probes) for 2 hours at room temperature, rinsed again, mounted on slides and coverslipped with Vectashield Mounting media (refractory index 1.45; Vector Laboratories, Burlingame, CA).

Control experiments were performed on serials by using the described immunohistochemical procedure, yet in the absence of the primary antibody. No immunolabelling occurred in these slices, confirming the specificity of the secondary antibody (data not shown).
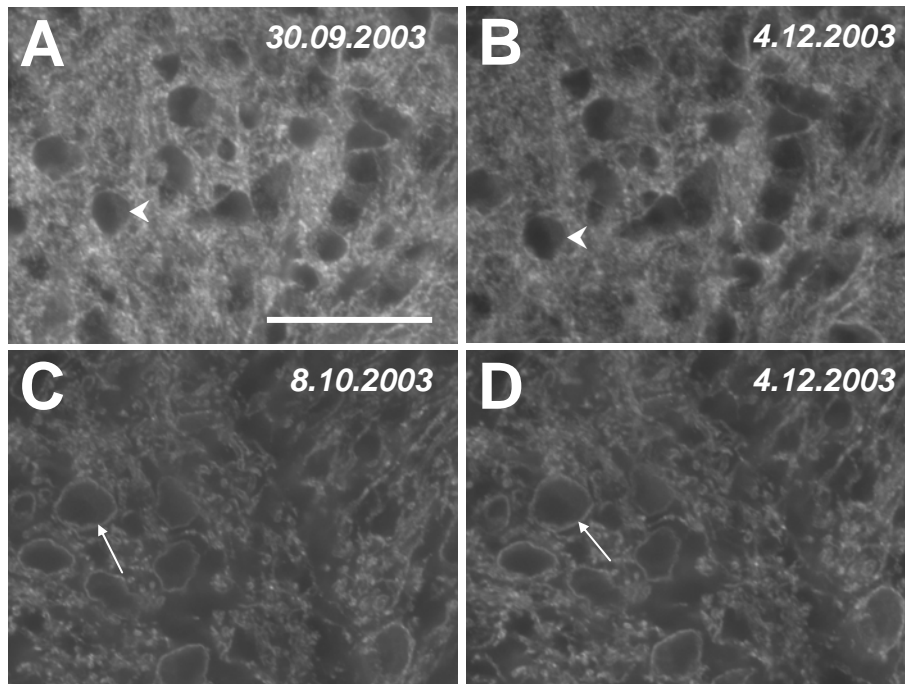
Figure 2.4: Comparison of the fluorescent signal in P4 (A and B) and P12 (C and D) animals after brain fixation with PFA, triton permeabilisation step and immunostaining protocol with KCC2 primary antibody form Dr. Delpire

At both ages the comparison shows no difference (or only a small difference at P4) in the intensity of the fluorescent signal after 2 months storage of the slices. This shows that the decreased signal after storage that was pointed in Figure 3 is due to SDS treatment but not to the quality of the antibody. In order to show that the same area has been photographed twice, the same cell body is marked with arrowheads (P4, panel (A) and (B)) or arrows (P12, panel (C) and (D)). Scale bar, 50 µm in all photomicrographs.
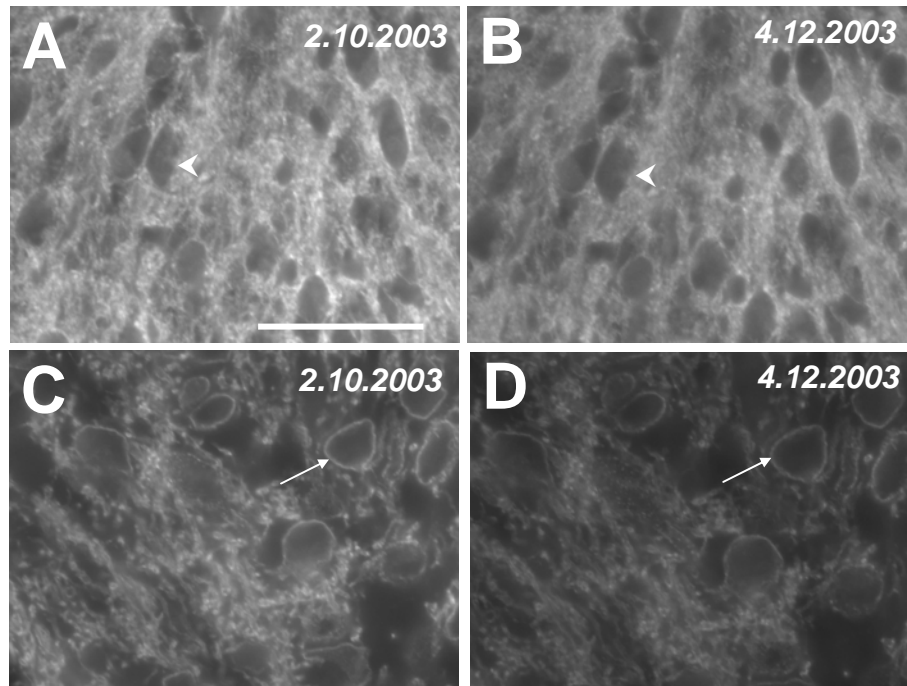
Figure 2.5: Comparison of the fluorescent signal in P4 (A and B) and P12 (C and D) animals after brain fixation with PFA, triton permeabilisation step and immunostaining protocol with KCC2 Upstate primary antibody

Note that with this protocol, high-intensity pictures are obtained. Moreover, at both ages, the comparison shows no difference in the intensity of the fluorescent signal after 2 months storage of the slices. In order to show that the same area has been photographed twice, the same cell body is marked with arrowheads (P4, panel (A) and (B)) or arrows (P12, panel (C) and (D)). Scale bar, 50 µm in all photomicrographs.

2.1.5   Evaluation of fluorescent images prior
to confocal microscopy

Labelled slices were carefully evaluated on a conventional fluorescent microscope (Axioskop 2; Zeiss, Göttingen, Germany) with filter set number 09 (BP 450-490; FT 510; LP 520), using 10x/0.3 and 20x/0.5 Plan-Neofluar objectives. Only high quality slices were taken for further analysis considering general tissue quality (including fixation and folding in the tissue) and high signal-to-noise ratio; only the brightest slices from each serial with present SOC nuclei were further analyzed by confocal microscopy.

2.1.6   Confocal microscopy

Confocal microscopy offers several advantages over conventional optical microscopy. It employs laser technology in the illumination and detection of fluorescence at a single point (optical plane) in a thick specimen. A plate with a small hole, called pinhole, is placed in front of the image detecting device (photomultiplier tube). This eliminates out-of-focus interference, thereby allowing structures to be sectioned optically. In Figure 2.6 a schematic representation of a confocal microscope is presented.
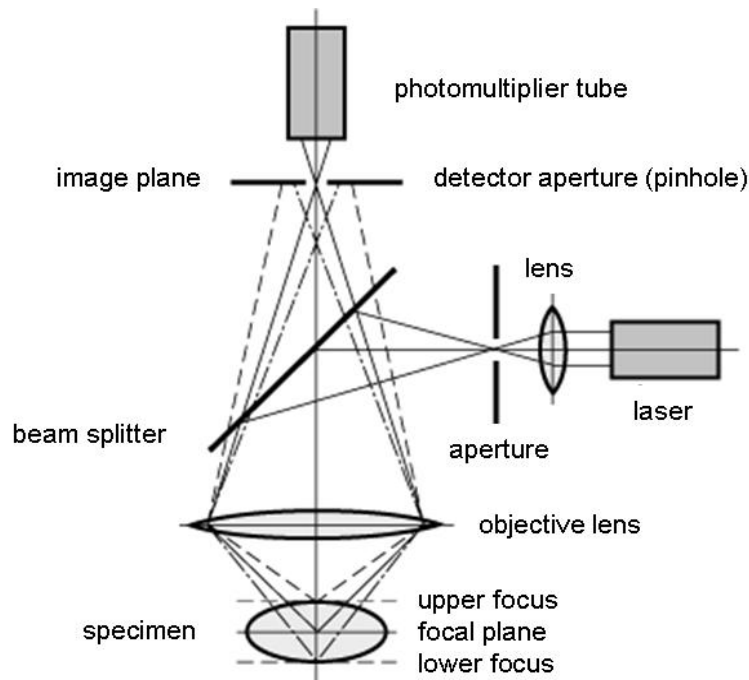
Figure 2.6: Schematic representation of a confocal microscope setup

The illumination light from the laser is scanned onto the specimen dot by dot through a scanner. The light emitted from the specimen is collected and de-scanned dot by dot. It then passes through the detecting pinhole and reaches the photomultiplier tube. The disadvantage of this collection strategy is the slow speed of data collection and longer exposure of the specimen to excitation illumination that can photobleach specimens. However, the confocal imaging approach provides an improvement in both axial and lateral resolution. Their theoretical values are determined by the diameter of the two apertures **(Fig. 2.6)** and the numerical aperture of the objective lens and are characteristics of the system. Values in the range of 0.2 μm in the plane of section and 0.5 μm along the z-axis are considered being minimal and allow accurate localization of the fluorescence signal. The confocal technique also provides a means for objective quantification by measuring image pixel intensities. Nevertheless, before imaging, a lot of parameters, including laser line selection and control of laser power, beam splitter selection, gain of photomultiplier tube and offset adjusting, detecting pinhole size, detecting spectral range, scan speed, frame format and zoom factor, have to be set up properly.

In the current investigation, a stack of 15 to 20 images (the optical plane of each stack is 0.5 μm) was taken with a laser scanning microscope (Axioplan 2, LSM 510; Carl Zeiss, Jena, Germany) and captured with Zeiss LSM Image Browser software (Version 2.80.1123, Carl Zeiss, Jena, Germany) provided by the system. The specimen was excited with an Argon laser with a wavelength of 488 nm (Alexa Fluor 488 goat anti–rabbit IgG was used as secondary antibody, **Fig. 2.7**).
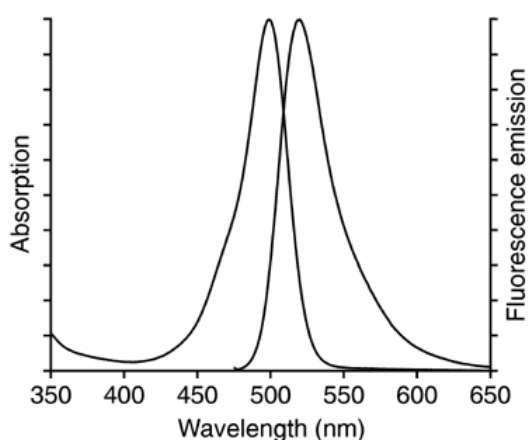
Figure 2.7: Absorption and fluorescence emission spectra (maxima at 495 nm and 519 nm, respectively) of Alexa Fluor 488 goat anti–rabbit immunoglobulin G (IgG) antibody in pH 8.0 buffer. From http://www.probes.com

The emission signal was imaged through a filter set, comprising a beam splitter (MBS:HFT 488) and a long-pass filter (LP 505 nm). The laser was operated at 10% of the maximum power. The pinhole was set between 66 μm and 71 μm. Images were collected with 1.60 μs pixel time, a compromise to avoid too long illumination and consequent bleaching effects, and the requirements for using the confocal setup. Each image was captured as 2048 x 2048 pixels scan format (digital image resolution). A 10x Plan-Neofluar lens (NA = 0.3) for overview pictures and a 40x oil Plan-Neofluar immersion lens (NA = 1.3) for high magnification pictures were used. Software zoom was not used and the zoom factor in both cases was set to 1.0.

One important principle of confocal microscopy must be considered: the combination of gain and offset adjustment on the photomultiplier tube produces an optimized image with balanced intensity and background noise on which further analysis can be done. Since these two parameters counteract each other, it was important to find an appropriate balance between them, still in the linear range in order to generate meaningful expression data. Linear range indicates the range of input signal intensities over which the detector can accurately measure intensity changes, such that a given degree of change in input signal generates the same degree of change in output signal. Data acquired outside this linear range (leading to underexposed or overexposed images) will not be measured accurately and, therefore, it will not be possible to generate statistically significant data.

In the present thesis, the gain and the offset were optimized for each nucleus such that the whole set of settings mentioned above were the same throughout all different age-groups and still in the linear range. For the overview pictures, the detector gain was set to 620 V and the amplifier offset to -0.10. For the high magnification pictures, the detector gain was set to 700 V for the LSO and the MSO, 750 V for the MNTB and 680 V for the SPN; the amplifier offset was set to -0.10 for LSO, -0.14 for MNTB and -0.12 for MSO and SPN.

To collect high magnification images from unlabeled control slices, included to check for background fluorescence (autofluorescence), the range of settings was the same as for the labelled tissue (for details see **Figs. 2.9–2.12**).

2.1.7   Data analysis and quantification

In the developmental series from five different ages (P0, P4, P8, P12 and P60), the staining intensities in the four different nuclei from SOC were evaluated. Because such developmental evaluations can lead to inaccurate conclusions, I had to consider some potential pitfalls. First, I took into account that litter-specific peculiarities can occur. Therefore, I obtained age-matched animals from two different litters. Second, because the slices from the 10 animals (2 animals in each age-group) were stained in separate sessions and during a period that extended over two months, I had to consider that the staining intensity may have been affected by changes in the quality of antibody, by seasonal variations or both. Fortunately, I found no such variability when both primary antibodies and the PFA fixation protocol were used **(Figs. 2.4, 2.5)**. Third, quantifying the intensity of data collected on the confocal microscope can be critical. Some factors to consider are: uneven illumination across the field of view, fluctuations as the system heats up, daily variations in the laser power, (mis)alignment of the system, bleaching of fluorophores, depth within a sample, variations in sample preparation and/or immunolabelling.

For quantification analysis of KCC2 immunoreactivity, z-series stacks of each nucleus, scanned at high magnification, were loaded from Zeiss LSM Image Browser to ImageJ 1.31u software (National Institute of Health, USA; http://rsb.info.nih.gov/ij/) via LSM Reader plug-in. A single image (optical section with 0.5 µm thickness) for each neuron was taken from the stack, zoomed offline and used to manually outline the two regions of interest: soma surface and the soma interior **(Fig. 2.8A)**. Then the pixel intensities (absolute gray values, AGV_s) were determined for soma surface **(Fig. 2.8B)** and soma interior **(Fig. 2.8C)**. Because the micrographs were taken with an 8-bit resolution, the pixels could have AGV_s between 0 (black) and 255 (white). Then the AGV_s related to the pixel number allow calculating the mean (the sum of the gray values of all the pixels in the selection divided by the number of pixels). The mean gray value of soma surface ($MGV_{soma\ surface}$) and soma interior ($MGV_{soma\ interior}$) from 20 single neurons was calculated in order to obtain an average value for each nucleus, region of interest and given age-group ($MGV_{group\ surface}$ and $MGV_{group\ interior}$). The MGV_{group} and standard deviation (SD) are shown in Tables 2.1 – 2.4. These values were used to objectively compare the immunoreactivity obtained with KCC2 antibody in a given nucleus between five different ages.
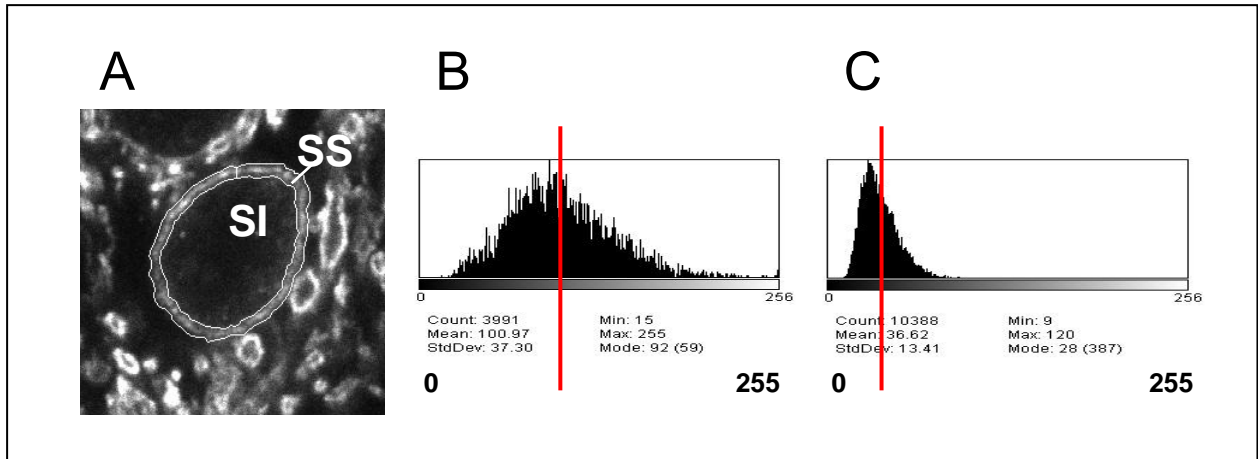
Figure 2.8: Photomicrograph of a representative LSO neuron at P12 (A) and the related histograms of AGV_s distribution for soma surface (B) and soma interior (C)

In this representative example, $MGV_{soma\ surface} = 101$ and $MGV_{soma\ interior} = 37$ (red vertical lines in panel B and C, respectively) of the neuron are close to the $MGV_{group\ surface} = 109$ and $MGV_{group\ interior} = 35$ of the given age-group.

AGV_s, absolute gray values, $MGV_{soma\ surface/interior}$, mean gray value; SS, soma surface; SI, soma interior

As mentioned above, high magnification images from control (unlabeled) slices were collected to check for background fluorescence (autofluorescence). To do so, for each nucleus the mean gray values from a 2048 x 2048 pixel scan frame (MGV_{frame}), taken with 40x Plan-Neofluar objective, were compared between untreated slices and immunostained slices for each nucleus (MNTB: **Fig. 2.9**; MSO: **Fig. 2.10**; LSO: **Fig. 2.11**; SPN: **Fig. 2.12**).
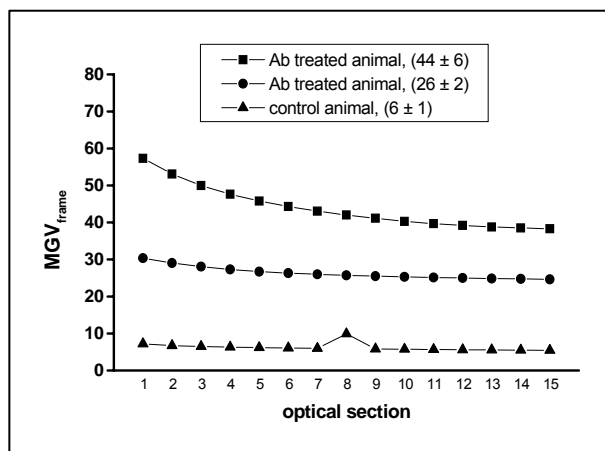
Figure 2.9: Plot of the MGV_{frame} along the z-stack in MNTB

The MGV_{frame} from a 2048 x 2048 pixel scan frame taken with 40x Plan-Neofluar objective from three different P12 animals are compared. The bottom line (-▲-) is from an unlabeled specimen and shows the background fluorescence (autofluorescence) in the MNTB. The middle (-●-) and the upper line (-■-) are from specimens from two different animals, treated with above mentioned immunohistochemical protocol. In the inset the mean of the MGV_{frame} from each optical section in a given stack ± SD are shown. Ab, antibody.
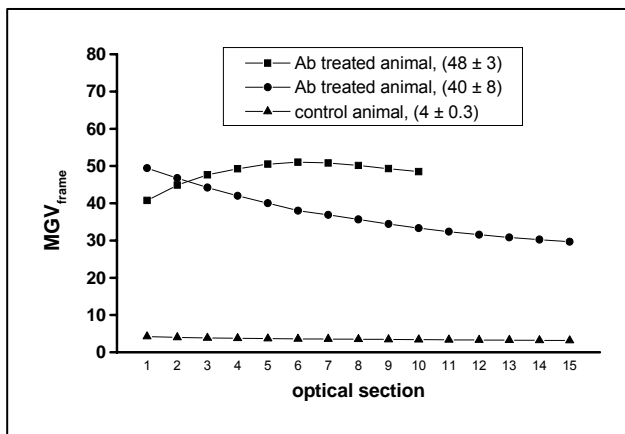
Figure 2.10: Plot of the MGV$_{frame}$ along the z-stack in MSO

The MGV$_{frame}$ from a 2048 x 2048 pixel scan frame taken with 40x Plan-Neofluar objective from three different P12 animals are compared. The bottom line (-▲-) is from an unlabeled specimen and shows the background fluorescence (autofluorescence) in the MSO. The middle (-●-) and the upper line (-■-) are from specimens from two different animals, treated with above mentioned immunohistochemical protocol. In the inset the mean of the MGV$_{frame}$ from each optical section in a given stack ± SD are shown. Ab, antibody.
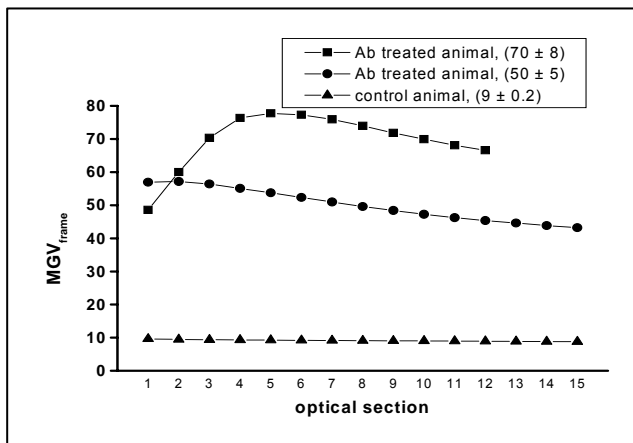
Figure 2.11: Plot of the MGV$_{frame}$ along the z-stack in LSO

The MGV$_{frame}$ from a 2048 x 2048 pixel scan frame taken with 40x Plan-Neofluar objective from three different P12 animals are compared. The bottom line (-▲-) is from an unlabeled specimen and shows the background fluorescence (autofluorescence) in the LSO. The middle (-●-) and the upper line (-■-) are from specimens from two different animals, treated with above mentioned immunohistochemical protocol. In the inset the mean of the MGV$_{frame}$ from each optical section in a given stack ± SD are shown. Ab, antibody.
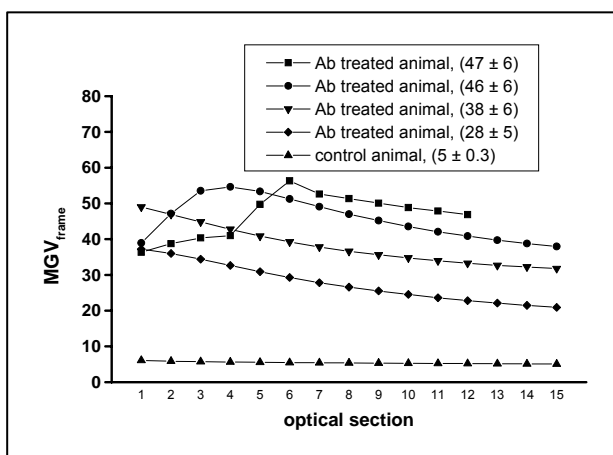
Figure 2.12: Plot of the MGV$_{frame}$ along the z-stack in SPN

The MGV$_{frame}$ from a 2048 x 2048 pixel scan frame taken with 40x Plan-Neofluar objective from three different P12 animals are compared. The bottom line (-▲-) is from an unlabeled specimen and shows the background fluorescence (autofluorescence) in the SPN. The rest lines denoted by (-●-), (-■-), (-▼-) and (-◆-) are from four different slices from two different animals, respectively, treated with above mentioned immunohistochemical protocol. In the inset the mean of the MGV$_{frame}$ from each optical section in a given stack ± SD are shown. Ab, antibody.

The comparison revealed that the background immunostaining levels were very low (in the range of 8-23%) and can therefore be neglected.

Further, an obvious difference in the pattern and intensity of the neuropil staining during development was noticed and it was analysed subsequently. Five consecutive images were taken from a stack and two cell body-free regions (ca. 100 000 pixels each) per animal were manually outlined. This area was defined as another region of interest, namely neuropil **(Fig. 2.13)**. In older animals (P12 and P60), the neuropil was defined by a rectangle, whereas in younger animals (P0-P8), a cell body-free area was randomly selected.
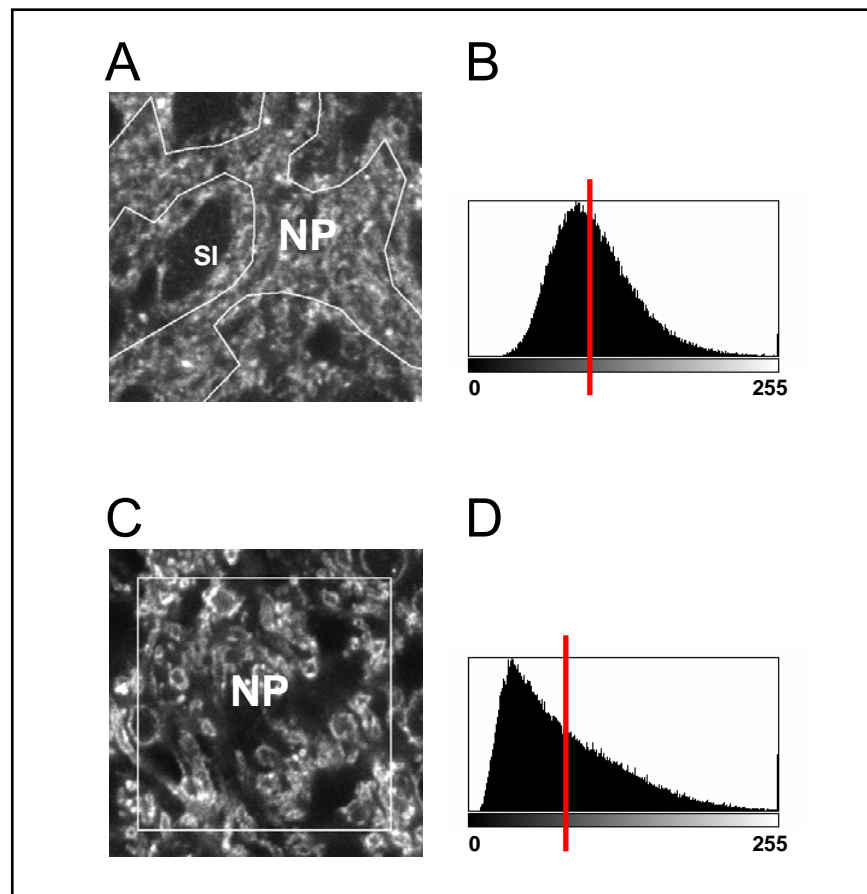
Figure 2.13: Photomicrographs of representative LSO neuropil outlines at P4 (A) and at P12 (C) and the related histograms of AGV$_s$ distribution at P4 (B) and at P12 (D)

In this representative example, the MGV$_{s\ neuropil}$ = 104 (P4) and MGV$_{s\ neuropil}$ = 79 (P12) (red vertical lines in panel B and D, respectively) and thus close to the MGV$_{group\ neuropil}$ = 104 (P4) and MGV$_{group\ neuropil}$ = 72 (P12). See results section where representative neuropil areas from all ages are presented. AGV$_s$, absolute gray values; MGV$_{neuropil}$, mean gray value of neuropil; NP, neuropil; SI, cell interior

The AGV_s were determined and the mean ($MGV_{s\ neuropil}$) was calculated. Note that $MGV_{s\ neuropil}$ were pooled, thus each data point was based on five optical sections from a given slice **(Figs. 2.23 - 2.26)**. In order to obtain the average value for each nucleus and age-group, $MGV_{group\ neuropil} \pm SD$ was calculated **(Table 2.5)**.

2.1.8   Statistical analysis

For statistical analysis, WinSTAT software, add-in for Microsoft Excel, was used. Statistically significant differences were determined using regression analysis and a parametric student *t-test* for two-group comparison. The significance of correlation was tested using Pearson test and p values were obtained. Significance of the data was accepted at $p < 0.05$. Its level according to the p values and the related symbols used in the figures and tables are as follows (Motulsky, 1995):

p	value wording	abbreviation
>0.05	not significant	ns
<0.05	significant	*p
<0.01	very significant	**p
<0.001	extremely significant	***p

2.2   Results

2.2.1   Overview of KCC2 immunoreactivity in the SOC

The focus of Chapter 2 of the present study was to investigate the KCC2 immunofluorescent signals in the four major nuclei of the rat's SOC, i.e. the MNTB, the MSO, the LSO, and the SPN. The free-floating immunohistochemical technique, used to visualize the KCC2 protein, revealed immunolabelled neuropil and cell bodies in all four nuclei. The immunoreactivity was already present at birth. Confocal low magnification images of KCC2 expression at five different ages (P0, P4, P8, P12, and P60) were obtained and they are shown in Figure 2.14. The pictures were taken at the same confocal settings to enable a direct comparison of the fluorescent signal intensity during development and between nuclei. The staining was confined to the neurons in a way that the boundaries of the different SOC nuclei were easily delineated. For the sake of clarity, the outlines were drawn only at P60 **(Fig. 2.14E)**. Some differences in the intensities of KCC2 immunoreactivity between the nuclei, however, did become apparent. The SPN and the LSO presented the highest immunofluorescent signal among the four nuclei. Extremely prominent immunoreactivity was found in the neuropil at P0. In contrast, the MNTB was less noticeable and remained weakly labelled throughout the investigated period. The MSO displayed a moderate labelling. This variance in the intensity of KCC2 staining was obvious from P0 to P12 **(Fig. 2.14A-D)**. At P60, the immunofluorescent signal from all nuclei seemed to be barely above the background and it seemed as if KCC2 protein declined when judged at low magnification **(Fig. 2.14E)**. However, at higher magnification **(Figs. 2.15, 2.17, 2.19, 2.21)**, it became clear that the decline was not in the soma surface, yet in the neuropil.

Due to KCC2 immunolabelling, it was also possible to observe the morphology of the cell bodies of the principle neurons in each nucleus: the MNTB cell bodies with their spherical or oval perikarya (Sommer et al., 1993), the narrow dorso-ventrally oriented column of neuronal somata of the MSO (Ramon y Cajal, 1907), the tightly packed cell bodies of bipolar LSO neurons aligned orthogonal along the long axis of the "S"-shape (Schwarz, 1992) and the heterogeneous SPN cell bodies with morphologies ranging from large cells with polygonal or rounded somata to medium and small, highly elongated or ovoid cell bodies (Saldana and Berrebi, 2000) and its relatively low cell density in comparison to the MNTB, the MSO and the LSO (Kulesza et al., 2000).
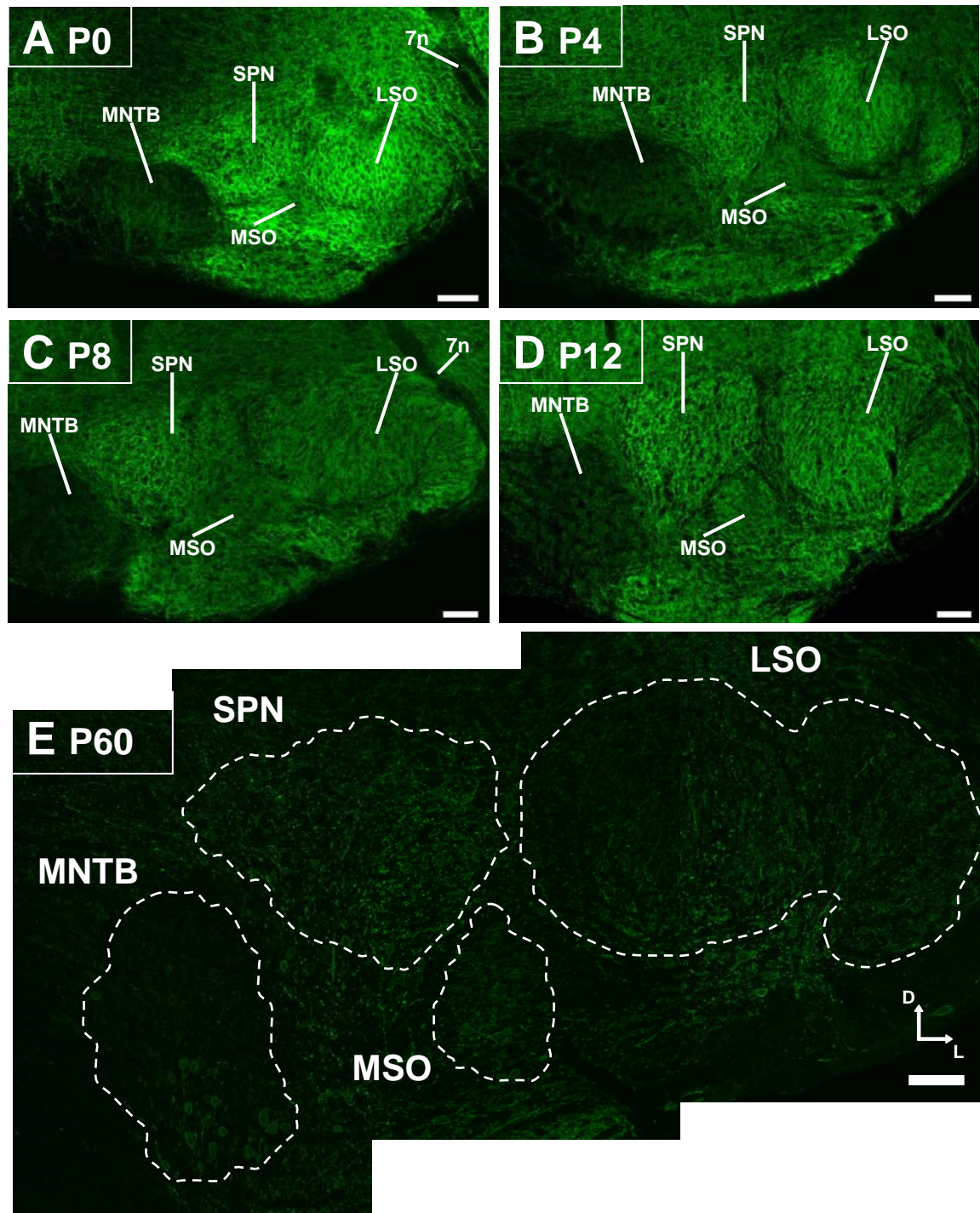
Figure 2.14: Confocal overview pictures for KCC2 immunoreactivity in the rat SOC at five different ages

The pictures were taken at the same confocal settings to enable a direct comparison of the fluorescent signal during development and between nuclei. The SPN and the LSO show the highest immunofluorescent signal intensity. The MNTB shows the lowest signal intensity and the MSO an intermediate one. The labelling pattern is obvious at P0 – P12. Note that at this magnification, it seems as the immunofluorescent signal in all nuclei declines between P12 and P60. Though, at higher magnification (Figs. 2.15, 2.17, 2.19 and 2.21), one can see that the decline is not in the soma surface, yet in the neuropil.

LSO, lateral superior olive; MNTB, medial nucleus of trapezoid body; MSO, medial superior olive; SPN, superior paraolivary nucleus; L, lateral; D, dorsal; 7n, facial nerve. Scale bar, 100 µm in all panels.

2.2.2   Detailed view of immunoreactivity of KCC2 in the SOC

To compare in more quantitative terms the distribution of KCC2 immunofluorescent staining, area-specific intensity profiles of the immunofluorescent signal were measured. Three regions of interest were distinguished: soma surface, soma interior and neuropil. The quantification was organised so that immunoreactivity was compared between P0 and P12 using regression analysis. In order to see whether the expression level attains the adult values at P12, a parametric student *t-test* was applied between P12 and P60.

In order to correlate the immunofluorescent appearance of the neurons and the quantitative data, representative cell bodies were pointed out in the high magnification confocal pictures. Also, the representative cell bodies were presented together with their related histograms of AGV_s distribution for soma surface and soma interior, respectively for each nucleus **(Figs. 2.16E, 2.18E, 2.20E, 2.22E)**.

2.2.2.1   MNTB

At P0 and P4, labelled cell bodies of MNTB neurons were barely visible and almost indistinguishable from the diffusely stained neuropil **(Fig. 2.15A,B)**. The KCC2 immunoreactivity was rarely related to membrane structures including cell bodies and dendrites. In Figures 2.15A and 2.15B, cell bodies are marked with small arrows in order to point to the soma surface. Interestingly, at P8 and P12, the pattern of the signal from the soma surface showed obvious "hot spots" (puncta) **(Fig. 2.15C,D)**. The two cell bodies, marked by open triangles for the puncta in Figure 2.15C, had almost the same $MGV_{soma\ surface}$ but they differed in their staining pattern. Whereas this necklace-like pattern was present in most somata at P8, at P12 soma surfaces with more continuous look were present **(Fig. 2.15D)**. It should be noted that for example the cell body in Figure 2.15D, marked by a double arrow, had $MGV_{soma\ surface} = 108$, thus close to $MGV_{group\ surface} = 107$ at P60 **(Table 2.1)**. At P8 and P12, the neuropil was almost devoid of signal **(Fig. 2.15C,D)**, but at P12, transversally cut dendrites could be seen for the first time. At P60, it was rare to find cell bodies with obvious necklace-like punctate soma surface, yet continuous appearance was common **(Fig. 2.15E)**. In the neuropil, transversally cut dendrites appeared more often than at P12.
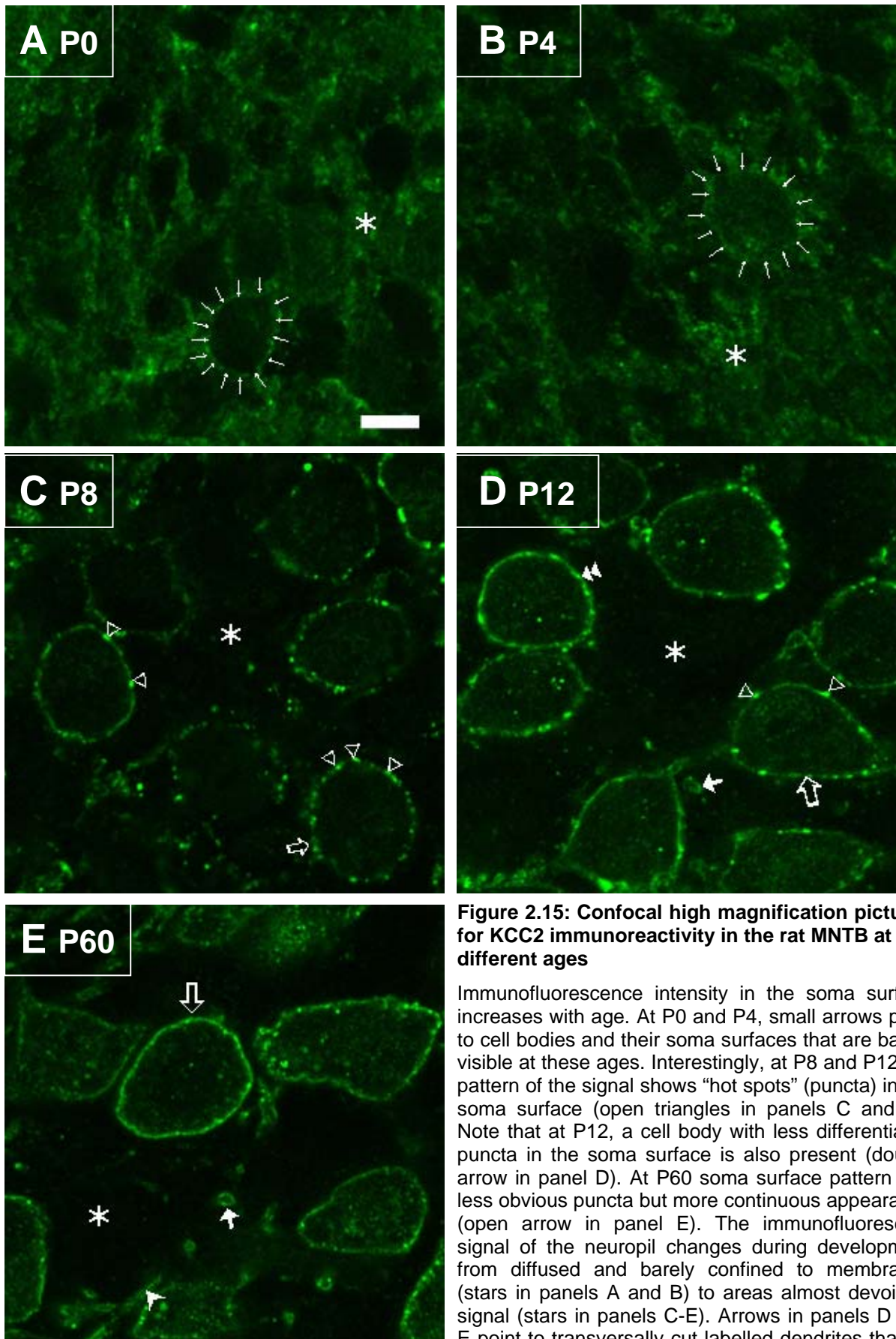
Figure 2.15: Confocal high magnification pictures for KCC2 immunoreactivity in the rat MNTB at five different ages

Immunofluorescence intensity in the soma surface increases with age. At P0 and P4, small arrows point to cell bodies and their soma surfaces that are barely visible at these ages. Interestingly, at P8 and P12 the pattern of the signal shows "hot spots" (puncta) in the soma surface (open triangles in panels C and D). Note that at P12, a cell body with less differentiated puncta in the soma surface is also present (double arrow in panel D). At P60 soma surface pattern has less obvious puncta but more continuous appearance (open arrow in panel E). The immunofluorescent signal of the neuropil changes during development from diffused and barely confined to membranes (stars in panels A and B) to areas almost devoid of signal (stars in panels C-E). Arrows in panels D and E point to transversally cut labelled dendrites that do not appear before P12. Small arrows in panels A and B and open arrows in panels C-E indicate representative somata. Scale bar, 10 µm in all panels.

The quantification of immunofluorescent signal intensity in the MNTB soma surface between P0-P12 animals and between P12-P60 animals is shown in Figures 2.16A and 2.16B, respectively. The results of soma surface analysis provided the expected and already noticed increase in the immunoreactivity with age. The statistical analysis showed an extremely significant linear increase from P0 to P12 (***$p=0.000006$) and no significant difference between P12 and P60 ($p=0.05$). The $MGV_{group\ surface}$ ($\pm SD$) for each age-group is shown in Table 2.1. Scatter plots of $MGV_{soma\ interior}$ between P0-P12 animals and between P12-P60 animals are shown in Figures 2.16C and 2.16D, respectively. The statistical analysis showed no significant difference from P0 to P12 ($p=0.4$) as well as between P12 and P60 ($p=0.4$). The $MGV_{group\ interior}$ ($\pm SD$) for each age-group is shown in Table 2.1. Photomicrographs with the representative MNTB cell bodies and the related histograms of AGV_s distribution for soma surface and soma interior are shown in Figure 2.16E.

In summary, the quantification analysis in the MNTB showed that the adult value of immunoreactivity in soma surface was attained at P12. For soma interior, no statistically significant change during the investigated period has been observed.

Figure 2.16: Quantification of immunofluorescent signal in the MNTB soma surface and soma interior during development

(A) and (B) Scatter plots of MGV_s in soma surface between P0-P12 animals and between P12-P60 animals, respectively. Statistical analysis shows a linear increase of the soma surface immunofluorescent intensity from P0 to P12 (***$p=0.000006$) and no significant difference between P12 and P60 ($p=0.05$)

(C) and (D) Scatter plots of MGV_s in soma interior between P0-P12 animals and between P12-P60 animals, respectively. Statistical analysis shows no significant difference of the soma interior immunofluorescent intensity from P0 to P12 ($p=0.4$) as well as between P12 and P60 ($p=0.4$).

(E) Photomicrographs of representative MNTB cell bodies at different ages (first row) and the related histograms of AGV_s distribution for soma surface (second row) and soma interior (third row), respectively. The values of $MGV_{group\ surface}$ ($\pm SD$) and $MGV_{group\ interior}$ ($\pm SD$) for each age-group are shown in Table 2.1.

AGV_s, absolute gray values; MGV_s, mean gray values of a single cell body; $MGV_{group\ surface/interior}$, mean gray values of a group for soma surface and soma interior, respectively; SS, soma surface; SI, soma interior.
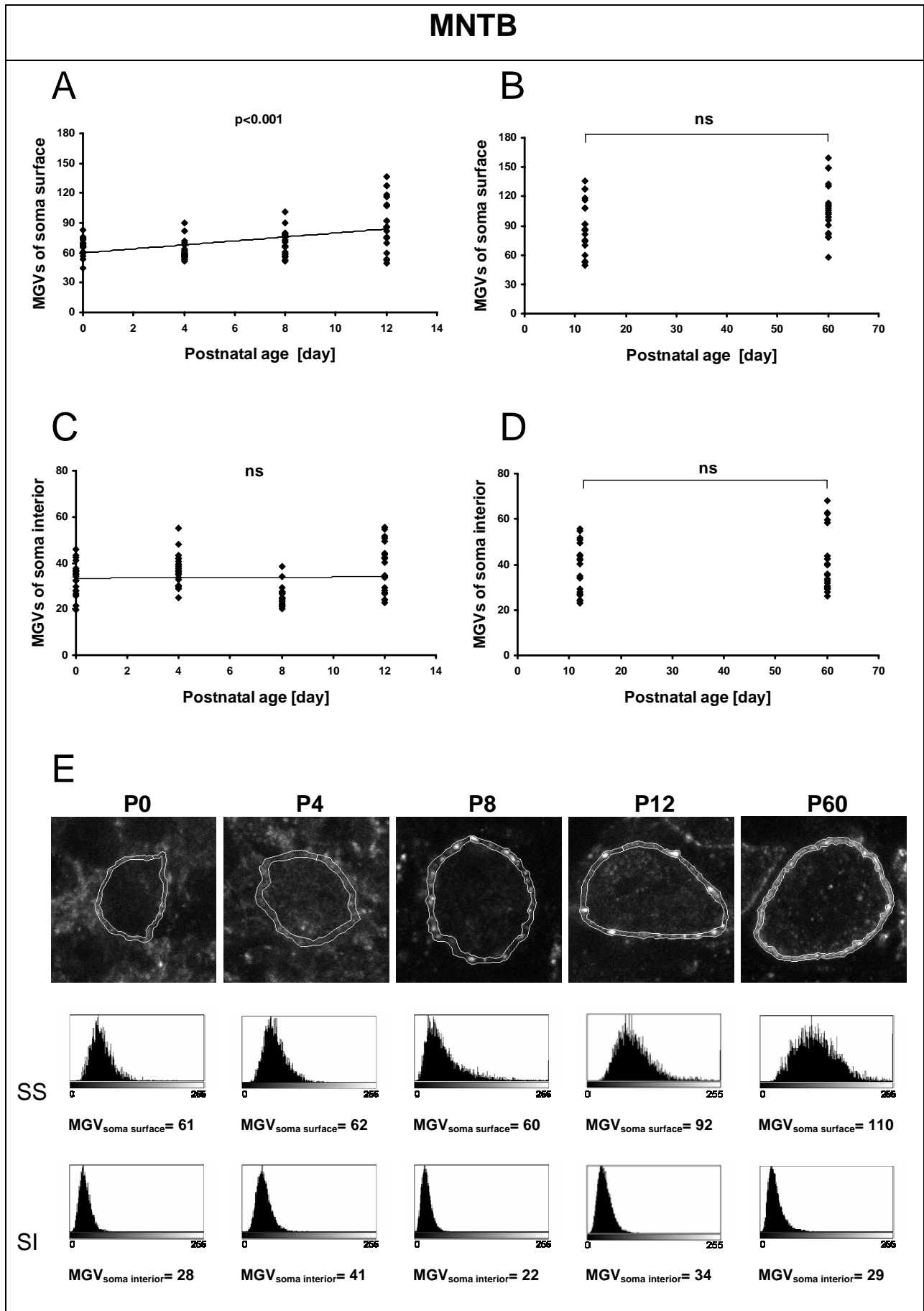
MNTB

Table 2.1: MGV$_s$ obtained for soma surface and soma interior in MNTB

Postnatal age	P0	P4	P8	P12	P60
N	20	20	20	20	20
MGV$_{group\ surface}$ ± SD	66 ± 9	62 ± 10	70 ± 13	90 ± 27	107 ± 27
MGV$_{group\ interior}$ ± SD	33 ± 7	37 ± 7	26 ± 4	38 ± 11	41 ± 14

2.2.2.2   MSO

In comparison to the MNTB at P0 and P4, here the cell bodies could be relatively easily outlined. The narrow vertical column of horizontally oriented bipolar neurons was clearly visible even in young animals **(Fig. 2.17A,B)**. In Figures 2.17A and 2.17B, cell bodies were marked with small arrows to point to the soma surface. The neuropil at these ages was diffusely stained, but already at P4, the signal started to become confined to soma surfaces and transversally cut dendrites appeared for the first time **(Fig. 2.17B)**. At P8 and P12, the soma surface staining was more defined and intensely stained, judged by eye. In the MSO, in contrast to the MNTB, a necklace-like labelling pattern of the soma surface was not observed, yet a continuous look throughout the development. At the same time the dendritic labelling became crisp and the signal confined to the membrane surface **(Fig. 2.17C,D)**. Dendrites cut along their length could be seen and distinguished from the rest neuropil as well as an increase in the number of transversally cut dendrites. The pattern of expression at P60 represented the situation at P12 aside from the appearance of many transversally cut dendrites and less amount of diffuse neuropil **(Fig. 2.17E)**.

The quantification of KCC2 immunofluorescent signal intensity in MSO soma surface between P0-P12 animals and between P12-P60 animals is shown in Figures 2.18A and 2.18B, respectively. The statistical analysis revealed a significant linear increase in the soma surface immunoreactivity from P0 to P12 (*p=0.04) and no significant difference of the signal between P12 and P60 (p=1). The MGV$_{group\ surface}$
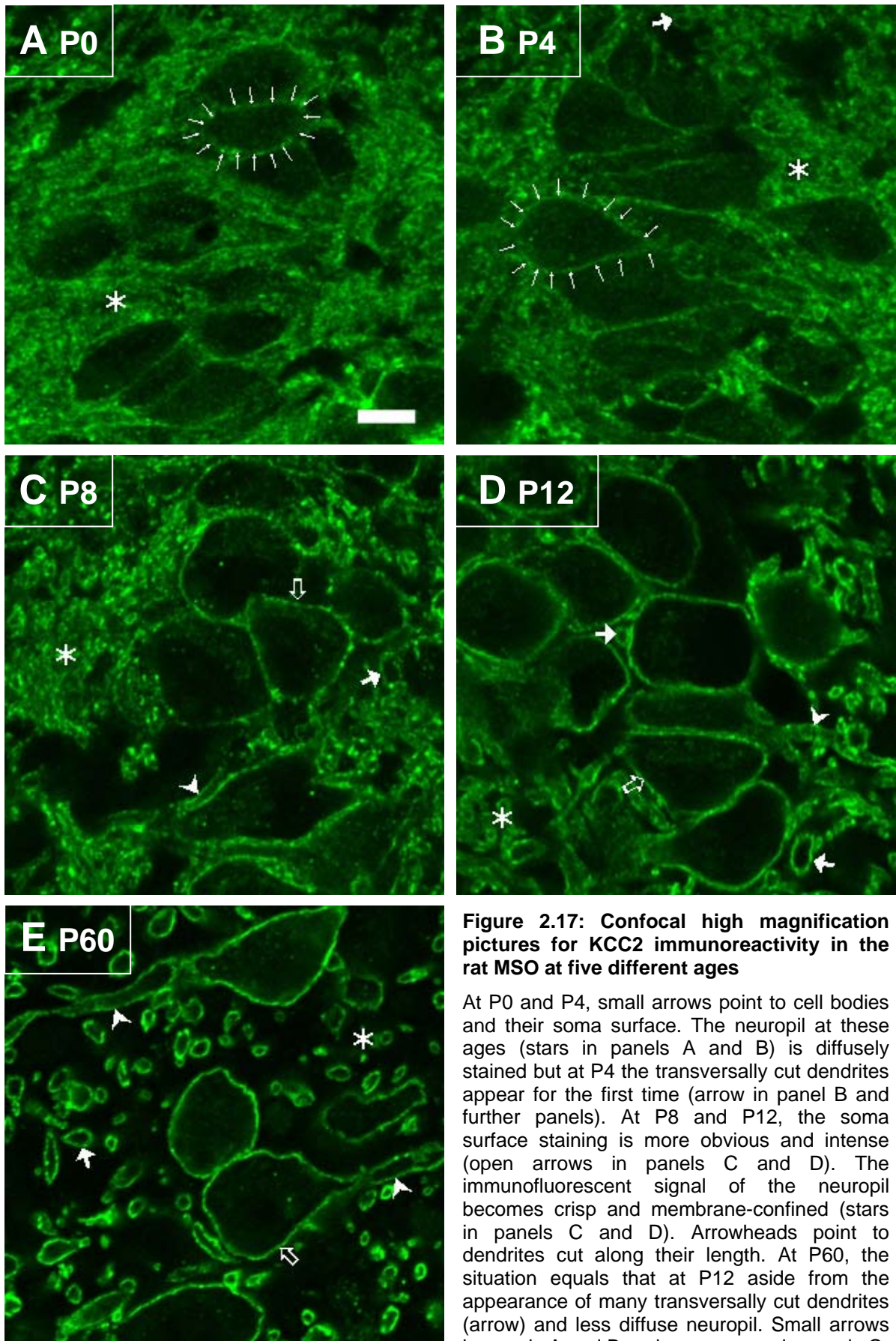
Figure 2.17: Confocal high magnification pictures for KCC2 immunoreactivity in the rat MSO at five different ages

At P0 and P4, small arrows point to cell bodies and their soma surface. The neuropil at these ages (stars in panels A and B) is diffusely stained but at P4 the transversally cut dendrites appear for the first time (arrow in panel B and further panels). At P8 and P12, the soma surface staining is more obvious and intense (open arrows in panels C and D). The immunofluorescent signal of the neuropil becomes crisp and membrane-confined (stars in panels C and D). Arrowheads point to dendrites cut along their length. At P60, the situation equals that at P12 aside from the appearance of many transversally cut dendrites (arrow) and less diffuse neuropil. Small arrows in panels A and B and open arrows in panels C-E indicate representative somata. Scale bar, 10 µm in all panels.

($\pm$SD) for each age-group is shown in Table 2.2. Scatter plots of $MGV_{soma\ interior}$ between P0-P12 animals and between P12-P60 animals are shown in Figures 2.18C and 2.18D, respectively. The statistical analysis showed an extremely significant linear decrease of the signal intensity from P0 to P12 (***p=5E-14) and no significant difference between P12 and P60 (p=0.4). The $MGV_{group\ interior}$ ($\pm$SD) for each age-group is shown in Table 2.2. Photomicrographs with the representative MSO cell bodies and the related histograms of AGV_s distribution for soma surface and soma interior are shown in Figure 2.18E.

In summary, the quantification analysis in the MSO showed that the adult values of immunoreactivity in both regions (soma surface and soma interior) were attained at P12.

Table 2.2: MGV_s obtained for soma surface and soma interior in MSO

Postnatal age	P0	P4	P8	P12	P60
N	20	20	20	20	20
$MGV_{group\ surface} \pm$ SD	82 ± 14	86 ± 18	95 ± 14	90 ± 20	90 ± 31
$MGV_{group\ interior} \pm$ SD	38 ± 5	41 ± 6	29 ± 4	25 ± 4	24 ± 7

Figure 2.18: Quantification of immunofluorescent signal in the MSO soma surface and soma interior during development

(A) and (B) Scatter plots of MGV_s in soma surface between P0-P12 animals and between P12-P60 animals, respectively. Statistical analysis shows a linear increase of soma surface immunofluorescent intensity from P0 to P12 (*p=0.04) and no significant difference between P12 and P60 (p=1).
(C) and (D) Scatter plots of MGV_s in soma interior between P0-P12 animals and between P12-P60 animals, respectively. Statistical analysis shows a linear decrease of the soma interior immunofluorescent intensity from P0 to P12 (***p=5E-14) and no significant difference between P12 and P60 (p=0.4).
(E) Photomicrographs of representative MSO cell bodies at different ages (first row) and the related histograms of AGV_s distribution for soma surface (second row) and soma interior (third row), respectively. The values of $MGV_{group\ surface}$ ($\pm$SD) and $MGV_{group\ interior}$ ($\pm$SD) for each age-group are shown in Table 2.2.
AGV_s, absolute gray values; MGV_s, mean gray values of a single cell body; $MGV_{group\ surface/interior}$, mean gray values of a group for soma surface and soma interior, respectively; SS, soma surface; SI, soma interior.

MSO

A — $p < 0.05$ — MGVs of soma surface vs. Postnatal age [day]

B — ns — MGVs of soma surface vs. Postnatal age [day]

C — $p < 0.001$ — MGVs of soma interior vs. Postnatal age [day]

D — ns — MGVs of soma interior vs. Postnatal age [day]

E — P0, P4, P8, P12, P60

SS
$MGV_{soma\ surface} = 83$ $MGV_{soma\ surface} = 88$ $MGV_{soma\ surface} = 99$ $MGV_{soma\ surface} = 104$ $MGV_{soma\ surface} = 106$

SI
$MGV_{soma\ interior} = 42$ $MGV_{soma\ interior} = 45$ $MGV_{soma\ interior} = 33$ $MGV_{soma\ interior} = 30$ $MGV_{soma\ interior} = 25$
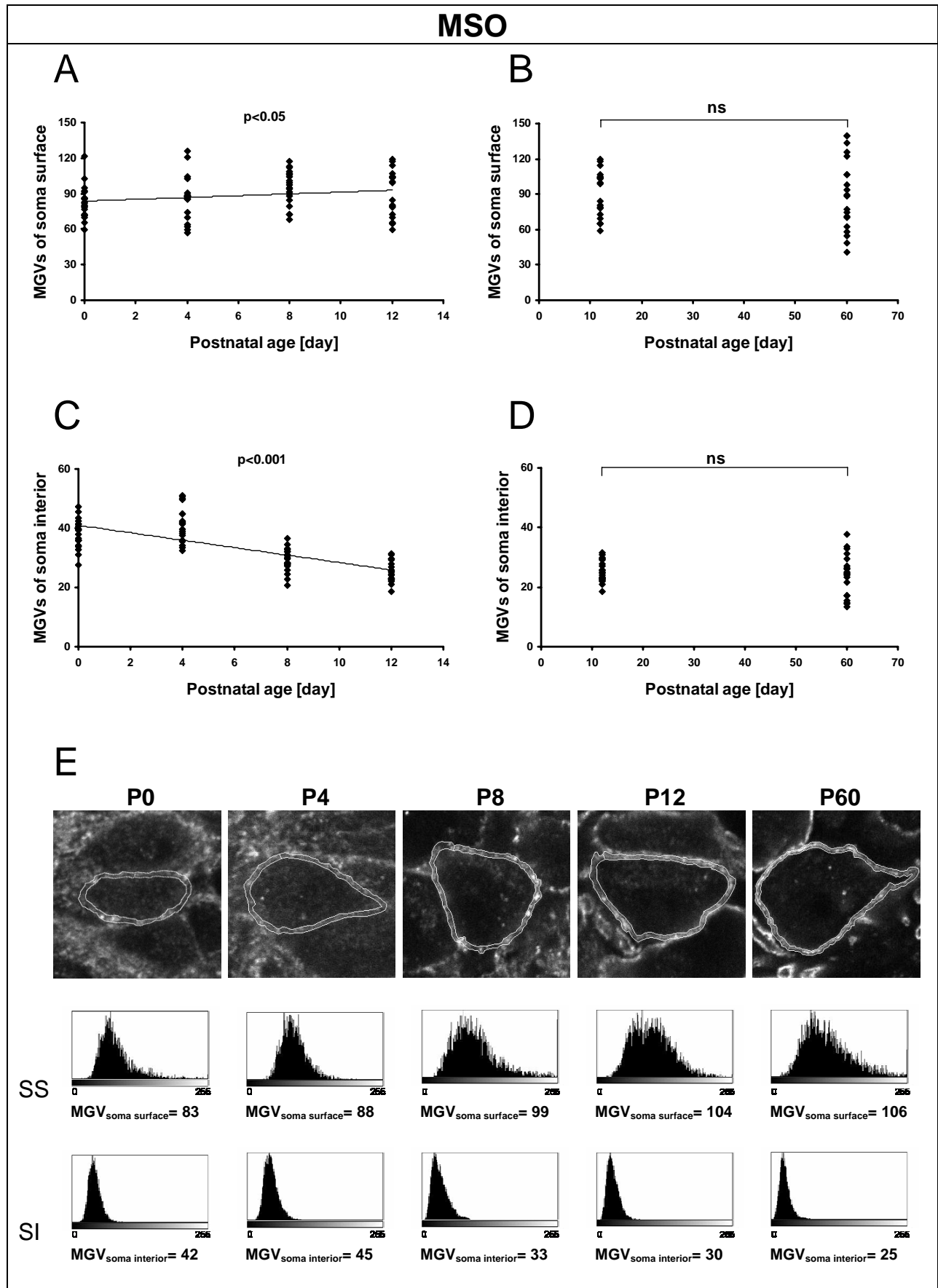
2.2.2.3   LSO

At P0 and P4, cell bodies of LSO neurons were easily distinguishable from the neuropil **(Fig. 2.19A,B)**. They appeared with moderate staining against the background of intensely stained neuropil, especially at P0, that tightly surrounded them. Close scrutiny at P0 revealed that the signal from the soma surface could not be distinguished from the signal originating from the multiple neuronal processes that coat the cell bodies at this age **(Fig. 2.19A)**. Considering this critical point, the data from the soma surface at P0 were not included into the quantitative analysis. The neuropil at P0 and P4 was diffusely stained, but at P4, the immunofluorescent signal started to become membrane-confined and transversally cut dendrites appeared for the first time as well as dendrites cut along their length **(Fig. 2.19B)**. At P8, the soma surface was stained intensely and the labelling of the neuropil became crisp and less diffuse **(Fig. 2.19C,D)**. "Hot spots" in the soma surface labelling were not observed, yet a continuous look throughout development. This developmental line continued until P12 with increasing signal intensity in the soma surface and the appearance of many transversally cut dendrites **(Fig. 2.19D)**. The expression pattern at P60 reflected the situation at P12 aside from the decreased number of immunopositive transversally cut dendrites. Due to this, in the overview picture at P60, it seemed that the KCC2 expression decreased in comparison to P12 **(Fig. 2.19E)**. In fact, only the neuropil intensity was decreased in P60 (for quantification see 2.2.2.5 Neuropil).

The quantification of immunofluorescent signal intensity in the LSO soma surface between P4-P12 animals and between P12-P60 animals is shown in Figures 2.20A and 2.20B, respectively. The statistical analysis revealed a very significant linear increase of the soma surface immunoreactivity from P4 to P12 (**p=0.003) and no significant difference of the signal between P12 and P60 (p=0.1). The $MGV_{group\ surface}$ (±SD) for each age-group is shown in Table 2.3. Scatter plots of $MGV_{soma\ interior}$ between P0-P12 animals and between P12-P60 animals are shown in Figures 2.20C and 2.20D, respectively. The statistical analysis showed an extremely significant linear decrease of the soma interior signal intensity from P0 to P12 (***p=7E-17) and no significant difference between P12 and P60 (p=0.06). The $MGV_{group\ interior}$ (±SD) for each age-group is shown in Table 2.3. Photomicrographs with the representative LSO cell bodies and the related histograms of AGV_s distribution for soma surface and soma interior are shown in Figure 2.20E.
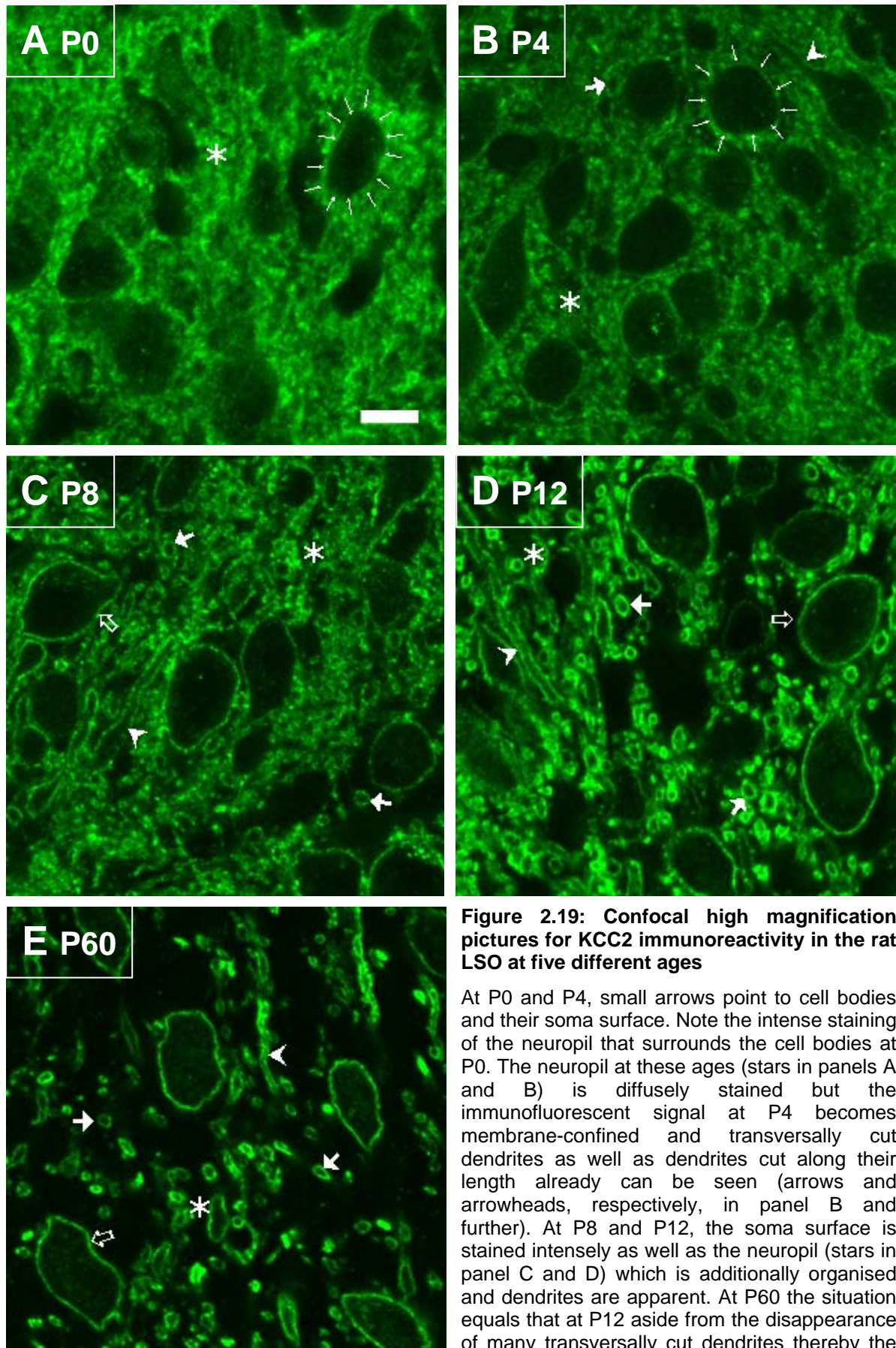
Figure 2.19: Confocal high magnification pictures for KCC2 immunoreactivity in the rat LSO at five different ages

At P0 and P4, small arrows point to cell bodies and their soma surface. Note the intense staining of the neuropil that surrounds the cell bodies at P0. The neuropil at these ages (stars in panels A and B) is diffusely stained but the immunofluorescent signal at P4 becomes membrane-confined and transversally cut dendrites as well as dendrites cut along their length already can be seen (arrows and arrowheads, respectively, in panel B and further). At P8 and P12, the soma surface is stained intensely as well as the neuropil (stars in panel C and D) which is additionally organised and dendrites are apparent. At P60 the situation equals that at P12 aside from the disappearance of many transversally cut dendrites thereby the neuropil appears less stained. Small arrows in panels A and B and open arrows in panels C-E indicate representative somata. Scale bar, 10 µm in all panels.

LSO

A

p<0.01

MGVs of soma surface

Postnatal age [day]

B

ns

MGVs of soma surface

Postnatal age [day]

C

p<0.001

MGVs of soma interior

Postnatal age [day]

D

ns

MGVs of soma interior

Postnatal age [day]

E

P0   P4   P8   P12   P60

SS

MGV$_{soma\ surface}$= 134   MGV$_{soma\ surface}$= 94   MGV$_{soma\ surface}$= 110   MGV$_{soma\ surface}$= 101   MGV$_{soma\ surface}$= 103

SI

MGV$_{soma\ interior}$= 51   MGV$_{soma\ interior}$= 40   MGV$_{soma\ interior}$= 35   MGV$_{soma\ interior}$= 37   MGV$_{soma\ interior}$= 31
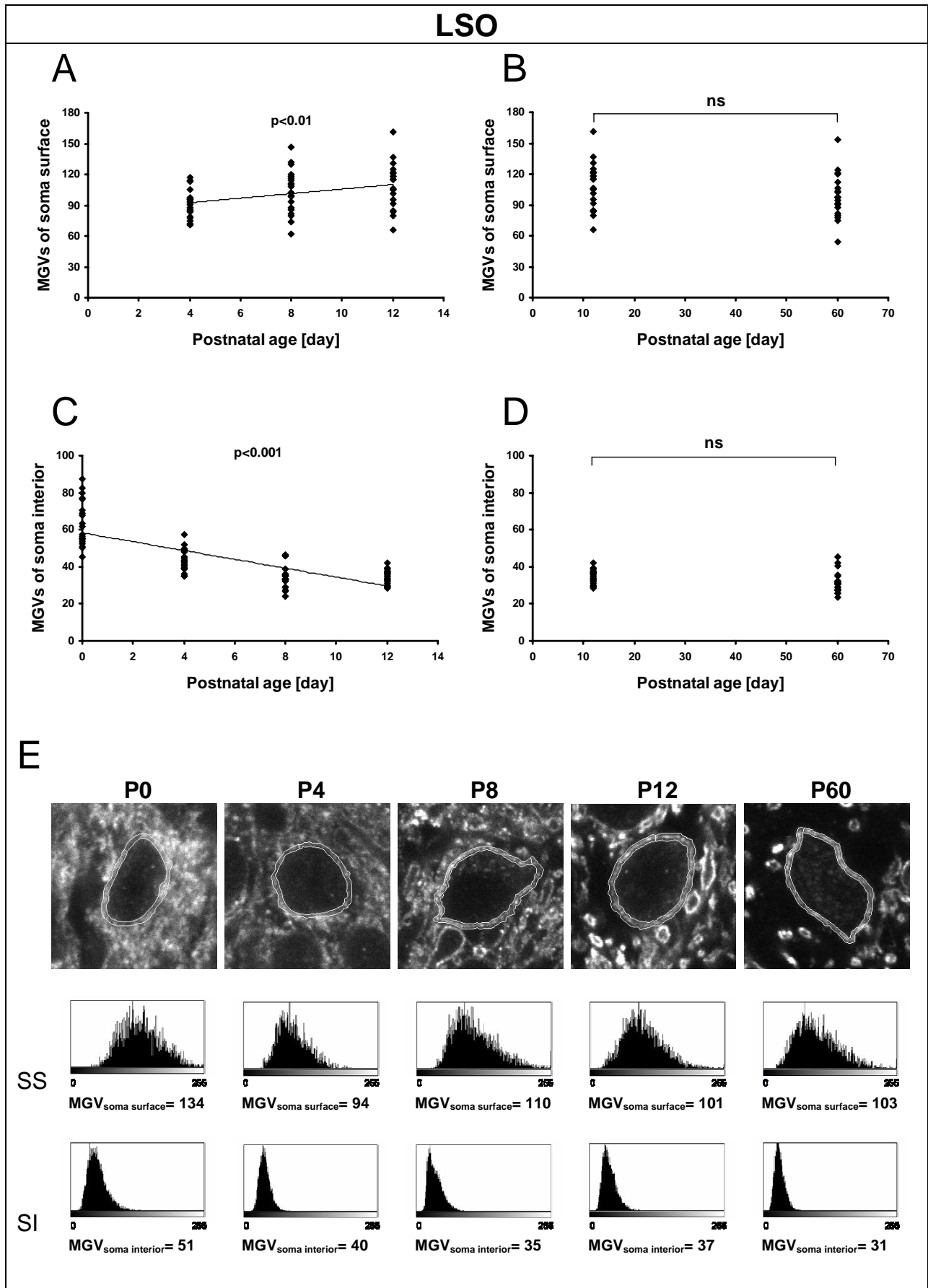
Table 2.3: MGV$_s$ obtained for soma surface and soma interior in LSO
*MGV$_{group\ surface}$ at P0 was very difficult to obtain. Therefore, the data were not included into quantification analysis.

Postnatal age	P0	P4	P8	P12	P60
N	20	20	20	20	20
MGV$_{group\ surface}$ ± SD	*135 ± 22	91 ± 14	103 ± 21	109 ± 22	98 ± 21
MGV$_{group\ interior}$ ± SD	63 ± 12	44 ± 6	34 ± 6	35 ± 4	32 ± 6

In summary, the quantification analysis in the LSO showed that the adult values of immunoreactivity in both regions (soma surface and soma interior) were attained at P12.

← *previous page*

Figure 2.20: Quantification of immunofluorescent signal in the LSO soma surface and soma interior during development

(A) and (B) Scatter plots of MGV$_s$ in soma surface between P4-P12 animals and between P12-P60 animals, respectively. Statistical analysis shows a linear increase of the soma surface immunofluorescent intensity from P4 to P12 (**p=0.003) and no significant difference of the signal between P12 and P60 animals (p=0.1).
(C) and (D) Scatter plots of MGV$_s$ in soma interior between P0-P12 animals and between P12-P60 animals, respectively. Statistical analysis shows a linear decrease of the soma interior immunofluorescent intensity from P0 to P12 (***p=7E-17) and no significant difference between P12 and P60 animals (p=0.06).
(E) Photomicrographs of representative LSO cell bodies at different ages (first row) and the related histograms of AGV$_s$ distribution for soma surface (second row) and soma interior (third row), respectively. The values of MGV$_{group\ surface}$ (±SD) and MGV$_{group\ interior}$ (±SD) for each age-group are shown in Table 2.3.
AGV$_s$, absolute gray values; MGV$_s$, mean gray values of a single cell body; MGV$_{group\ surface/interior}$, mean gray values of a group for soma surface and soma interior, respectively; SS, soma surface; SI, soma interior.

2.2.2.4   SPN

In contrast to the other three nuclei at P0, in the SPN, cell bodies and their soma surfaces were visible and discernible from the neuropil **(Fig. 2.21A)**. The neuropil was to some extent diffusely stained but, interestingly, all characteristic features mentioned in the other nuclei as being present in older animals (at P4 in MSO and LSO, at P12 in MNTB), here were manifested already at P0: both, transversally cut dendrites and dendrites cut along their length were labelled. The staining pattern at P4 reflected that seen at P0 with respect to soma surface and neuropil immunofluorescent signal **(Fig. 2.21B)**. At P8 and P12, the soma surface was intensely stained and the neuropil signal became crisp and membrane-confined to dendrites **(Fig. 2.21C,D)**. At P60, the pattern resembled that at P12 aside from the disappearance of many immunopositive transversally cut dendrites; thereby the neuropil seemed less stained **(Fig. 2.21E)**.

The quantification of immunofluorescent signals in soma surface between P0-P12 animals and between P12-P60 animals is shown in Figures 2.22A and 2.22B, respectively. Statistical analysis revealed an extremely significant linear increase of soma surface immunofluorescent signal intensity from P0 to P12 (***p=0.00005) as well as a significant increase from P12 to P60 (*p=0.03). The $MGV_{group\ surface}$ (±SD) for each age-group is shown in Table 2.4. Scatter plots of $MGV_{soma\ interior}$ between P0-P12 animals and between P12-P60 animals are shown in Figures 2.22C and 2.22D, respectively. Statistical analysis showed an extremely significant linear decrease of the soma interior immunofluorescent signal intensity from P0 to P12 (***p=0.0000004) and no significant difference between P12 and P60 (p=0.4). The $MGV_{group\ interior}$ (±SD) for each age-group is shown in Table 2.4. Photomicrographs with the representative SPN cell bodies and the related histograms of AGV_s distribution for soma surface and soma interior are shown in Figure 2.22E.

In summary, the quantification analysis in the SPN showed that the adult values of immunoreactivity in soma interior were attained at P12, whereas an additional increase in the KCC2 immunofluorescence occurred in the soma surface after P12.
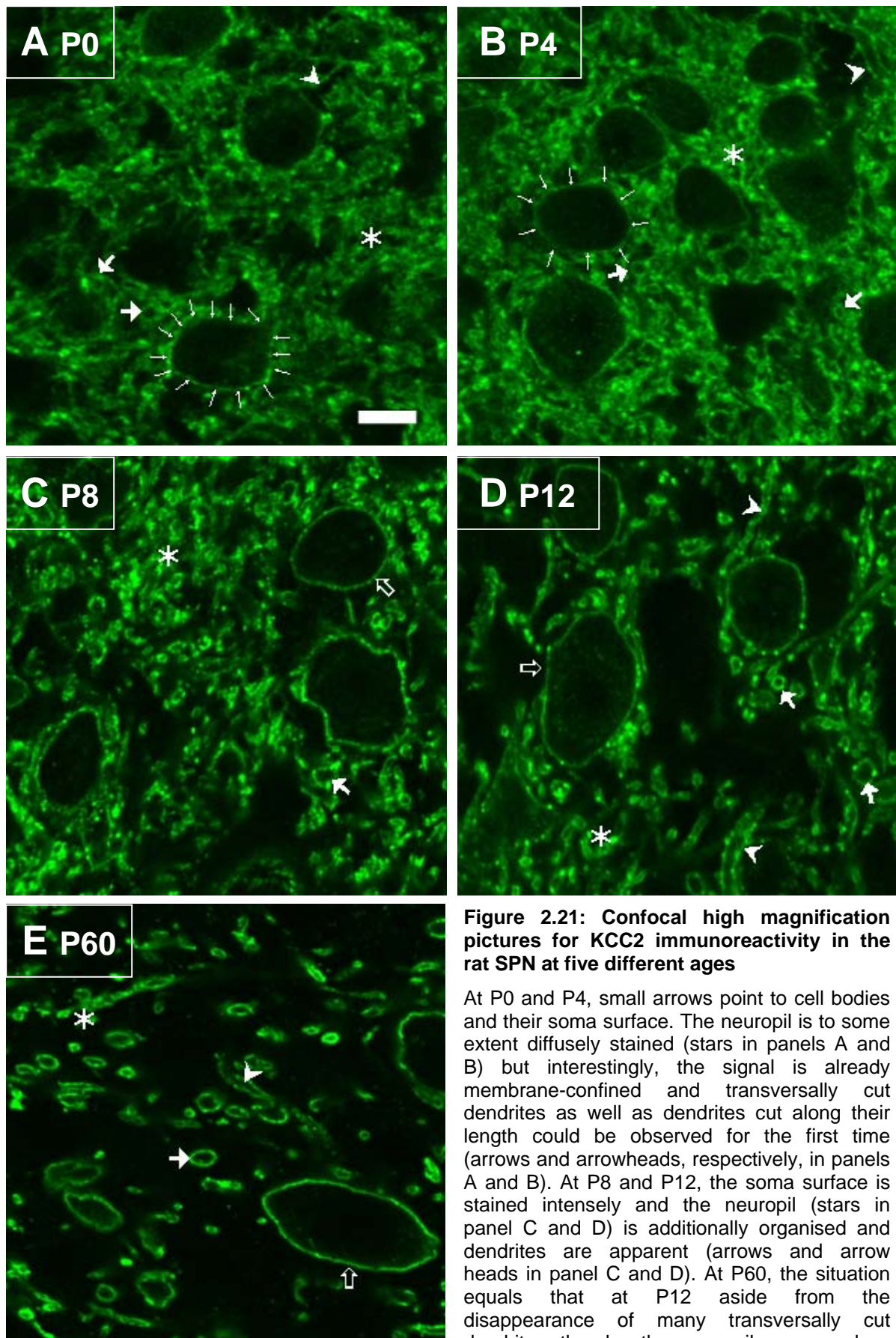
Figure 2.21: Confocal high magnification pictures for KCC2 immunoreactivity in the rat SPN at five different ages

At P0 and P4, small arrows point to cell bodies and their soma surface. The neuropil is to some extent diffusely stained (stars in panels A and B) but interestingly, the signal is already membrane-confined and transversally cut dendrites as well as dendrites cut along their length could be observed for the first time (arrows and arrowheads, respectively, in panels A and B). At P8 and P12, the soma surface is stained intensely and the neuropil (stars in panel C and D) is additionally organised and dendrites are apparent (arrows and arrow heads in panel C and D). At P60, the situation equals that at P12 aside from the disappearance of many transversally cut dendrites thereby the neuropil appears less stained. Small arrows in panels A and B and open arrows in panels C-E indicate representative somata. Scale bar, 10 µm in all panels.

SPN

A — $p < 0.001$ (MGVs of soma surface vs. Postnatal age [day])

B — $p < 0.05$ (MGVs of soma surface vs. Postnatal age [day])

C — $p < 0.001$ (MGVs of soma interior vs. Postnatal age [day])

D — ns (MGVs of soma interior vs. Postnatal age [day])

E

P0	P4	P8	P12	P60

SS

$MGV_{soma\ surface} = 83$ $MGV_{soma\ surface} = 81$ $MGV_{soma\ surface} = 85$ $MGV_{soma\ surface} = 96$ $MGV_{soma\ surface} = 114$

SI

$MGV_{soma\ interior} = 28$ $MGV_{soma\ interior} = 28$ $MGV_{soma\ interior} = 23$ $MGV_{soma\ interior} = 31$ $MGV_{soma\ interior} = 19$
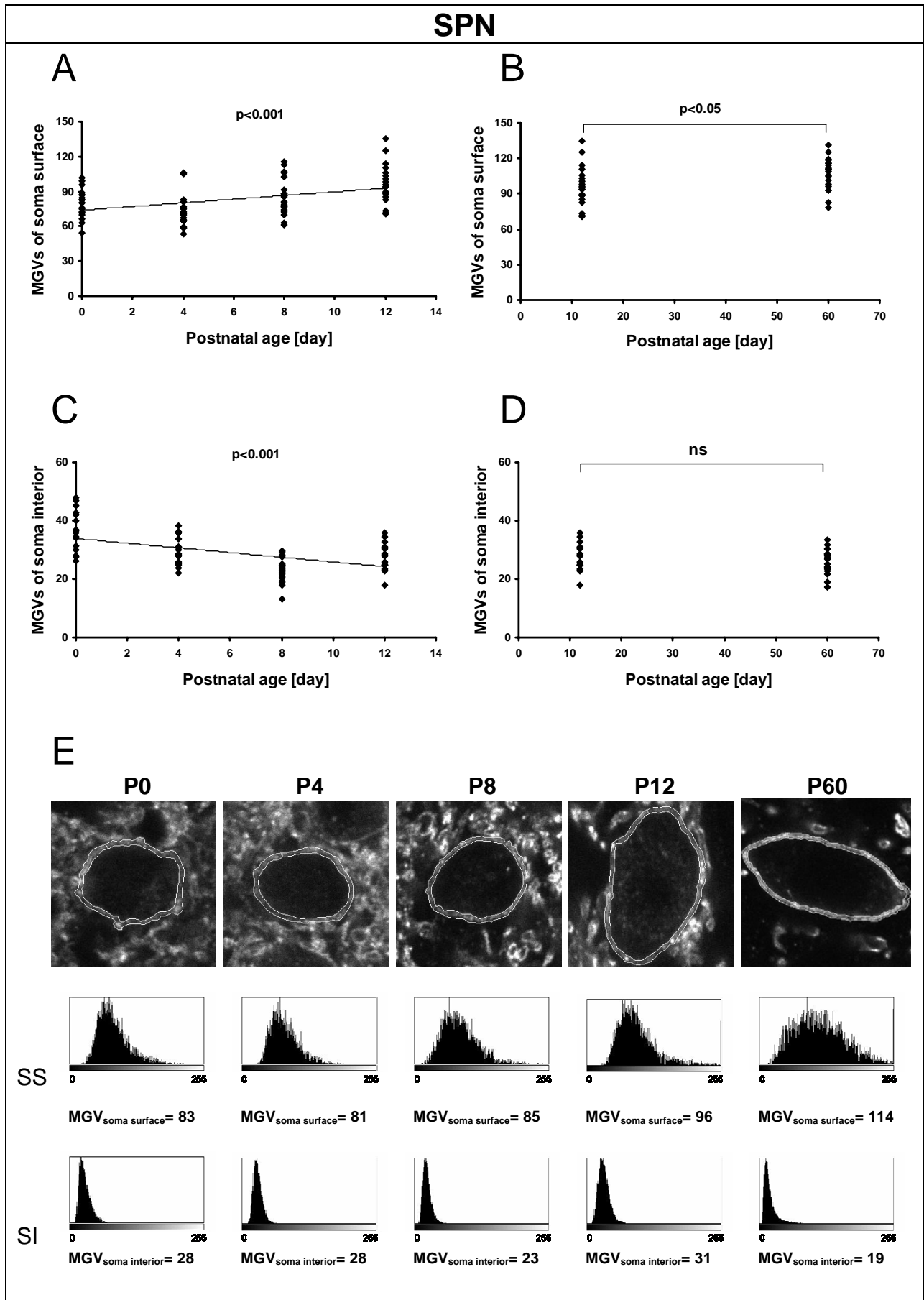
Table 2.4: MGV$_s$ obtained for soma surface and soma interior in SPN

Postnatal age	P0	P4	P8	P12	P60
N	20	20	20	20	20
MGV$_{group\ surface}$ ± SD	79 ± 12	72 ± 14	85 ± 16	96 ± 17	107 ± 14
MGV$_{group\ interior}$ ± SD	36 ± 7	30 ± 5	23 ± 4	28 ± 4	26 ± 4

2.2.2.5   Neuropil

The developmental changes of the neuropil have already been described briefly and qualitatively in the sections above. It became obvious that the most prominent change in the KCC2 immunolabelling pattern in the SOC nuclei occurred in the neuropil. Therefore, this region of interest was also quantified. The intensity of the neuropil was measured in cell body-free areas and the data were pooled from five consecutive optical slices (for details see 2.1.7 Data analysis and quantification).

For all four nuclei, the quantification of immunofluorescent signal intensity in the neuropil between P0-P12 animals displayed a linear decrease (MNTB: **Fig. 2.23A**; MSO: **Fig. 2.24A**; LSO: **Fig. 2.25A**; SPN: **Fig. 2.26A**), yet with different levels of significance. The statistical analysis also revealed a significant decrease of the signal between P12 and P60 animals in all nuclei (MNTB: **Fig. 2.23B**; MSO: **Fig. 2.24B**; LSO: **Fig. 2.25B**; SPN: **Fig. 2.26B**). The MGV$_{group\ neuropil}$ (±SD) for each age-group are shown in Table 2.5.

← *previous page*

Figure 2.22: Quantification of immunofluorescent signal in the SPN soma surface and soma interior during development

(A) and (B) Scatter plots of MGV$_s$ in soma surface between P0-P12 animals and between P12-P60 animals, respectively. Statistical analysis shows a linear increase of soma surface signal intensity from P0 to P12 (***p=0.00005) and significant difference between P12 and P60 animals (*p=0.03).
(C) and (D) Scatter plots of MGV$_s$ in soma interior between P0-P12 animals and between P12-P60 animals, respectively. Statistical analysis shows a linear decrease (***p=0.0000004) of soma interior signal intensity between P0 and P12 and no significant difference between P12 and P60 (p=0.4).
(E) Photomicrographs of representative MSO cell bodies at different ages (first row) and the related histograms of AGV$_s$ distribution for soma surface (second row) and soma interior (third row), respectively. The values of MGV$_{group\ surface}$ (±SD) and MGV$_{group\ interior}$ (±SD) for each age-group are shown in Table 2.4. AGV$_s$, absolute gray values; MGV$_s$, mean gray values of a single cell body; MGV$_{group\ surface/interior}$, mean gray values of a group for soma surface and soma interior, respectively; SS, soma surface; SI, soma interior.
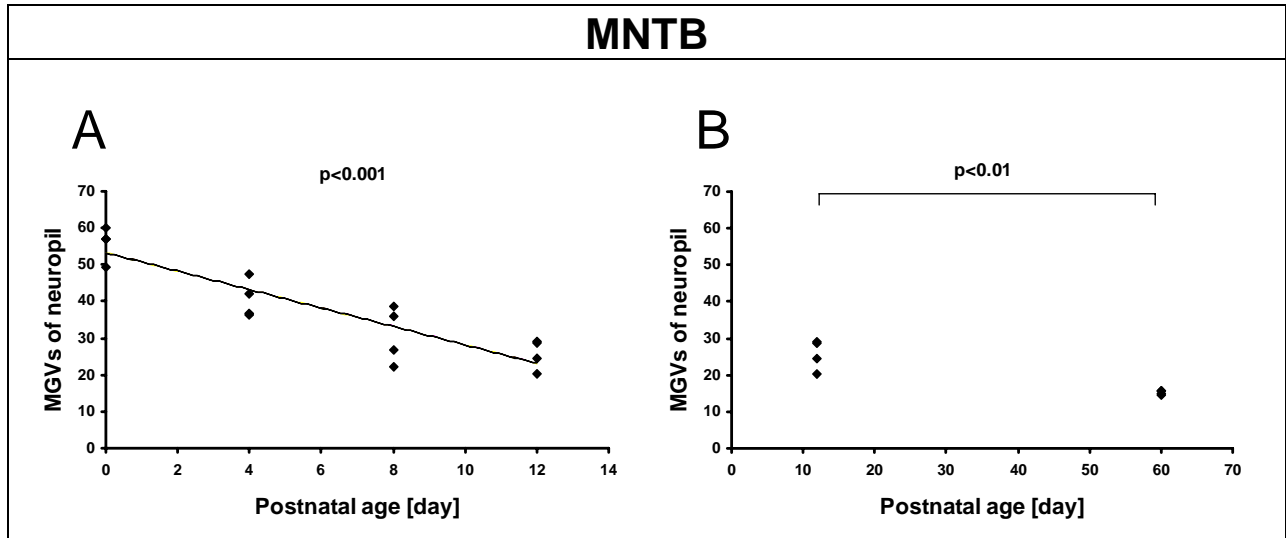
Figure 2.23: Quantification of immunofluorescent signal in the MNTB neuropil during development

(A) and (B) Scatter plots of MGV_s in neuropil between P0-P12 animals and between P12-P60 animals, respectively. Statistical analysis shows a linear decrease of neuropil immunofluorescent signal intensity from P0 to P12 (***p=0.000001) and a significant difference between P12 and P60 animals (**p=0.003). The $MGV_{group\ neuropil}$ (±SD) for each age-group are shown in Table 2.5.
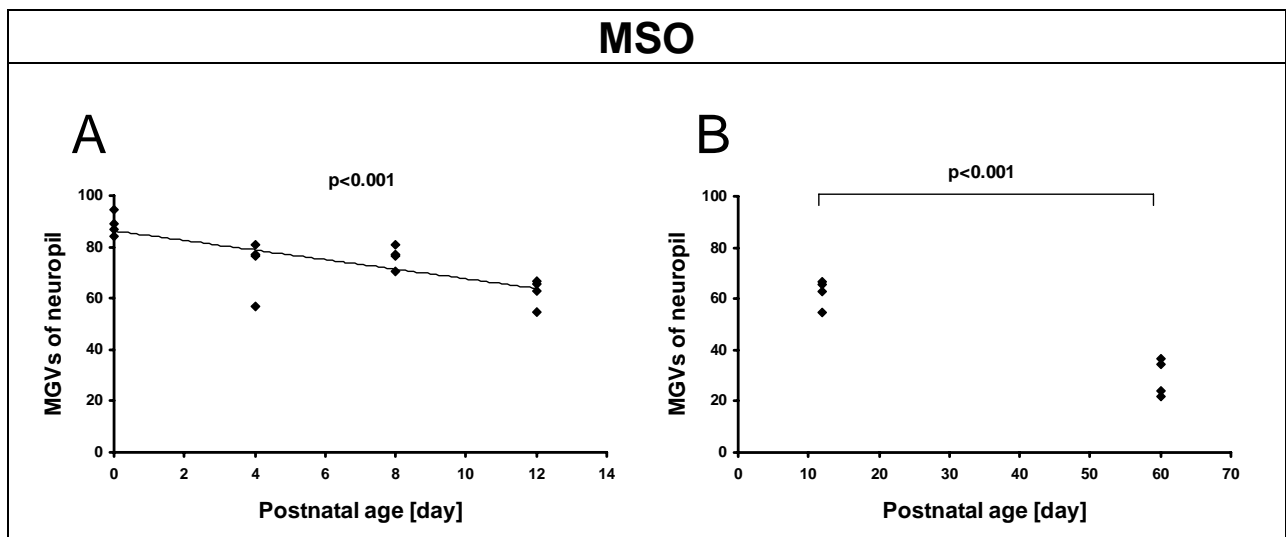
Figure 2.24: Quantification of immunofluorescent signal in the MSO neuropil during development

(A) and (B) Scatter plots of MGV_s in neuropil between P0-P12 animals and between P12-P60 animals, respectively. Statistical analysis shows a linear decrease of neuropil immunofluorescent signal intensity from P0 to P12 (***p=0.0003) and a significant difference between P12 and P60 animals (***p=0.00008). The $MGV_{group\ neuropil}$ (±SD) for each age-group are shown in Table 2.5.
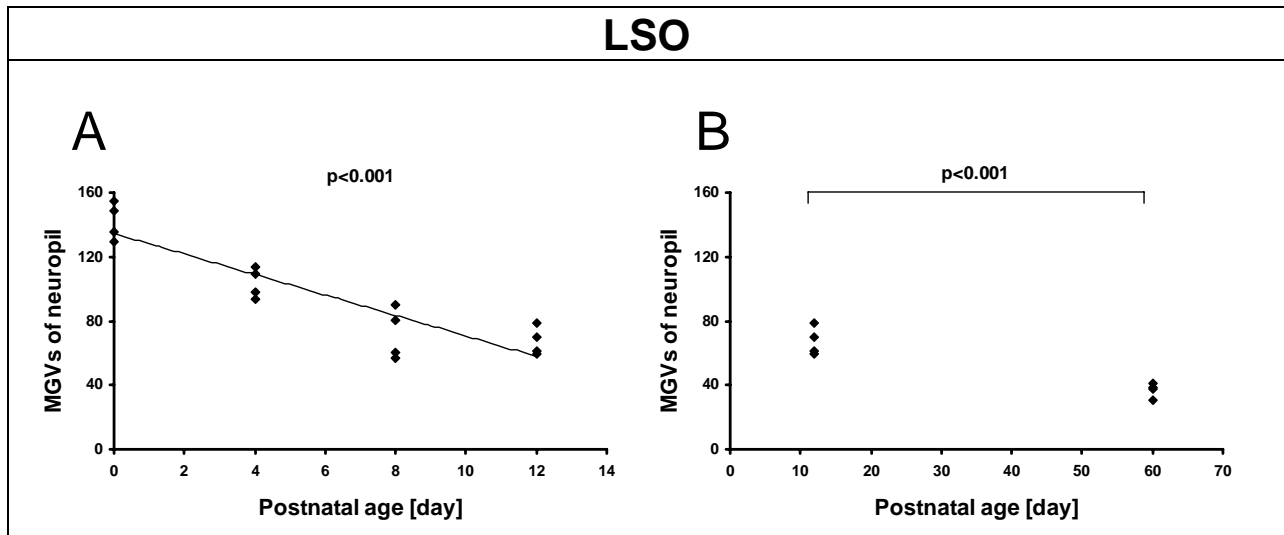
Figure 2.25: Quantification of immunofluorescent signal in the LSO neuropil during development

(A) and (B) Scatter plots of MGV_s in neuropil between P0-P12 animals and between P12-P60 animals, respectively. Statistical analysis shows a linear decrease of neuropil immunofluorescent signal intensity from P0 to P12 (***p=0.0000008) and a significant difference between P12 and P60 animals (***p=0.00096).
The $MGV_{group\ neuropil}$ (±SD) for each age-group are shown in Table 2.5.
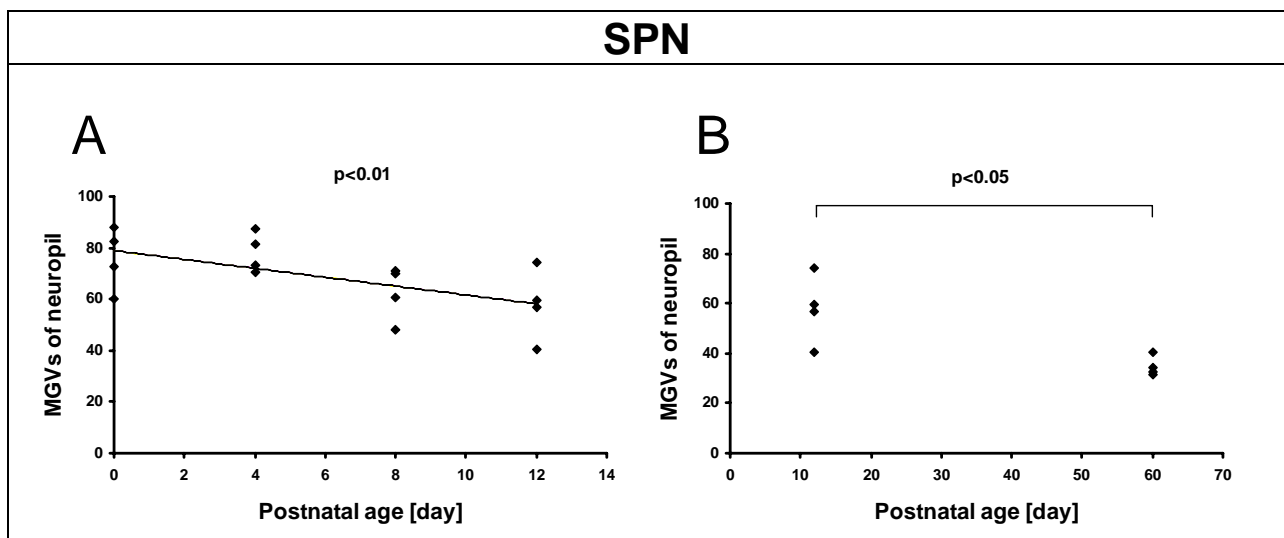
Figure 2.26: Quantification of immunofluorescent signal in the SPN neuropil during development

(A) and (B) Scatter plots of MGV_s in neuropil between P0-P12 animals and between P12-P60 animals, respectively. Statistical analysis shows a linear decrease of neuropil immunofluorescent signal intensity from P0 to P12 (**p=0.007) and a significant difference between P12 and P60 animals (*p=0.02).
The $MGV_{group\ neuropil}$ (±SD) for each age-group are shown in Table 2.5.

Table 2.5: MGV$_s$ obtained for neuropil in four different nuclei

Postnatal age MGV $_{group\ neuropil}$ ± SD	P0	P4	P8	P12	P60
MNTB	56 ± 5	41 ± 5	31 ± 8	26 ± 4	15 ± 1
MSO	89 ± 4	73 ± 11	76 ± 4	62 ± 5	29 ± 7
LSO	142 ± 12	104 ± 9	72 ± 16	67 ± 9	37 ± 4
SPN	76 ± 12	78 ± 8	63 ± 10	58 ± 14	35 ± 4
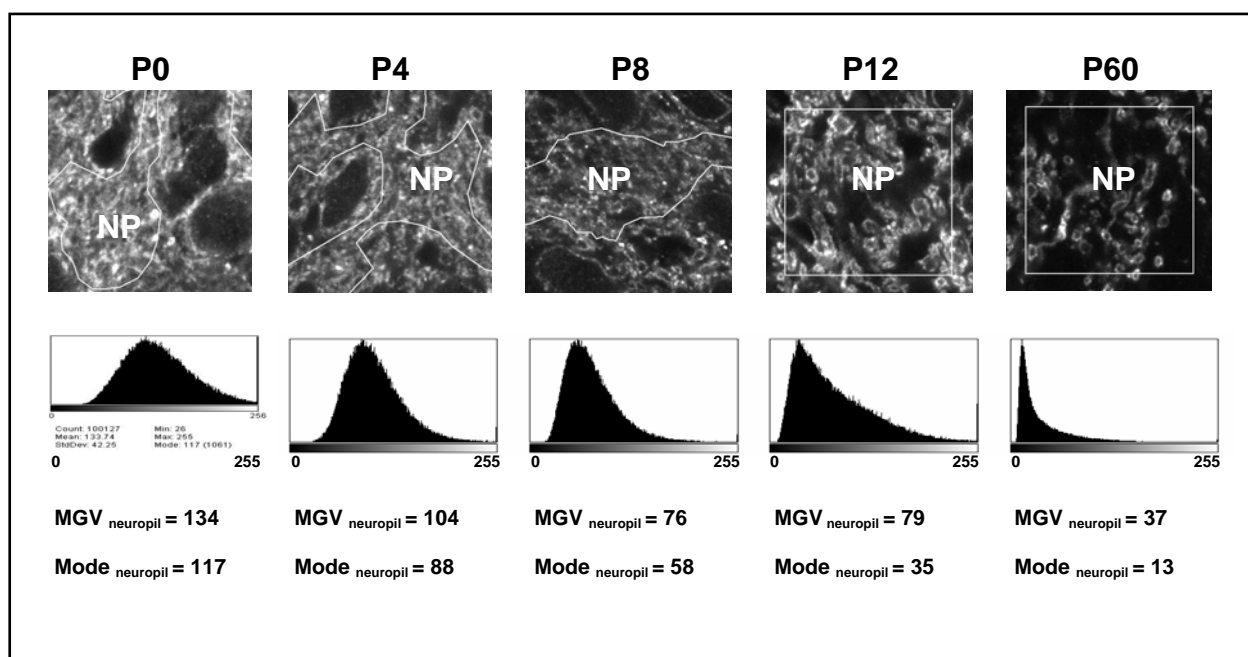
Figure 2.27: Photomicrographs of representative LSO neuropil areas (first line) and the related histograms of AGV$_s$ distribution (second line)

In this representative example, MGV of the selected neuropil was close to the MGV$_{group\ neuropil}$. The MGV$_{group\ neuropil}$ (±SD) for each age-group are shown in Table 2.5. Mode $_{neuropil}$ corresponds to the highest peak in the histogram that is moved from higher gray values (white) in young animals to lower gray values (black) in adult.

AGV$_s$, absolute gray values; NP, neuropil; MGV $_{neuropil}$, mean gray value of neuropil; Mode $_{neuropil}$, modal gray value.

In Figure 2.27, representative photomicrographs of the LSO neuropil and the related histograms of AGV_s distribution are shown. In addition to the $MGV_{neuropil}$ that decreases during development **(Fig. 2.25)**, modal gray values of the neuropil (Mode $_{neuropil}$) are also shown. Mode $_{neuropil}$ is the most frequently occurring gray value within the selection and in the case of a heterogeneous region, as the neuropil, it was also reasonable and meaningful to show the modal gray values. Mode $_{neuropil}$ corresponds to the highest peak in the histograms. It changed from high gray values (white) in young animals (Mode $_{neuropil}$ =115 at P0) to low gray values (black) in adult (Mode $_{neuropil}$ =15 at P60). Equivalent micrographs and histograms from the neuropil in the other SOC nuclei are not shown because the situation equalled that in the LSO neuropil. A specific pattern was present in the MNTB where the neuropil developed to areas almost devoid of signal (Mode $_{neuropil}$ = 44 at P0; Mode $_{neuropil}$ = 9 at P60).

In summary, the quantification analysis in the SOC nuclei showed that the immunoreactivity in the neuropil decreased with age and attained adult values at P60, yet two stages in developing pattern of KCC2 immunoreactivity were noticed: from P0 to P12, the immunoreactivity developed from a diffuse signal to a membrane-confined pattern. Moreover, labelling of dendrites became apparent. At P60, the situation equalled that at P12 except that disappeared many transversally cut dendrites, although the remaining KCC2-stained dendrites became thicker and the signal became stronger, judged by eye. Thus, qualitative and quantitative changes occurred until P12. After P12, the changes were only of quantitative nature.

2.3   Discussion

2.3.1   Presence of KCC2 protein already at birth

Chapter 2 of the present study demonstrates that KCC2 protein in the rat brain stem auditory nuclei is present already at birth (P0). In a previous investigation, using *in situ* hybridization, single-cell RT-PCR, and Western blot analysis, Balakrishnan et al. (2003) showed that the KCC2 mRNA and the protein in the SOC are expressed during both the depolarizing (P3) and hyperpolarizing period (P12) of GABA/glycine signalling. In contrast, in the other regions investigated so far (hippocampus, cerebellum, neocortex, and retina), it was shown that the expression of KCC2 on both the transcriptional and the translational level is up-regulated postnatally (hippocampus: Rivera et al., 1999; Gulyás et al., 2001; Balakrishnan et al., 2003; cerebellum: Lu et al., 1999; neocortex: Clayton et al., 1998; DeFazio et al., 2000; 1999; retina: Vu et al., 2000). In the mouse brain stem and the spinal cord, KCC2 protein was found as early as E15.5 (Stein et al., 2004). However, hippocampal expression in the same species was observed not earlier than postnatally (Stein et al., 2004). Protein levels in the spinal cord and brain stem were established at birth, but in the hippocampus, cerebellum, and cortex around the end of the second postnatal week (Stein et al., 2004). Together with this, the switch from depolarization to hyperpolarization of GABA and glycine in the spinal cord takes place before birth (Hübner et al., 2001), in the brain stem ranging from a prenatal change (in the SPN, Srinivasan et al., 2004a) to a change after the second postnatal week (in the MNTB: Awatramani et al., 2004; Srinivasan et al., 2004a), in the hippocampus during the second postnatal week (Ben-Ari et al., 1989; Zhang et al., 1990; Cherubini et al., 1991). Thus, a striking difference in KCC2 development between the SOC nuclei and higher brain regions was found concerning the correlation of the KCC2 mRNA and protein with changes in the polarity of GABA/glycinergic responses. Therefore, if there is up-regulation of KCC2 protein in the brain stem, it should occur before birth. This is also together with the notion that the maturation of KCC2 expression (mRNA as well as protein) follows a caudal-to-rostral axis (i.e. caudal parts develop earlier than rostral ones, Alvarez-Bolado and Swanson, 1996): the KCC2 expression starts earlier in phylogenetically older parts of the neuraxis (Clayton et al., 1998; Williams et al., 1999). A similar KCC2 expression pattern in humans, with the early up-regulation in the older parts, like spinal cord and brain stem, might explain why

GABA$_A$ receptor agonists are useful in neonatal brain stem epilepsy but work for epilepsy involving the rostral part of the CNS only later in life. In contrast to Balakrishnan et al. (2003), a recent study using single-cell RT-PCR showed that only two of seven LSO neurons from P0-P3 rats expressed KCC2 (Shibata et al., 2004). However, no explanation for this discrepancy was given, yet it was suggested that KCC2 mRNA levels are too low to be detected in many neonatal LSO neurons. In an early study, it was predicted that the expression of KCC2 at birth can vary between adjacent neurons due to the intrinsic heterogeneity present among immature neurons (Ben-Ari, 2002).

It was surprising to find a disagreement between the absence of KCC2 protein change, reported in the rat brain stem during postnatal development (Balakrishnan et al., 2003) and looking at low magnification pictures. From my results, it appears that KCC2 protein decreases from P0 to P60 in the brain stem nuclei. A closer look and quantification analysis, however, showed that this was the case only for the neuropil. The application of an independent technique, as Western blot analysis, with tissue from MNTB, MSO, LSO, and SPN at different postnatal ages, incubated with the same anti-KCC2 antiserum, will allow a comparison of the total amount of KCC2 protein in each nucleus during development as well as between the nuclei.

In the current investigation, differences in the intensities of KCC2 immunofluorescent signal between the nuclei became apparent: the SPN and the LSO had the strongest immunoreactivity among the nuclei, the MNTB had the weakest signal, and the MSO had a moderate one. This diversity, however, was evaluated only by eye. A comparison of the absolute immunofluorescent intensities between the nuclei from high magnification images cannot be performed due to different confocal settings for each nucleus.

2.3.2 Differences in the intensities of KCC2 immunofluorescence between the nuclei

The low magnification pictures were taken at the same confocal settings and this enabled a direct comparison of the fluorescent signal among the nuclei. The main difference was found between the MNTB that remained weakly labelled throughout the investigated period and the other three nuclei, which showed moderate (MSO) to heavy

(SPN, LSO) immunoreactivity. Stein and co-workers (2004), demonstrated by *in situ* hybridization and Western blot that the time course of protein expression closely parallels the detection of KCC2 transcripts. Moreover, it was found that the MNTB neurons express KCC2 mRNA at lower levels at P3 and at P12 in comparison to MSO, LSO, and SPN (Balakrishnan et al., 2003). One possible explanation for the lower KCC2 expression in the MNTB is the source of inhibition in this nucleus. In contrast to the other three nuclei, the primary inhibitory input, which MNTB neurons receive, comes from recurrent collaterals of their own axons (Guinan and Li, 1990; Kuwabara and Zook, 1991; Sommer et al., 1993; Smith et al., 1998; review: Thompson and Schofield, 2000). Additionally, the MNTB receives inhibitory input from neurons in the ventral nucleus of the trapezoid body (Ostapoff et al., 1997) and the SPN (Helfert et al., 1989). In fact, the MNTB is very often viewed as a relay station, providing inhibitory input from the contralateral CN to the ipsilateral MSO, LSO, and SPN (Sommer et al., 1993) and the presence of inhibition onto MNTB neurons was often omitted. Only recently, it was proposed that excitatory transmission in the MNTB might be subject to inhibition, strong enough to offset the massive excitatory input from the calyx of Held (Kopp-Scheinpflug et al., 2003). In addition, an optical imaging study with voltage-sensitive dyes showed that the switch from depolarization to hyperpolarization of GABA and glycine in the MNTB does not occur until P10 (Srinivasan et al., 2004a). The inhibition becomes profound in its magnitude and kinetics only after P20 (Awatramani et al., 2004).

It was hypothesized that KCC2 is important for postsynaptic inhibition (Williams et. al., 1999), and different studies showed that KCC2 was highly colocalized with $GABA_A$ and glycine receptor (GlyR) subunits: in the rat cerebellum granular cell layer, KCC2 was colocalized with $GABA_A$ receptor $\beta 2/\beta 3$ subunits at synaptic and extrasynaptic sites (Williams et al., 1999); in the rat hippocampus, KCC2 was found in the vicinity of excitatory synapses, perhaps again in close association with extrasynaptic $GABA_A$ receptors (Gulyás et al., 2001); in the mouse spinal cord, KCC2 was shown to be predominantly, but not exclusively, colocalized with gephyrin (Hübner et al., 2001), a postsynaptic protein involved in the clustering of glycine and $GABA_A$ receptors (Kneussel and Betz, 2000). In the brain stem nuclei, a colocalization study for GABA or glycine receptor subunits and KCC2 is missing. However, anatomical studies suggest that among the SOC nuclei, the adult-type glycine receptor $\alpha 1$ subunit mRNA accumulates slower in the MNTB and does not peak before the third week after birth

(Piechotta et al., 2001). The density of GlyR α1 immunoreactive puncta in the MNTB was also much lower, resulting in a scattered, rather than a ring-like, appearance and was restricted to the somata and not associated with the proximal dendrites or the neuropil, in contrast to the other three SOC nuclei (Friauf et al., 1997). Inhibitory GABAergic boutons on the somata of MNTB neurons have been demonstrated by immunocytochemical labelling (Roberts and Ribak, 1987; Adams and Mugnaini, 1990), originating from neurons in the ventral nucleus of trapezoid body (Ostapoff et al., 1997) or in the SPN (Helfert et al. 1989).

In summary, less KCC2 mRNA in the MNTB together with anatomical and physiological data for the delay in development of inhibitory machinery in this nucleus can explain the barely visible KCC2 labelling during the investigated period. Moreover, since the MNTB provides well-timed inhibition to the other main nuclei in the SOC, the glycinergic modulation of MNTB activity could have profound consequences in the sound localization after hearing onset.

2.3.3   Early presence of KCC2 in the soma surface

A recent study from our laboratory investigated the temporal expression of KCC2 and showed the presence of the protein throughout postnatal development, yet the protein becomes functional only at P12 (Balakrishnan et al., 2003). As a possible reason for this discrepancy, a subcellular redistribution of KCC2 was proposed and a later incorporation of the protein in the membrane, consistent with transporter functionality and the shift in GABA/glycine responses.

In adult rat (older than P15) hippocampal interneuronal somata, immunogold and DAB techniques showed no association of KCC2 with the Golgi apparatus or the endoplasmic reticulum, but immunogold particles were found frequently on the membranes of transport vesicles inside the dendrites very early in development (P2) (Gulyás et al., 2001). It was hypothesized that this is an indication of a rapid transfer of the synthesized protein to the plasma membrane or masking of the C terminus epitopes in the endoplasmic reticulum. Thus, it was not surprising that KCC2 immunoreactivity in the auditory brain stem nuclei was present very early in the region of the plasma membrane, whereas a colocalization within the biosynthetic secretory pathway was not found during the first 2 postnatal weeks (Blaesse et al., 2004). This correlates also with

the earlier prenatal appearance of KCC2 in the brain stem (Hübner et al., 2001; Stein et al., 2004) in comparison to the hippocampus.

In a high-resolution study in the rat hippocampus, a diffuse KCC2 immunolabelling and an association with the plasma membrane of distal dendrites as well as with the membranes of transport vesicles inside the dendrites was frequently observed at P0-P2 by electron microscopy (Gulyás et al., 2001). At P4, the number of KCC2-immunoreactive transport vesicles was gradually decreased and most of the reaction products were observed on the cytoplasmic surface of the plasma membrane. Therefore, considering the earlier development of KCC2 expression in the brain stem than in the hippocampus, it is likely that the signal from the neuronal somata in the brain stem nuclei at birth was from the plasma membrane.

A critical point in the present study was the insufficient resolution of the confocal microscope and the lack of membrane markers to really show the presence of KCC2 in the soma and dendrite plasma membranes. A similar phenomenon, how far one can rely on the resolution given from confocal microscopy regarding biological processes, has been seen in a colocalization study where kidney cells were stained for the Na^+-dependent potassium chloride cotransporter NKCC2 (Gimenez and Forbush, 2003). Only electron microscopy resolution has been able to discriminate between the amount of NKCC2 found within 0.10 µm from the cell membrane before (40.1% of the NKCC2 molecules) and after (62.0% of the NKCC2 molecules) vasopressin treatment. The change represented a 1.55-fold increase in the number of NKCC2 transporters available at the membrane for solute transport. In confocal pictures, this redistribution of the transporter in close vicinity to the apical membrane remained overlooked. Considering this remark, I used the term "soma surface" to describe the presence of KCC2 in the region of the plasma membrane.

A result from the present study was the early presence, already at birth, of KCC2 immunoreactivity in the soma surface in all auditory brain stem nuclei investigated. However, due to reasons mentioned above, the possibility remains that KCC2 is close to, but not within, the plasma membrane. Another possibility could be that it is in the plasma membrane but not functional, or functional but not powerful enough to change the polarity of GABA/glycine signalling (the SPN is an exception). Thus, the change from depolarizing to hyperpolarizing GABA/glycine activity occurs after the KCC2 protein is localized for some time in the soma surface. This indicates that functionality is

not merely determined by the incorporation of the protein into the plasma membrane. Considering the present study, however, it seems that at least partly the KCC2 expression in the rat brain stem between P0-P12 developed through an increasing signal in the soma surface and this was observed in all auditory nuclei. In addition, this result demonstrated that it is unlikely that the presence of glial cells interferes with the penetration of the antibodies in older animals.

2.3.4   An increase of KCC2 immunofluorescence in the soma surface during development

The increase of KCC2 signal in the soma surface was statistically significant in all nuclei between P0 and P12. No changes in the KCC2 intensities in this region were found later on, i.e. the adult values were attained by P12. One exception was found in the SPN. In this nucleus, the increase in the soma surface KCC2 signal appeared significant between P12 and P60. Note that among the nuclei in the SOC, the SPN displays the earliest shift in the polarity of GABA/glycine-evoked responses, i.e. before birth (Srinivasan et al., 2004a). However, the functional implications of the early inhibitory synapse maturation in this nucleus and the extended period of increase in KCC2 soma surface signal intensity are not known. In an optical imaging study with voltage-sensitive dyes, it was speculated that the maturation of one nucleus in the brain stem may influence the others (Srinivasan et al., 2004a).

Nevertheless, looking at Table 2.6, the increase in the soma surface immunoreactivity among the nuclei ranged from 1.1 to 1.6-fold, i.e. it was negligible in comparison to the change in the neuropil signal intensity (2.2 to 3.8-fold), which decreases with age. Thus, I conclude that a small increase in the soma surface KCC2 immunofluorescence intensity (recruitment of the protein) during the first two postnatal weeks is only of minor importance and does not explain the change in KCC2 functionality: in the MNTB after P20 (Awatramani et al., 2004); in the MSO at P5, in the LSO between P4 and P6, in the SPN between E18 and E20 (Srinivasan et al., 2004a).

2.3.5   Transient appearance of KCC2 immunofluorescent puncta in soma surface of the MNTB neurons

Interestingly, at P8 and P12, the pattern of the signal from the soma surface in the MNTB showed "hot spots" (puncta). A possible explanation was found considering the predominant colocalization of KCC2 with inhibitory (GABA$_A$) postsynaptic receptors (Williams et al., 1999, Gulyás et al., 2001, Hübner et al., 2001). Moreover, in the SOC there is an early developmental stage at which inhibitory receptors (GlyRs) are diffusely distributed and focal clusters on the neuronal surfaces are formed only subsequently during the first postnatal week (Friauf et al., 1997). However, in the MNTB, the labelling pattern differed from that in the other SOC nuclei in the lower density of GlyR puncta, resulting in a scattered, rather than a ring-like appearance (Friauf et al., 1997). Thus, if KCC2 is colocalized with GlyR, it will also appear as "hot spots" on the MNTB soma surface. This punctate profile for both inhibitory receptors and KCC2 coincided with the period of still missing or weak inhibition in the MNTB (Awatramani et al., 2004, Srinivasan et. al., 2004a). The maturation of inhibitory synapses (after P20) correlated with the time when the punctate pattern of soma surface disappeared, yet a continuous uniform appearance was common. Similar observations of punctate KCC2 signal were made in primary retinal cultured neurons (Williams et al., 1999). In these retinal cultures, KCC2 protein exhibited a distinctly punctate distribution at the plasma membrane of amacrine cell somata and dendrites, and the highest expression was observed in regions where cells contacted each other, consistent with the idea that KCC2 is localized predominantly at synapses. In the same study, in slices of rat cerebellum it was shown that much of the KCC2 immunostaining in the molecular layer was punctate, indicating that KCC2 may localize at specific sites along the numerous dendrites that occur in this region, especially from Purkinje cells. Also KCC2 immunoreactivity was distributed in a punctate manner in the retinal middle stratum layer (Vardi et al., 2000) and inner plexiform layer (Vu et al., 2000) and this pattern also resembled staining for clusters of GABA$_A$ and glycine receptors (Vardi et al., 1992; Sassoé-Pognetto et al., 1994; Koulen et al., 1996). Nevertheless, an open question remains why only in the MNTB punctate labelling was observed. It can be speculated that this appearance might exist in the other nuclei, too, but prenatally.

2.3.6　A decrease of KCC2 immunofluorescence in the soma interior during development

The decrease of KCC2 signal intensity in the soma interior was statistically significant in all nuclei between P0 and P12 and it ranged from 1.4 to 2-fold. Probably, it was in relation to the increased immunofluorescence in soma surface during the same developmental period and the proposed (weak) intracellular trafficking process of KCC2. One exception was found in the MNTB, where no statistically significant change in the KCC2 intensity in the soma interior was found during the investigated period (P0-P60). Considering also the unusual transient appearance of "hot spots" in the soma surface of MNTB, it is possible that the KCC2 expression has a distinct developmental line in this nucleus.

2.3.7　The main developmental reorganization of KCC2 immunofluorescence was observed in the neuropil

As mentioned above, the quantification analysis showed that the increase in the soma surface KCC2 immunofluorescence intensity among the nuclei ranged from 1.1 to 1.6-fold and thus cannot explain the change in transporter functionality. However, the quantification of the signal intensity in the neuropil revealed a statistically significant decrease throughout development (P0-P60), regarding all SOC nuclei, and the change ranged from 2.2 to 3.8-fold. On the other hand, the immunofluorescent signal of the neuropil changed also its pattern during development, following the already described changeover: from diffusely stained neuropil early in development (P0-P4) to a crisp and membrane-confined signal later on (P8-P60), with single dendrites becoming apparent. The exception was found in the MNTB, where the neuropil became almost unlabeled. Thus, the main qualitative as well as quantitative changes in the KCC2 immunoreactivity in the auditory brain stem nuclei were observed in the neuropil. In addition, some correlation was found between structure and function, namely, the appearance of the specific membrane-confined *dendritic* pattern correlated with the time of change in GABA/glycine polarity, i.e. with the shift from depolarization to hyperpolarization, in the different nuclei **(Table 2.6)**.

Table 2.6: Correlation between structure and function

	increase in soma surface immunoreactivity	appearance of "hot spots"	decrease in neuropil immunoreactivity	appearance of *dendritic* pattern	** shift from depolarization to hyperpolarization
MNTB	1.6-fold	at P8	3.7-fold	**at P12**	**no shift until P10**
MSO	1.1-fold	no	3.1-fold	**at P4**	**at P5**
LSO	* 1.1-fold	no	3.8-fold	**at P4**	**at P4-P6**
SPN	1.3-fold	no	2.2-fold	**at P0**	**at E18-20**

* for the LSO consider the time between P4 and P60
** from Srinivasan et al. (2004a)

At birth, the presence of KCC2 in the soma surface was not paralleled by the presence of KCC2 in the dendrite surface (the SPN is an exception). However, once KCC2 became functional/powerful enough to change the polarity of GABA/glycine response, the KCC2 signal appeared confined to the dendrites' surface in a specific, membrane-confined *dendritic* pattern **(Table 2.6)**. As the dendrites provide a much large membrane surface than the soma (e.g. 97% of the surface area of a motor neuron, excluding the axon, is dendritic surface (Ulfhake and Kellerth, 1981)), it is logical that if the neuron needs an efficient Cl^- outward transport system, the KCC2 molecules have to be incorporated into the dendritic plasma membrane. Although, the localization in the membrane (regardless of whether it is in the soma or in dendrites), does not imply presence of functional cotransporter and switch of GABA/glycine signalling. In other words, KCC2 function is determined by something else than merely membrane insertion. Another inconsistency was the decrease of KCC2 signal in the neuropil during development (P0-P60) in opposition to the increase of KCC2 signal in the soma surface (P0-P12). In my opinion, this concern, at least in part, the age-related reduction of dendritic branches by a presumed pruning mechanism which is a common phenomenon in motor (Ramirez and Ulfhake, 1991) and sensory (Yamasaki and Ramoa, 1993) systems. Also, Rietzel and Friauf (1998) described considerable remodelling that takes place in the LSO between P4 and P36 with a selective loss of distal dendritic branches

in the third postnatal week; a mechanism by which the appropriate pattern of synaptic connections is formed. However, by means of this process of physical elimination of dendrites alone, it is not possible to explain the pronounced (2.2 to 3.8-fold) decrease in the KCC2 immunofluorescence intensity in the neuropil, although the remaining KCC2-stained dendrites became thicker and the signal became stronger. Therefore, I tried to find some reason why in the neuropil KCC2 immunoreactivity undergoes such transition with age and whether this reorganization is related to the main function of this cotransporter to switch the GABA/glycine transmission.

2.3.8   Possible role of KCC2 in ion homeostasis in dendrites

Considering the role of KCC2 in controlling the polarity of GABA/glycine responses, I asked the question why KCC2 is found in the dendrites if inhibitory inputs are observed to be preferentially localized to the soma and proximal dendrites (…………………….). It was expected that the change in the KCC2 expression will affect mostly the signal in the soma surface. The distal dendritic area is known to be mostly the target of excitatory inputs (…………………). Therefore, at first sight, the result of qualitative as well as quantitative reorganization process mainly occur in the neuropil was considered as a rather unexpected finding in light of the fact that KCC2 is necessary in close proximity to inhibitory inputs, regarding its role for maintaining intracellular Cl^- concentration and keeping the Cl^- equilibrium potential below the membrane resting potential, and thus, responsible for the hyperpolarizing action of GABA and glycine.

This apparent contradiction can be explained by the presence of extrasynaptic $GABA_A$ receptors on the dendrites as it is proposed in different studies (Nusser et al., 1995b; Brickley et al., 1996, 2001; Banks and Pearce, 2000; Gulyás et al., 2001). It is known that extrasynaptic, high-affinity $GABA_A$ receptors are involved in the tonic inhibition in the brain (review in Mody, 2001). The tonic (due to an ambient GABA) and phasic (due to a vesicular GABA release) inhibition can be pharmacologically separated (Nusser and Mody, 2002; Yeung et al., 2003). The magnitude of the tonic inhibition can be surprisingly high, with the total charge transfer greatly exceeding that generated by phasic GABA release (Brickley et al. 1996; Nusser and Mody 2002). The specific role of tonic inhibition is unknown, but it would clearly have a large effect on brain excitability

and hyperexcitatory disorders, such as epilepsy. Anticonvulsants that increase the extracellular concentration of GABA may primarily increase the tonic inhibitory conductance (Overstreet and Westbrook, 2001). Interestingly, the role of the tonic inhibition was shown in controlling passive electrophysiological characteristics and excitability of cerebellar granule cells (Brickley et al., 1996, 2001) and that extrasynaptic GABA$_A$ receptors were seen at glutamatergic synapses (Nusser et al., 1996) without their functional role to be known (Nusser, 1999). Recently, in the cerebellum, KCC2 was found in the plasma membrane around the cell bodies of the granule cells, which were also stained for GABA$_A$ receptors (Williams et al., 1999) that are believed to be extrasynaptic as the granule cells have no inhibitory inputs on their cell bodies. This is consistent with the hypothesis that the inhibition is transmitted via spillover of GABA (Nusser et al., 1998; Rossi and Hamann, 1998). In the hippocampus, KCC2 was highly expressed in the vicinity of synapses responsible for excitatory transmission (Gulyás et al., 2001). The most direct evidence for this conclusion was provided by the ultrastructural localization of KCC2 with preferentially asymmetrical, but not symmetrical, synapses (Gulyás et al., 2001). The authors claim that this can be explained by the presence of extrasynaptic GABA$_A$ receptors in the neuronal dendrites.

To my knowledge, a colocalization study in the brain stem for KCC2 and GABA$_A$ receptor has not been performed so far. But, a strong expression of GABA β2/β3 receptor subunits was demonstrated in the LSO neuropil of neonatal gerbils (Korada and Schwartz, 1999). Unlike the punctate staining of GlyRs seen at P14, the distribution of the β2/β3 subunits of the GABA$_A$ receptor at P4 did not appear as precisely confined to clusters, suggesting an extrasynaptic localization of some GABA$_A$ receptors in the LSO. Together with the present result, showing the intensely stained neuropil (and dendrites) for KCC2, especially in younger animals, it is conceivable that KCC2 cotransporter is situated close to these extrasynaptic GABA$_A$ receptors on the neuronal dendrites also in the brain stem nuclei. However, the open question is: what is the functional significance of KCC2 being close to extrasynaptic GABA$_A$ receptors and close to excitatory glutamatergic synapses?

Figure 2.28 illustrates a scenario that points to the importance of KCC2 in mediating interactions among postsynaptic excitation, inhibition, and neuronal volume transients. It was described in the rat hippocampus and it was proposed that the

neuron-specific cotransporter KCC2, indeed, has a role in the regulation of water and ion homeostasis in the dendrites (Gulyás et al., 2001).
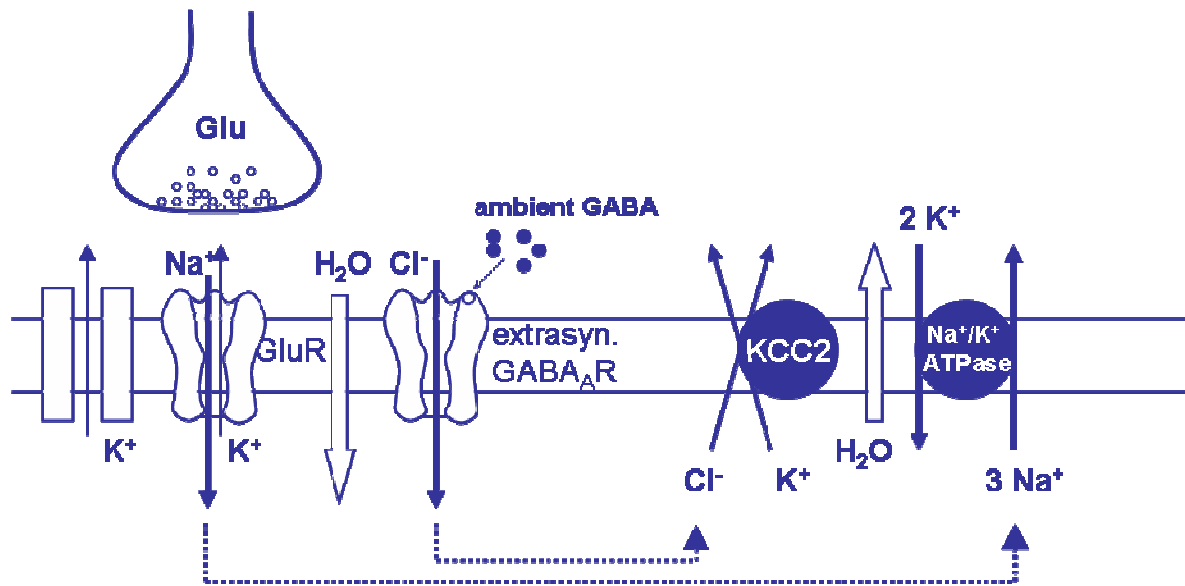
Modified from Gulyás et al. (2001)

Fig 2.28: Possible role of the neuron-specific KCC2 cotransporter in regulation of ion homeostasis in the dendrites of auditory brain stem nuclei

At the excitatory synapses, a conductive Na^+ influx via GluR is paralleled by an influx of Cl^- via, the proposed in close vicinity, extrasynaptic $GABA_A$ receptors ($GABA_A$Rs) and the presence of ambient GABA. This ionic uptake together with osmotically obligated water may result in a dendritic swelling. The activity of the Na^+/K^+ pump (stimulated by the increase in intracellular Na^+ concentration) will extrude the sodium and in concert with the outward-directed chloride cotransporter (KCC2) (largely driven by the elevated intracellular Cl^- concentration) will act to restore the ionic and water balance in the dendrites to the steady state level.
Glu, glutamate; GluR, glutamate receptor

In rat midbrain cultured neurons, the KCC2 transport mechanism was shown to be localized primarily in the dendrites (Jarolimek et al., 1999). Under normal physiological conditions, KCC2 actively extrudes Cl^- from nerve cells using the outwardly directed K^+ chemical gradient (Kaila, 1994) that in turn is maintained by the Na^+/K^+ pump also with a preferentially dendritic expression (Brines et al., 1995). It is known that both primary and secondary active ion transporters influence the concentration of osmolytes in the intracellular and extracellular space (Kaila, 1994) which will also affect the cellular volume (Basavappa and Ellory, 1996; Lang et al., 1998). Several studies showed that a profound postsynaptic swelling takes place in response to intensive excitatory input

(Dietzel et al., 1980; Rothman, 1985; McBain et al., 1990; Jarvis et al., 1999). It is proposed that such activity-induced neuronal/dendritic swelling appears to be the result of net uptake of Na^+ (Rose et al., 1999), Cl^- (Gulyás et al., 2001), and osmotically obliged water. Hence, it was proposed that during intense excitation, the combined entry of Na^+ (via AMPA/NMDA-type glutamate receptors) and Cl^- (via extrasynaptic $GABA_A$ receptors) at excitatory inputs leads to an osmotic load larger than it is caused by the influx of Cl^- during effective synaptic inhibition (Kaila, 1994; Destexhe and Pare, 1999; Gauck and Jaeger, 2000).

In light of the present study and KCC2 expression on the dendrites, possibly in close vicinity to extrasynaptic $GABA_A$ receptors, KCC2 may function to counteract the abnormal Cl^- load (via extrasynaptic $GABA_A$ receptors) and to protect the dendrites from excitatory-induced swelling. Evidence for the presence of AMPA receptor subunits in the SOC is provided by an immunocytochemical study (Caicedo and Eybalin, 1999). Only recently, it was shown that these receptors are functional in LSO neurons (Vitten et al., 2004). Interestingly, in the retina and cerebellar granule cells, swelling-associated excitotoxic cell death can be prevented by blocking inhibitory ionotropic channels (Chen et al., 1999). Functional and ultrastructural studies suggested such an extrasynaptic $GABA_A$ action in the hippocampal pyramidal neurons (Banks and Pearce, 2000), dentate granule cells (Nusser et al., 1995b) and cerebellar granule cells (Brickley et al., 1996, 2001). However, such studies for $GABA_A$ receptor functionality and colocalization with KCC2 and glutamate receptors are missing in the brain stem nuclei. Therefore, this remains to be investigated further: 1) a colocalization study for KCC2 and inhibitory (GABA/glycine) receptor subunits at different developmental ages; 2) an extensive ultrastructural and physiological proof for the presence and the functionality of extrasynaptic $GABA_A$ receptors in the auditory brain stem nuclei; 3) colocalization of extrasynaptic $GABA_A$ receptors and glutamate receptors in the brain stem nuclei; 4) electrophysiological data whether there is a difference in Cl^- regulation between the soma and the dendrites in the SOC neurons and possible change with age.

In addition, Brickley and co-workers (1996) discovered a clear temporal correlation between the development of the negative shift in GABA reversal potential and of tonic inhibition. The tonic inhibition was virtually absent in neurons with depolarizing $GABA_A$ responses. Therefore, I concluded that the involvement of the KCC2 in the dendritic ion homeostasis occur only in the period of hyperpolarizing GABA/glycine action. In the

present study, the appearance of a specific membrane-confined *dendritic* pattern **(Table 2.6)** was correlated with the time of change in GABA/glycine polarity in the auditory brain stem nuclei (Srinivasan et al., 2004a).

As it was mentioned before, the pruning mechanism and the elimination of dendritic branches can explain, in part, the pronounced decrease in KCC2 immunofluorescence signal in the neuropil. Considering the present hypothesis that KCC2 function as protective mechanism against the dendritic swelling, on one hand, anatomical studies suggest a decrease of extrasynaptic $GABA_A$ receptors (Korada and Schwartz, 1999). On the other hand, physiological studies show a reduction of KCC2 activity in the dendrites with age (Jarolimek et al., 1999; Woodin et al., 2003). In the SOC, the general decrease of extrasynaptic GABA ß2/ß3 receptors with age is more profound in the neuropil (Korada and Schwartz, 1999). Moreover, a profound transition from GABAergic to glycinergic transmission in the gerbil LSO during the first 2 postnatal weeks was observed (Kotak et al., 1998). Such a transition from GABAergic to glycinergic synaptic transmission is also present in newly formed spinal networks (Gao et al., 2001). Woodin et al. (2003) proposed that the somatodendritic differences in intracellular Cl^- concentration in hippocampal neurons (Jarolimek et al., 1999) are due to a higher KCC2 activity in the dendrites, being capable of creating local changes in intracellular Cl^- concentration and thus, differences in the reversal potential of GABA in comparison to the soma. Also, they showed that the coincident activity, that followed the maturation of the neuronal network, leads to a reduction of KCC2 activity which eliminated the somatodendritic difference. Taken together, I suppose that the contribution of the extrasynaptic $GABA_A$ receptor-induced inhibition, thus, the abnormal Cl^- load in the dendrites decreases during development.

Considering the KCC2 immunofluorescent signal in the neuropil, an independent studies observed no KCC2 immunoreactivity along axons and glial cells: in the cerebellum, it was proposed postsynaptic distribution of KCC2, consistent with its neuron-specific localization (Payne et al., 1996; Williams et al., 1999); in the embryonic spinal cord, no colabelling of KCC2 with the neurofilament-associated antigen, an axonal marker, was found (Hübner et al., 2001); electron micrographs taken from KCC2/immunogold-stained hippocampal sections of rats confirmed the expression of KCC2 in the plasma membrane of dendrites and its absence in axons (Gulyás et al., 2001). Therefore, it is most likely that the distinctive processes that appeared in the

neuropil and were labelled for KCC2 were dendrites but not axons. Additional proof in favour of the dendritic, but not axonal, presence of KCC2 was provided by a study in the brain stem that used antibodies against the dendritic marker MAP2 (microtubule-associated protein) (Blaesse et al., 2004), although, it was a bit surprising that colocalization of KCC2 with MAP2 was not observed at P4 and P12. Other studies in adult hippocampus and cerebellum (Lu et al., 1999) and in embryonic spinal cord (Hübner et al., 2001) showed a correlation of the KCC2 signal with the expression pattern of MAP2. At this time the reason for this difference is not clear.

In summary, I suppose that KCC2 performs a dual task: first, to shift the polarity of GABA/glycine responses in the soma; second, locally in the dendrites, to maintain the cellular ionic homeostasis and to prevent dendritic swelling. The pronounced decrease of KCC2 immunofluorescent intensity in the neuropil can be explained, in part, with the absence of abnormal Cl^- load via extrasynaptic $GABA_A$ receptors, together with the pruning mechanism that occurs with age.

2.3.9   What leads to KCC2 activation?

The two postulated physiological roles of KCC2 in the CNS underscore the importance of defining how the function of this transporter is regulated. It was concluded that the onset of transporter activity does not correlate with the amount of mRNA or with the mere presence of KCC2 protein (Kelsch et al., 2001). Based on the examination of both the expression and the functional status of KCC2 in deaf gerbils, it was concluded that the transporter was well expressed in these animals, yet the chloride extrusion was functionally disrupted (Vale et al., 2003). The functional status of the transporter was assessed via three different pharmacological treatments that suppressed chloride cotransport (bumetanide, cesium, and genistein) and had little or no effect on neurons from deafened animals in comparison to neurons from controls. This suggested that normal auditory activity regulates inhibitory synaptic strength through the functional status of a chloride transporter.

2.3.9.1   Posttranslational modifications

Recent studies support the idea that the maturation of inhibitory synapses follows several steps, including posttranslational modifications of inward or outward

transporters which result in changes of the phosphorylation (Bize et al., 2000) and/or the glycosylation status (Hiki et al., 1999). Indeed, cation-chloride cotransporters are regulated by phosphorylation/dephosphorylation events (Russell, 2000). In the thesis of Balakrishnan (2004), LSO neurons were treated with the protein phosphatase inhibitor calyculin A in order to increase the phosphorylation of proteins in general (Ishihara et al., 1989). This experiment demonstrated a decline in the intracellular Cl^- concentration and a possible role of phosphorylation (possibly of KCC2) in the process of inhibitory synapse maturation.

The KCC2 protein contains five consensus phosphorylation sites for protein kinase C as well as one consensus tyrosine protein kinase phosphorylation site (Payne et al., 1996). Serine/threonine phosphorylation has been shown to regulate KCC2 activity in oocytes (Strange et al., 2000), while cytosolic tyrosine kinase activity regulates K/Cl cotransport activity (possibly via KCC2) during maturation of hippocampal neurons (Kelsch et al., 2001). In these neurons, the tyrosine phosphorylation site at position 1087 is important for the activation of KCC2 and it is required to maintain the active conformation state of the proteins and/or that they function as sites for essential regulatory protein-protein interactions.

A broad study from our laboratory showed that no splice variants of KCC2 are predicted by bioinformatics. Such splice variants were also not found by RT-PCR analysis in samples from P3 and P12 rat brain stem (Blaesse, 2003; Blaesse et al., 2004). In contrast to our previous hypothesis, that KCC2 trafficking is regulated in an age-dependent manner, the present study and the investigation by Blaesse et al. (2004) have provided strong evidence that KCC2 activity in the brain stem is regulated by age-dependent posttranslational modifications and/or interactions with modulatory proteins.

Results from various investigations differ with respect to the KCC2 phosphorylation state during development in different brain regions. In mouse spinal cord motoneurons and hippocampal pyramidal cells, phosphorylated KCC2 protein was already present early in development, even before the switch of GABA activity (Stein et al., 2004). The authors raised the question of whether the GABA switch is the result of the expression level of KCC2 or whether an activation of the protein has to occur. They claimed that tyrosine phosphorylation appears to be less important than the transcriptional up-regulation of KCC2 that occurs during development. This is in contrast to previous studies (in cultured hippocampal neurons: Kelsch et al., 2001, in brain stem slices:

Balakrishnan et al., 2003), where the authors claimed that transcriptional mechanisms are not sufficient for the introduction of KCC2 activity. Further evidence in the brain stem, supporting the last statement, was provided from my present result: although, the presence of KCC2 protein and its localization in the region of plasma membrane (regardless of whether it is in the soma or in dendrites), this does not imply presence of functional cotransporter. Therefore, differences in the KCC2 regulation between different brain regions are likely to be present.

2.3.9.2   Involvement of growth factors

Recent studies proposed trophic factors, such as brain-derived neurotrophic factor (BDNF) (Rivera et al., 2002; Aguado et al., 2003) or insulin-like growth factor (IGF) (Kelsh et al., 2001), to account for the functional expression of KCC2 via changing of trafficking KCC2 to the membrane and/or via kinetic modulation on the postsynaptic cell.

Immunohistochemical studies showed that the normal developmental distribution of BDNF in the mammalian auditory brain stem occurs during the first two postnatal weeks, and it is in parallel with the developmental expression of its cognate receptor TrkB (Hafidi et al., 1996; Hafidi, 1999; Tierney et al., 2001). BDNF expression is virtually absent from all auditory nuclei in the brain stem at birth (in rat: Hafidi, 1999) as well as TrkB receptor expression (in gerbil: Hafidi et al., 1996). One week before the onset of hearing, BDNF and TrkB are already expressed in the nuclei and the increase of their expression correlates with the appearance of sound-evoked activity, suggesting a role primarily in the maintenance and/or modulation of postnatal and adult functions. Such a modulatory role would complement the long-lasting effect of neurotrophins on KCC2 expression (Rivera et al., 2002; Aguado et al., 2003). BDNF signalling has been shown to down-regulate KCC2 mRNA expression by 50%, leading to an impairment of Cl⁻ extrusion in rat hippocampal slice cultures and acute slices (Rivera et al., 2002). In BDNF-overexpressing embryos, it was suggested that BDNF controls and coordinates network activity via increased synaptogenesis, GABA production and up-regulation of KCC2 expression in rat hippocampal slices (Aguado et al., 2003). The obviously opposite action of BDNF on KCC2 expression in immature versus mature neurons in the same brain region is likely to reflect the activation of the distinct TrkB-linked signalling pathways, as it was proposed recently (Rivera et al., 2004).

In summary, it has to be emphasized that it is not possible to make a general statement about how grow factors influence KCC2 expression because of complex and various aspects that they have on the neuronal modulation (for reviews see: Bibel and Barde, 2000; Poo, 2001; Chao, 2003), namely: to mediate the differentiation and the survival of neurons; as synaptic modulators inducing changes in synaptic efficacy and morphology; to modulate the response of growth cones to guidance molecules. Studies of mutant mice and analysis of heterozygous animals have shown the importance of the neurotrophins in learning (Linnarsson et al., 1997), locomotor and feeding behaviours (Lyons et al., 1999; Kernie et al., 2000).

2.3.9.3   Involvement of thyroid hormone

It is well documented that thyroid hormone plays a critical role in brain development and plasticity (Chan and Kilby, 2000; Anderson et al., 2003; Vara et al, 2003). In the thesis from Balakrishnan (2004), the role of thyroid hormone in the maturation of inhibitory synapses was tested. He found that hypothyroid rats display an abnormality in the shift from depolarization to hyperpolarization as it did not occur during the investigated time frame (P5-P12). Thus, it was suggested that the thyroid hormone may act as a possible induction factor in the developmental switch of the polarity of GABA/glycine response. Further investigations need to be performed to address whether KCC2 expression is also affected in these animals.

2.3.10   Down-regulation of KCC2 expression/function

Changes in chloride cotransporter expression/function are observed under physiological (e.g. development) as well as under pathophysiological conditions:

1) deafness leads to an alteration of the balance between inhibitory and excitatory synaptic drive and to a depolarization of the inhibitory synaptic reversal potential (Kotak and Sanes, 1996; Vale and Sanes, 2000, 2002). In deaf animals, a functional decrease of chloride transport occurs without a change in KCC2 mRNA or protein expression (Vale et al., 2003); in contrast, Shibata et al. (2004) showed that the expression of KCC2 mRNA in LSO neurons from P14-P16 rats is dependent on auditory experience and either ipsi- or contralateral ablation of the cochlea or implanted strychnine pellets lead to a lack of KCC2 mRNA in some neurons. A possible reason for this discrepancy

can be that these two studies have investigated different brain regions: the inferior colliculus and the LSO, respectively. This provides further evidence that the correlation between function and expression of the KCC2 cotransporter differ among the brain regions.

2) KCC2 expression levels in the dorsal motor neurons of the vagus were down-regulated following axotomy (Nabekura et al., 2002) and different traumatic insults (concussion, epileptic seizures, or hypoxia-ischemia) (van den Pol et. al., 1996; Thomas-Crusells et al., 2000; Chung and Payne, 2001; Rivera et al., 2002). There is some indication that epilepsy is also associated with improper chloride balance (Cohen et al., 2002), and protein tyrosine phosphorylation was suggested to modify the neuronal function under this pathological condition (Sanna et al., 2000). In humans, the KCC2 gene is located on chromosome 20q, containing 2 epileptic genes but without direct linkage in between them (Delpire and Mount, 2002). This does not exclude the possibility that KCC2 constitutes a risk factor for epilepsy, due to observations in mouse model with lower threshold for epileptic seizures (Hübner et al., 2001). In general, the importance of the cation-chloride cotransporter gene family is demonstrated by human diseases like Bartter syndrome and Gitelman disease (Kurtz, 1998), and Andermann syndrome (Deleu et al., 1997).

An interesting question, then, is: what could be the functional significance of the loss of KCC2 protein/function and the following depolarizing action of GABA after injury? Although, it appears that the reversion to depolarization would be harmful and would contribute to excitotoxicity, it was proposed that the trauma might cause neurons to revert to a state of immature neurons where they have greater developmental flexibility, perhaps needed in sprouting and retargeting (Payne et al., 2003).

2.3.11   Importance of KCC2 regulation in the brain

KCC2 was found to be responsible for extruding both K^+ and Cl^- from neurons, thus, actively regulating the intraneuronal Cl^- concentration or buffering extracellular K^+ (Payne et al., 2003). During developmental plasticity, the up-regulation of KCC2 activity switches the depolarizing GABA responses into hyperpolarizing ones (Rivera et al., 1999; DeFazio et al., 2000; Ganguly et al., 2001). A similar developmental shift occurs in glycine signalling (in rat spinal cord: Wu et al., 1992b; in rat brain stem: Backus et al.,

1998; Ehrlich et al., 1999). The excitatory action of GABA and glycine in the immature animals is believed to be important for the development of the nervous system, as the trophic action induces a rise in intracellular Ca^{2+} (through membrane depolarization) and ultimately leads to neuronal differentiation, growth and maturation of synapses (Cherubini et al., 1991; Yuste and Katz, 1991; Barker et al., 1998; Gulyás et al., 2001; Maric et al., 2001). In addition, GABA operates in synergy with NMDA channels in immature neurons at the excitatory glutamatergic synapses, which initially lack functional AMPA receptors (Ben-Ari et al., 1997). The GABA-induced depolarizing currents (the principle source of depolarization at this stage) remove the voltage-dependent magnesium block from NMDA channels and induce an increase of intracellular Ca^{2+} (Ben-Ari et al., 1997). This will further increase neuronal activity in the network and facilitate the generation of synchronized patterns of activity that are a hallmark of developing networks (for review see: Ben-Ari, 2002). Moreover, the correspondence between the time course of refinement in the inhibitory network and the development of inhibition supports the idea that this refining mechanism relies on the excitatory properties of immature GABA and glycinergic synapses (Kandler et al., 2002).

Therefore, via manipulating the duration of the depolarizing phase of GABA/glycine transmission, it will be interesting to analyze its effect on the maturation of postsynaptic morphology. One possibility to achieve this task is via analysis in loss-of-function KCC2 knock-out animals. Mice with disruption of the Slc12a5 gene, which codes for KCC2 protein, and 95% reduction of the KCC2 protein are used in the second part (Chapter 3) of my PhD Thesis. There, I address the question of the effect of Cl^- homeostasis on different morphometric parameters as nucleus volume, neuron number and soma cross-sectional area.

2.4   Summary of chapter 2

1.   It was demonstrated that in the rat auditory brain stem nuclei, the KCC2 protein is present already at birth.

2.   A difference appeared in the KCC2 immunofluorescent intensity between the nuclei during development; the MNTB remained weakly labelled throughout the investigated period. In my opinion, this is due to a delay in the development of the inhibitory machinery in the MNTB in comparison to the other brain stem nuclei.

3.   KCC2 was localized in the region of the plasma membrane already at birth (P0) and its expression in the rat auditory brain stem developed via an increase of the immunofluorescent signal intensity between P0-P12. However, this change is with a moderate magnitude. I conclude that it is only of minor importance and does not explain the change in KCC2 functionality.

4.   The transient (at P8 and at P12) appearance of KCC2 immunofluorescent puncta in the soma surface of the MNTB neurons is consistent with: 1) weaker KCC2 labelling in this nucleus throughout the investigated period and a delay in the development of an inhibitory machinery in comparison to MSO, LSO, and SPN; 2) an initial period of missing or less powerful inhibition and colocalization of KCC2 with immature inhibitory synapses. I speculate that transient puncta in the soma surface of the other nuclei may be present prenatally, in correlation with the earlier maturation of inhibitory synapses.

5.   The main developmental reorganization (in qualitative as well as in quantitative aspects) of KCC2 immunoreactivity in the brain stem auditory nuclei was observed in the neuropil. I suppose that, at least in part, the decrease in the signal intensity can be explained by an age-related reduction of dendritic branches via the pruning mechanism and with the absence of an abnormal Cl^- load via extrasynaptic $GABA_A$ receptors. This is consistent with the proposed additional role of KCC2, namely to maintain the cellular ionic homeostasis and to prevent dendritic swelling (Gulyás et al., 2001).

6.   Neither the increase in the KCC2 soma surface signal intensity, nor the reorganization in the neuropil, can be strictly related to the developmental switch in GABA/glycine signalling and the onset of KCC2 function, although some correlation (the appearance of a specific membrane-confined *dendritic* pattern) between structure and function was found. Further implication of different molecular methods, regarding the proposed posttranslational modification of KCC2, will shed light upon the question of what leads to the functional activation of the cotransporter.

3   Morphometric analysis in KCC2 knock-out animals

3.1   Materials and Methods

3.1.1   Animals

Experiments were performed using the C57BL/6JO1aHsd strain as a genetic background for KCC2 (+/+) and KCC2 (-/-) mice. KCC2 (+/-) mice were kindly given by Dr. Delpire (University Medical Center, Nashville, USA). The protocol for inactivation of KCC2 was published elsewhere (Delpire et al., 2002). Disruption of the *Slc12a5* gene, which codes for the KCC2 protein, resulted in a >95% reduction of protein expression as measured by Western blot analysis (Lu et al., 1999). Further mating of KCC2 (+/-) mice, in order to obtain KCC2 (-/-) animals, was performed in the animal facilities of the University of Kaiserslautern.

The animals were randomly selected. No more than two were used from a given litter. In appearance and gross behaviour, the KCC2 (-/-) animals at P3 were indistinguishable from the other animals at this age. In this case, for all KCC2 animals at P3, standard genotyping procedure was used. To do so, separate Polymerase Chain Reaction (PCR) was performed on tail DNA to amplify fragments specific to control and modified genes. The sequences of the primers used to amplify the control gene were: forward 5'AGCGTGTGTCCGTGTGCGAGTG3' and reverse: 5'ATCGCCGTCCTCGC GTCCGTC3'. The forward primer was also used to amplify the mutant gene. The sequence of the reverse primer for the mutant gene was: 5'CCAGAGGCCAC TTGTGTAGCGC3'. The reaction volume of 50 µl contained: 1 µl of the genomic DNA, 1 µl of each primer, 5 µl of 10x PCR Y buffer (with 20 mM $MgCl_2$, Peqlab), 1 µl (0.2 mM) dNTP, 1 µl DMSO and 0,2 µl Taq Polymerase (5u/µl; Peqlab). Thirty-five cycles of PCR were performed, each consisting of a denaturation step at 94°C for 90 sec, an annealing step at 62°C for 60 sec, and an extension step at 72°C for 90 sec. Both sets of oligonucleotides generated a 0.2 kb PCR product that was isolated on a 1% agarose gel.

The KCC2 (-/-) mice presented a distinct phenotype barely visible at P6-P7 but becoming obvious at P12. The KCC2 (-/-) animals were smaller that the KCC2 (+/+) animals at P12; they demonstrated an abnormal posture and a gait consisting of standing and walking on stiff limbs. Therefore, a genotyping procedure for P12 KCC2

animals was not performed. The life expectancy of KCC2 (-/-) animals is short (Delpire et al., 2002), and in our animal facilities, KCC2 (-/-) mice died within 3 weeks. By contrast, only occasional deaths of KCC2 (+/+) and KCC2 (+/-) were observed.

3.1.2   Perfusion, fixation and tissue procedure

Four to fourteen animals were used in every category. Before perfusion, the body weight of the animals was obtained. Thereafter, they were perfused and fixed (for details see 2.1.2 Perfusion and fixation). At the end of the postfixation period, the olfactory bulb was removed and the brain was weighed on a microbalance. Coronal sectioning was performed on a freezing microtom at a thickness of 25 µm. The brain was placed with the rostral part on the platform and with the dorsal part facing the knife. A serial of coronal sections was collected and every second slice was mounted on gelatine-coated slides, air-dried overnight and stained with thionine for Nissl substance. The slides were then coverslipped in Entellan (Merck). Only one side of the brain in every animal was analysed.

3.1.3   Identification of the nuclei

A critical point for accurate volume calculation was the correct identification of each nucleus of interest.

The **cochlear nuclear complex (CN)** was subdivided into the ventral cochlear nucleus (VCN) and the dorsal cochlear nucleus. In the present investigation, only the VCN was analysed. No differentiation between anterior and posterior parts of the VCN was made. Part of the caudal boundary of the VCN was defined by the eighth nerve root. The medial edge of the nucleus was clearly bounded by the spinal track and principal sensory nucleus of the trigeminal nerve anteriorly and by the restiform body (inferior cerebellar peduncle) posteriorly. The VCN is surrounded by a well-developed small cell shell, which contains a high concentration of granule cells and numerous small stellate neurons (Osen, 1988; Trettel and Morest, 2001). These cells were not included in the outlines of the nucleus.

The **superior olivary complex (SOC)** is located in the caudal pons immediately dorsal to the pontine gray close to the ventral border of the brain stem. Three nuclei in

the SOC were analysed: the MSO, the LSO and the MNTB. The caudal border of the SOC complex corresponded to the appearance of the nucleus of the facial nerve. The borders of LSO and MNTB were relatively easy discerned by the distinct morphologies, arrangement of neurons and their location.

From caudal and rostral direction, the **MNTB** was readily recognized mainly by the appearance of very characteristic cell body with its spherical or oval pericarya. The most rostral and caudal slices with MNTB neurons were outlined even when less than ten somata were present. The number of large-fiber bundles running through the MNTB increased with age; it was not possible to subtract these fibers when the nucleus cross-sectional area was outlined and they contributed to its value and further to the absolute volume calculation (see 3.1.5 Stereological analysis. Volumetric data).

The **MSO** nucleus was identified as a narrow vertical column of horizontally oriented bipolar neurons, situated between the MNTB and the LSO. The size of the nucleus shows a large interspecies variation (Harrison and Irving, 1966) and is relatively small in rats and mice (around 600 cells). As it was noticed in the rat (Kulesza et al., 2002), MSO expands more caudal and especially more rostral to the LSO. After the LSO disappeared in the more rostral sections, the MSO expanded dorso-ventrally and shifted more dorsal. Its cross-sectional area nearly tripled in size.

From the caudal part, the **LSO** was readily recognized after the facial nucleus and the most caudal part of the lateral nucleus of trapezoid body (Kulesza et al., 2002). The LSO was clearly detected by the "S"-shape and its tightly packed bipolar neurons. They are aligned with their cell bodies orthogonal along the long axis of the "S"-shape. At this level, the lateral nucleus of trapezoid body was constricted and it occupied a small territory underneath the LSO. The LSO was not present in the most rostral sections of the SOC and the lateral nucleus of trapezoid body was expanded dorsally, shifted laterally and occupied the LSO's place (Kulesza et al., 2002).

3.1.4   Data analysis

The slides were analysed under a conventional microscope (Axioskop 2; Zeiss, Göttingen, Germany) using 10x and 20x Plan-Neofluar objectives, and a high-resolution digital camera (C4742-95-12NR, 1280x1024 pixels; Hamamatsu, Japan). Pictures were

stored and analysed with AnalySIS Software Imaging System (version 3.1, Münster, Germany).

The outlines of the cross-sectional area of the four investigated nuclei (VCN, LSO, MNTB and MSO) and the outlines of the somata cross-sectional area (see 3.1.6.2 Soma cross-sectional area) were hand drawn using a digitiser (Intuos; Walcom, Neuss, Germany). The data were saved as Microsoft Excel 2000 file and the further calculations were performed there.

3.1.5   Stereological analysis. Volumetric data

The calculation of the nucleus volume was done from a series of sections according to Cavalieri's Principle (Gundersen and Jensen, 1987). This method numerically integrates a curve of cross-sectional area measurements (A) plotted against the section number (n). The total nucleus volume ($V_{nucleus}$) was estimated by multiplying each cross-sectional area measurement with the distance (d = 50 µm) between the sections analysed and summing the obtained values **(Fig. 3.1)**; the d should not be confused with the slice thickness (t = 25 µm).

$$V_{nucleus} = d \sum (A_n),$$

where A_n is the cross-sectional area of the n-th section through the morphometric region. No correction for possible tissue shrinkage during fixation was made.
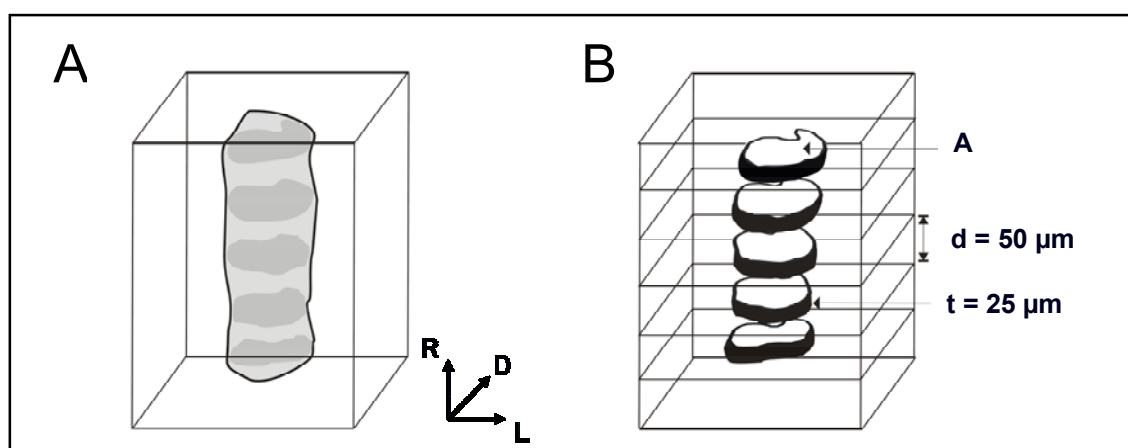
Figure 3.1: Cavalieri's principle for calculation of the nucleus volume

(A) Schematic three-dimensional drawing of the LSO in rostro-caudal extension. R, rostral; L, lateral; D, dorsal
(B) Coronal planes of cutting and outlined surface areas of the LSO. Only every second slice is mounted, outlined and used for nucleus volume calculation (only these slices are illustrated).
A, cross-sectional area; d, distance between analysed sections; t, slice thickness

3.1.6   Morphometric analysis

3.1.6.1   Neuron number

Here, modification of optical disector technique or "3D-counting box" was used (for details, see 3.1.9 Methodological considerations). The essential idea is to define a sample volume (disector probe or rectangular block) within the section of a tissue and then count all somata within that volume as well as half of all neurons that intersect its outer surface. This number is then used to calculate the number of neurons in an
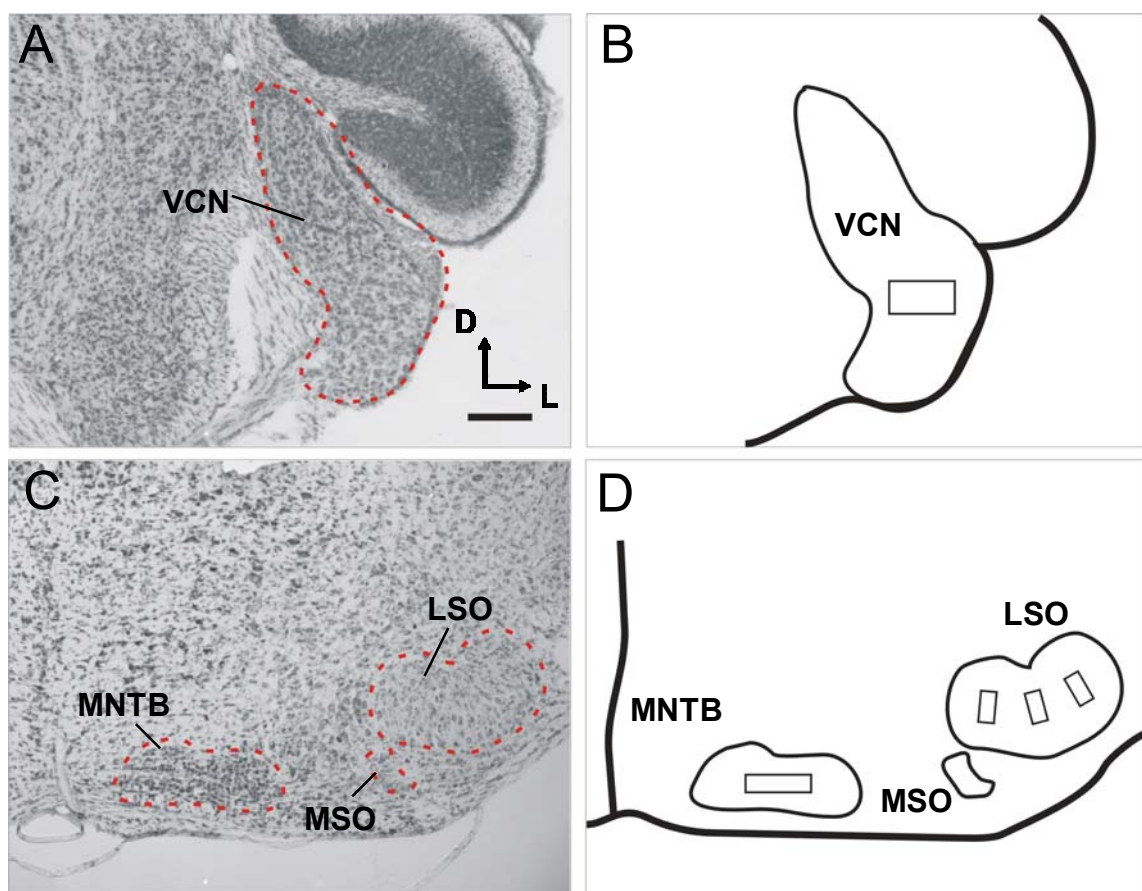
Figure 3.2: Identification and outline of the nuclei

(A), (C) Nissl-stained coronal sections from mouse brain (P12) with outlined ventral cochlear nucleus (VCN) (A) and the three main nuclei of the SOC (C): the lateral and the medial superior olivary nucleus (LSO and MSO, respectively) and the medial nucleus of trapezoid body (MNTB). D, dorsal; L, lateral. Scale bar, 200 µm in both panels.
(B), (D) Drawings based on panels (A) and (C). The rectangular blocks for cell counting are depicted in the VCN, the LSO, and the MNTB. In the MSO no rectangular block is used. The arrow in (B) denotes the distance of the counting block from the ventral tip of the VCN. With reference to approximately the same dorso-ventral position in this nucleus at both ages, the length of the arrow was 200 µm and 300 µm for P3 and P12, respectively.

already known volume of the current nucleus. Sections at approximately the 75% level from the caudal-to-rostral extension were chosen in every nucleus. The somata were then counted in the rectangular block drawn as a frame in Analysis Software **(Figs. 3.2, 3.3)**. The third (z) dimension was given by the slice thickness (t = 25 µm). The neuron somata could easily be identified and distinguished from the glial cells, especially at P12. Neuron identification criteria included: a single, darkly stained nucleolus and abundant Nissl substance in the cytoplasm. Those somata that were located completely within this rectangular block were counted for one each (see **Fig. 3.3**, marked by ✗). Somata that crossed the block were counted for 0.5 (half) cell (see **Fig. 3.3**, marked by ✓). In the VCN, the somata were counted in a rectangular block with a size of
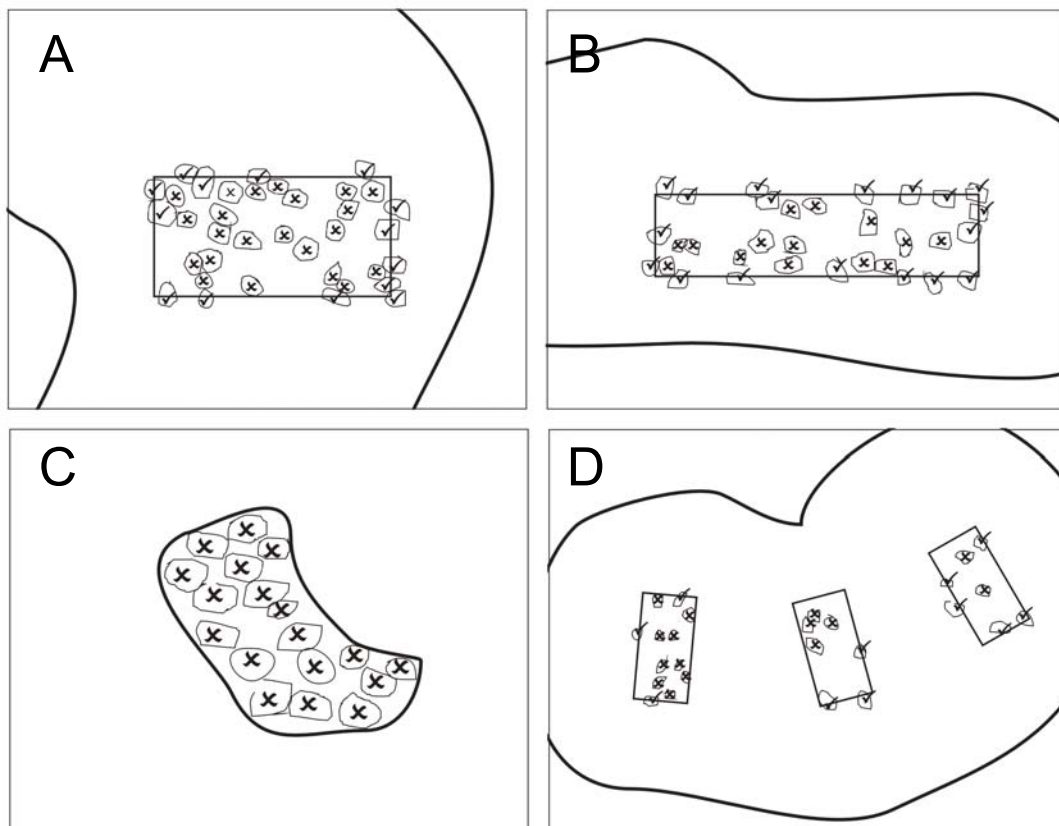
Figure 3.3: Detailed drawings of the four nuclei ((A) VCN, (B) MNTB, (C) MSO, (D) LSO)

Thus, ✗ depicts cell somata that were located completely within the rectangular block; they were counted for 1 each. ✓ depicts cell somata that crossed the block and they were thus counted for 0.5 (half cell). In the MSO, all cells in the outlined area were counted. VCN, ventral cochlear nucleus; MNTB, medial nucleus of trapezoid body; MSO, medial superior olivary nucleus; LSO, lateral superior olivary nucleus

200 μm x 100 μm x 25 μm. The block was put approximately 200 μm (for P3) or 300 μm (for P12) dorsally to the ventral tip of the VCN **(Figs. 3.2B, 3.3A)**. This was done to analyse approximately the same dorso-ventral area at both ages. By means of analysing, three rectangular blocks were used for the MNTB to test whether the impaired inhibition in KCC2 (-/-) animals influences the neurons along the tonotopic axis in a different way. In the MNTB, the somata were counted in a rectangular block with a size of 200 μm x 50 μm x 25 μm **(Fig. 3.3B)**. For both categories at P3, counting in three slices through the rostro-caudal extension of the nucleus was performed (at 25%, 50% and 75% level, respectively). This was done after statistical difference in neuron number during the development appeared. For each animal, the estimated somata number in the MNTB at P3 is provided as the arithmetic mean, based on these three counts. Due to its relatively small size, no rectangular block was used in the MSO. Instead, the counting was performed in a slice at the 75% level from the caudal border of the MSO in the whole nucleus cross-sectional area **(Fig. 3.3C)**. In the LSO, the somata were counted in three different rectangular blocks with a size of 50 μm x 100 μm x 25 μm each, located in the medial, middle and lateral part of LSO **(Fig. 3.3D)**. The reason was the finding obtained in gerbils (Sanes et al., 1987; Sanes and Wooten, 1987; Sanes and Silvers, 1991; Sanes and Chokshi, 1992) that the inhibitory (glycinergic) transmission from the MNTB, which contributes to the maturation of the postsynaptic neurons in the LSO, appeared to be more prominent within the high-frequency area of the LSO. This is the area having the greatest density of glycine receptors (Sanes et al., 1987); approximately 70% of the MNTB neurons project to this region (Sanes and Silvers, 1991); it has a two-fold higher neuron packing density (Sanes and Wooten, 1987); the neurons have spatially more restricted dendritic arbours (Sanes and Chokshi, 1992).

3.1.6.2   Soma cross-sectional area

The somata of all counted neurons were outlined using a 20x objective. The measurements were made in the same section in which neuronal counting was performed. In the MNTB, although at P3 somata were counted in three slices (see above), only somata in the most rostral slice were outlined for the analysis of soma

cross-sectional area at this age. In the LSO, somata in all three rectangular blocks were measured and the mean value was finally obtained.

3.1.6.3 Somata area occupation

This value represents the sum of the somata surface area located completely within a current rectangular block (see **Fig. 3.3**, marked by ✗) plus half of the sum of the somata surface area of the neurons that crossed the rectangular block (see **Fig. 3.3**, marked by ✓). This is valid for the VCN, the MNTB, and the LSO. For the MSO, somata area occupation represents the sum of the somata surface area of all neurons in a current slice. The somata area occupation represents an absolute value; it was not taken as a result but to calculate the relative somata area (see 3.1.7.2 Relative somata area).

3.1.7   Relative calculations

3.1.7.1 Nucleus volume / brain weight

This value represents the relative volume and it was calculated in order to normalize the obtained nucleus volume to the brain weight i.e. to the brain volume.

3.1.7.2 Relative somata area

This value represents the measured somata area occupation within the frame (see 3.1.6.3 Somata area occupation) divided by the surface area of the frame. The surface area of the frame was as follows: for the VCN 20 000 μm^2; for the MNTB 10 000 μm^2; for the LSO 15 000 μm^2. In the MSO, no frame but the nucleus cross-sectional area was used instead.

3.1.8   Statistical analysis

For the statistical analysis of the morphometrical differences between (-/-) animals and (+/+) animals and during development, WinSTAT software, add-in for Microsoft Excel, was used. The first analytical step showed that all data were normally distributed (Gaussian distribution). Thus, parametric student *t-test* for two-group comparison was

applied. One-way ANOVA test was applied for three-group comparison in the case of the LSO regarding the data obtained from the medial, middle and lateral region. For the level of significance and the related symbols of the p values used in the figures and tables, refer to 2.1.8 Statistical analysis. The statistical errors for all data are standard deviations (SD). In some case, the coefficient of variance (CV=SD/mean) was calculated in order to evaluate the precision of the measurement in the groups (see 3.3.2 Absolute and relative volume of the nuclei).

3.1.9   Methodological considerations

3.1.9.1   Representativeness of the sample

The body weight of the animals tends to vary due to their number in the litter. To avoid the correlated differences in the brain weight, between 7 and 9 animals were analysed in each category. In this case, the investigated group is sampled randomly and closely represents the given population.

3.1.9.2 Tissue shrinkage

Unfortunately, this methodological problem is inevitable. Differential tissue shrinkage as a function of age and level of fixation might be expected to affect directly two quantitative measures in this study: nucleus volume and soma cross-sectional area; indirectly it can affect the neuron number. Related to the nucleus volume a possible error may occur in all three dimensions, namely, in the size of the outlined nucleus cross-sectional area or/and in the number of slices, in which the given nucleus appears (i.e. in the rostro-caudal extent of the nucleus); thus, assume that the shrinkage is uniform in all directions. Data from the nucleus cross-sectional area in the rat LSO at midrostro-caudal level showed that the cross-sectional area increased 1.4-fold between P4 and P12 in rat (Rietzel and Friauf, 1998). This was comparable with my data from the LSO cross-sectional area that increased 1.6-fold between P3 (+/+) and P12 (+/+) mice. The result revealed that the possible histological shrinkage was probably at the same level in young and in old animals and the factor of difference between them was preserved during the experiment. Further evidence that the tissue shrinkage can be ignore as methodological problem in the current study are taken from previous reports

in mice VCN (Webster and Webster, 1980; Webster, 1988a). The authors have shown little change in the volume of this nucleus over the first three days after birth. However, from P6 to P12, the VCN volume increases more than double-fold (Webster, 1988a). Regarding my results, the VCN volume increases by the factor of 2.7 between P3 (+/+) and P12 (+/+) animals. Therefore, I assume that if the brains at different ages are treated with the same fixation protocol, the variations in the level of fixation and in the subsequent different tissue shrinkage can be ignored. Besides this, some experiments with unfixed brain and cryostat technique were performed in the present study. The results showed that the volume of the two LSO nuclei analysed ($0.041 \ \mu m^3$ and $0.043 \ \mu m^3$) was not significantly different ($p>0.05$) from the mean LSO volume obtained after the fixation procedure ($0.039 \ \mu m^3$).

With respect to soma cross-sectional area, quantitative data in auditory brainstem nuclei in mice (Webster and Webster, 1980) demonstrate a rapid growth between P3 and P12. The results showed that soma cross-sectional area almost doubled in size during this period. In agreement with this, my data for this parameter showed an increase between P3 and P12 by a factor of 1.8 for the VCN somata, by a factor of 1.7 for the MNTB somata and by a factor of 1.5 for the LSO somata.

In summary, my results could be considered independent of the factor tissue shrinkage. Moreover, the aim of this study was to obtain not just absolute values but rather comparing knockout vs. control, young vs. old.

3.1.9.3 Neuron number

There are two fundamental approaches used to estimate the total number of objects in a structure. One method involves the estimation of both the volume of the structure and the absolute number of the objects. However, in the majority of neuronal systems, a direct absolute determination of the total number of neurons is almost impossible, mainly due to their large amount. Therefore, estimates or approximations, based on limited sampling are preferred and easier to approach if the estimates are unbiased and the variance between the individuals is acceptable.

This second method, and the currently used one, is the well-known **fractionator approach** and involves the determination of the number of neurons in a known fraction of sections (for example, 1 every 3 sections) and all objects are counted in these

chosen section. This counted number must be multiplied by fractions to recompose the absolute number of neurons in the given area (Pakkenberg and Gundersen, 1988; West et al., 1991). The method involve a placement of geometrical probes (*disector*), and a counting rule was described in terms of the presence of sectional profiles of objects on two appropriately spaced sections (Sterio, 1984), hence the name "*di*-sector". The volume of disector probe is defined by the area that is sampled on one of the sections and the distance between the corresponding surfaces of the two sections (West, 1999). Counting with *disectors* involves determining whether a particular object is associated with a particular *disector*, using rules that insure that all objects have equal probability of being found in the volume defined by the *disector*. Variants of use disector counting technique have been used to estimate the total neuron number in a diverse range of neural structures stained with different techniques (West et al., 1991; Janson and Moller, 1993; West et al., 1996; Baldwin et al., 1997; Pakkenberg and Gundersen, 1997; West and Slomianka, 1998). This method is part of a collection of mathematical methods, namely stereology that implies quantitation of three-dimensional geometric characteristics of an object (e.g. volume, surface area, length and number) that relate to two-dimensional measurements, made on sections through the structure. The stereological techniques for counting objects (i.e. neurons and synapses) can be divided into two general categories. The first of these categories includes the assumption-based methods, which have been used for decades (Abercrombie, 1946; Chalkley et al., 1949). The other ones include the design-based methods, which have been popularised in the recent years (Sterio, 1984; Gundersen, 1988; Hedreen, 1999; Baddeley 2001, von Bartheld 2002).

The **design-based techniques**, is characterized by 3D probes (rectangular block or counting box) that enable one to count directly the objects in a define volume of tissue (Sterio, 1984; Williams and Rakic, 1988; West, 1999). The important feature of this technique is that no knowledge or assumption about the size, shape or orientation of the objects being counted is required which circumvents the major problem associated with assumption-based techniques (West, 1999; 2001). A source for incorrect extrapolations comes from simple counts of sectioned material that invariably overestimate the number of the neurons in the nucleus because the counted neurons are cut during sectioning and can appear in more than one section. One possibility to avoid this is reducing the neuron to a unique sampling point. For the Nissl-stained

neural tissue, an appropriately unique sampling point is the nucleolus of the neuron. Thus, every neuron will be counted only once because the possibility to have its nucleolus in two slices is very small. However, in sections containing large numbers of object profiles, there are difficulties associated with finding the corresponding parts of the two physically separated sections that define each *disector*. To avoid this, it was suggested (Gundersen, 1986) to use optical sections in thicker histological sections by focussing through a known volume of the section and counting the number of new objects that come into focus (i.e. neuron nucleoli). This method of counting has been referred into the literature as the **optical disector probe** (Gundersen et al., 1988b; West, 1993; Mayhew and Gundersen, 1996; Coggeshall and Lekan, 1996; West, 1999) and the original approach employing two physically separate sections is now referred as the physical disector probe to distinguish between the two. Optical disector or "3D counting box" is thought to be more efficient (West et al., 1991; Coggeshall and Lekan, 1996). The defining of the upper and/or lower focal planes and the optical disector counting is performed by superimposing the counting frame on the image and moving the counting frame a known distance, through the thickness of the section, with the focus control of the microscope.

In this sense, some methodological considerations concerning the currently used modification of optical disector should be mentioned:

1) I did not sample throughout the slice; I assumed that the upper and the lower focal planes of my *disector* (rectangular block) coincide with the physical borders of the slice i.e. the distance between them (z-axis) is 25 µm. On one hand, this was due to the absence of reasonable equipment (e.g. special stereological toolbox for PCs, motorised specimen stage and computer-controlled automatic sampling for the x- and y-axis, a mobile stage to measure the z-axis). However, it was shown that although the commercially available stereological analysis systems can expedite design-based analyses, they are not essential and design-based sampling and counting can be performed properly with inexpensive equipment (Pakkenberg and Gundersen, 1988; Busch, 1997). Moreover, it was empirically confirmed that there is no difference between the counting done in 2D images (fixed focus plane) and focussing through the slice. In addition, optical disector requires thick sections – between 35 and 50 µm. However, these sections have the disadvantages that penetration of stains may be less than optimal and it may be difficult to focus through the entire section. Thus, I have used

25 µm sections, which were still thick enough to be used for optical probe but also to allow optimal staining.

2) The real section thickness may not be always 25 µm due to the substantial slice shrinkage after drying and coverslipping (Abercrombie, 1946; Guillery and Herrup, 1997). However, this source of error would also refer to the volume calculation according to Cavalieri's principle. This means that when the total number of neurons rather than the density of neurons were estimated in the volume, the error of "incorrectly" assumed z-axis of the counting box would be spread throughout the nucleus volume. In this case, it is not worth to consider the real section thickness (Guillery and Herrup, 1997).

3) There are different ways to obtain unbiased counts of the number of profiles per unit area (frame) of a section. Since the Danish stereologist Hans Gundersen demonstrated the overestimation caused the edge effect, two borders of a frame have been systematically considered "forbidden", and all structures hit by these borders are not considered in the counts (Gundersen, 1977). I modified this counting rule in a way that all neurons that touch the border of the frame were counted for half cell (0.5).

4) Although, most authors consider the disector method unbiased (Bendtsen and Nyengaard, 1989; Fiala and Harris, 2001), I agree with Guillery and Herrup (1997) that all methods of quantification underlie some assumptions and principles, which must be carefully considered in relation to the problem that has to be solved, to the type of tissue available and to the level of accuracy needed.

In summary, I considered the modified optical disector counting technique and the modified disector counting rule, used in my present analysis, as adequate and suitable for the aim of the study: to obtain not just absolute neuron number, yet to compare this parameter between the four categories.

3.1.9.4   Only one counting

A source of error could be how representative is the counting in only one slice in the rostro-caudal extension of the nucleus. I tested the hypothesis of the possible biased sampling strategy. To do so, three rectangular blocks in the MNTB of P3 animals were used at 25%, 50% and 75% of the rostro-caudal extension of the nucleus. The

lack of significant difference in the case of using one or three counting blocks revealed no need to do the same for the other nuclei.

3.1.9.5   VCN neuron number definition

The neurons in the VCN were counted in the region of bushy cells, as they are the main source of input to the SOC (for review: Thompson and Schofield, 2000). However, one should take into account the presence of octopus cells in the most caudal part of the VCN. This part was already taken to calculate the reference nucleus volume, thus, to calculate the total number of neurons. In respect to this, the number of neurons for the VCN considered both bushy and octopus types in the VCN.

3.1.9.6   Variability of estimates

The reliability of a counting method can be evaluated by repeated counts made by the same investigator two times or by another person. I tested the reliability and performed a second counting of MNTB somata in the P3 (+/+) and P12 (+/+) animals 2 months later. The old values for P3 (+/+) animals (3951 ± 657, mean ± SD) and P12 (+/+) animals (5317 ± 546, mean ± SD) revealed no significant difference (p>0.05) with the new values respectively for P3 (+/+) mice (4144 ± 494, mean ± SD) and P12 (+/+) mice (5454 ± 422, mean ± SD).

3.2   Results

The focus of Chapter 3 was four nuclei in the mouse central auditory system: VCN, LSO, MNTB and MSO. The animals were put into four categories considering the age and the genotype: P3 (+/+), P3 (-/-), P12 (+/+) and P12 (-/-). All investigated parameters (body weight, brain weight, absolute and relative volume of the nuclei, neuron number, soma cross-sectional area and relative somata area) were compared between (-/-) and (+/+) group as well as between the two ages (P3 and P12).

3.2.1   Brain weight and body weight

Scatter plots of the brain weight as a function of the body weight from P3 (-/-) animals and P3 (+/+) animals showed that the data from these two characteristic features were dispersed at this age **(Fig. 3.4A)**. Only the body weight values for P3 (-/-) animals were shifted towards smaller values; their average body weight was 91% of the body weight determined in P3 (+/+) animals **(Table 3.1)**. Further statistical analysis between (-/-) and (+/+) animals at P3 related to the body weight **(Fig. 3.4B)** showed that the difference was significant. However, no significant difference was present between P3 (-/-) and P3 (+/+) animals related to the brain weight **(Fig. 3.4C)**. The data (mean ± SD) obtained for the brain and the body weight at P3 as well as the p values and the level of significance is presented in Table 3.1.

P12 (-/-) animals were obviously smaller than P12 (+/+) animals when judged by eye. This difference was not related to any disproportional changes in the brains. At first sight, the brain morphology in P12 (-/-) animals was similar to that of P12 (+/+), with the obvious exception that all structures were smaller. Further qualitative observation after Nissl staining procedure revealed also a normal cytoarchitecture in P12 (-/-) animals. The scatter plots of the brain weight as a function of the body weight from P12 (-/-) and P12 (+/+) animals showed that the values across the two categories were clearly separated **(Fig. 3.5A)**; those from (-/-) animals occupied the left bottom part of the graph whereas those from (+/+) animals occupied the right top part. In P12 (-/-) animals, the body weight was 54% of the value determined in P12 (+/+) animals **(Table 3.1)**. Moreover, the brain weight in P12 (-/-) animals was 81% from this in P12 (+/+) animals **(Table 3.1)**. Further statistical analysis revealed extremely significant differences between both the body weight and the brain weight values **(Fig. 3.5B,C)**. This, together

with the statistically significant difference between the two categories in the body weight at P3, shows that the body weight in (-/-) animals was more affected by the loss of KCC2 than the brain weight. The data (mean ± SD) obtained for the brain and the body weight at P12 as well as the p values and the level of significance is presented in Table 3.1. During development, there was an extremely significant increase of the body and the brain weight in both (-/-) and (+/+) animals **(Table 3.1)**. The body weight in (-/-)
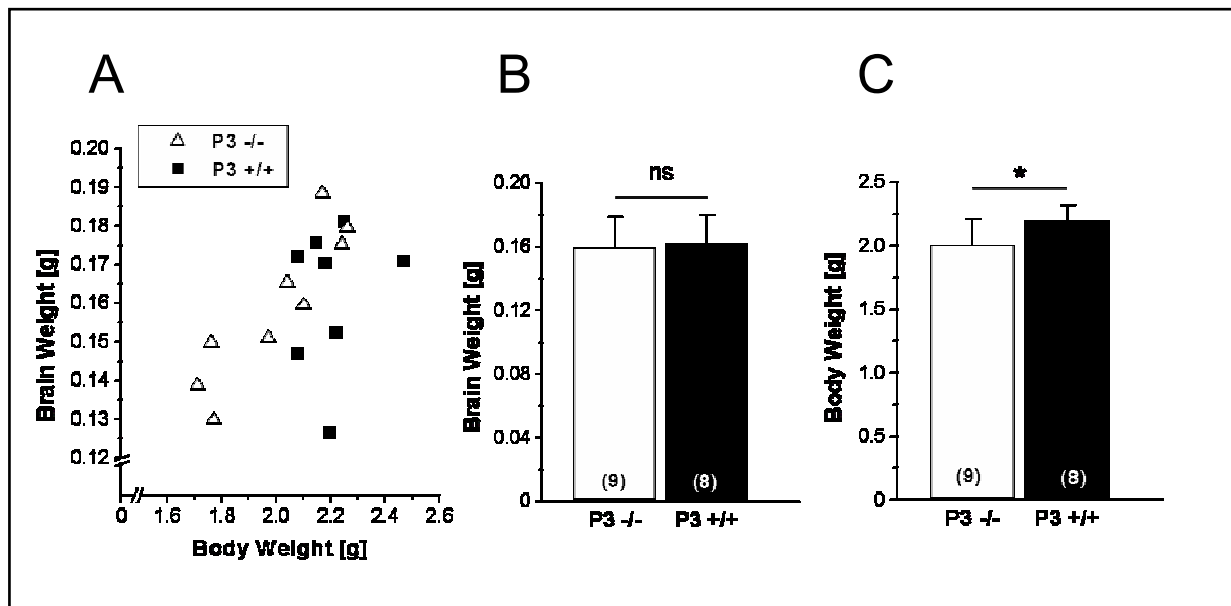
Figure 3.4: Comparison of brain weight and body weight at P3 between KCC2 homozygous null mice (-/-) and KCC2 wild-type mice (+/+)

(A) Scatter plots of brain weight against body weight for both categories. Open triangles (Δ) depict (-/-) mice and solid squares (■) (+/+) mice. The data were dispersed and only the body weight values for P3 (-/-) animals were slightly shifted to smaller values.
(B) Bar graph with mean body weight (±SD) of P3 (-/-) and P3 (+/+) mice. The body weight of P3 (-/-) animals was significantly lower than the body weight of (+/+) mice (p<0.05).
(C) Bar graph with mean brain weight (±SD) of P3 (-/-) and P3 (+/+) mice. There was no significant difference (p>0.05). Open bars depict (-/-) mice and solid bars (+/+) mice; asterisks refer to the presence of significant difference; ns refers to no significance; the number of animals for each category is shown in brackets; all this is also valid for subsequent figures.
The exact values of the mean (±SD) as well as the p values and the level of significance are shown in Table 3.1.
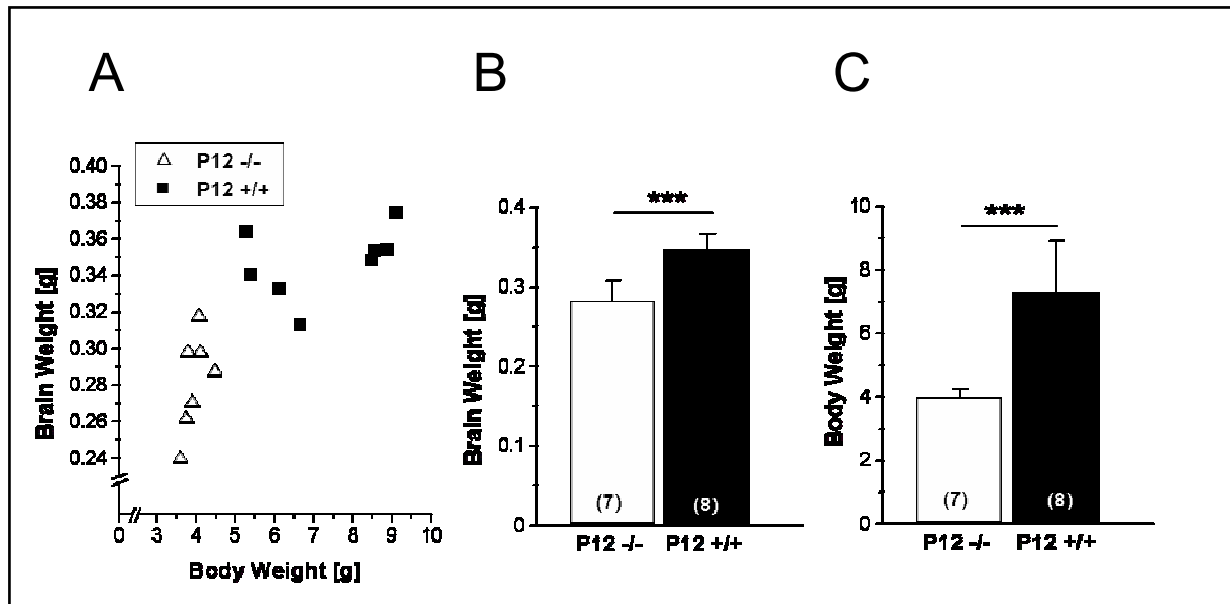
Figure 3.5: Comparison of brain weight and body weight at P12 between (-/-) and (+/+) mice.

(A) Scatter plots of brain weight against body weight for both categories. Open triangles (△) depict (-/-) mice and solid squares (■) (+/+) mice. The values across the two categories were clearly separated; those from (-/-) animals occupy the left bottom part of the graph whereas those from (+/+) animals occupy the right top part.

(B) and (C) Bar graphs with mean body weight (±SD) and mean brain weight (±SD) respectively, for P12 (-/-) and P12 (+/+) mice. For both parameters, values in P12 (-/-) animals were lower and the difference was extremely significant (p<0.001).

The exact values of the mean (±SD) as well as the p values and the level of significance are shown in Table 3.1.

Table 3.1: Data obtained for the brain weight and body weight

		Body Weight [g]		p	Brain Weight [g]		p
		-/-	+/+	-/- vs. +/+	-/-	+/+	-/- vs. +/+
	P3	2.00 ± 0.21	2.20 ± 0.12	*p=0.03	0.16 ± 0.02	0.16 ± 0.02	p=0.8
	P12	3.95 ± 0.29	7.31 ± 1.16	***p=0.0001	0.28 ± 0.03	0.35 ± 0.02	***p=0.00009
p	**P3 vs. P12**	***p=0.0000000003	***p=0.0000004		***p=0.00000004	***p=0.00000000001	

animals increased by a factor of 2.0. In comparison, the body weight in (+/+) animals increased by a factor of 3.3. Thus, the increase in body weight was much slower in (-/-) group. The brain weight in (-/-) animals increased by a factor of 1.8 and in (+/+) animals by a factor of 2.1. Thus, the increase in body weight during development in (+/+) animals was more pronounced than the increase in the brain weight. In contrast in (-/-) animals, the body weight increased by approximately the same factor during development as did the brain weight.

In other words, despite the body weight impairment observed in the KCC2 null animals, which was in part related to the seizure activity preventing normal feeding (Woo et al., 2002), the brains of these animals were less affected in terms of brain weight.

3.2.2   Absolute volume of the nuclei

The volume calculation of the four nuclei (VCN, LSO, MNTB, and MSO) was performed according to Cavalieri's principle (see 3.1.5 Stereological analysis. Volumetric data). The effect of KCC2 null mutation was different across the nuclei regarding this parameter **(Fig. 3.6)**. The values for nucleus volume (mean ± SD) as well as the p values and the level of significance are presented in Table 3.2.

The *VCN* volume was not significantly different between P3 (-/-) animals and P3 (+/+) animals **(Fig. 3.6A; Table 3.2)**. In contrast, the mean volume of the VCN in P12 (-/-) animals was 75% of the value determined in P12 (+/+) animals and the difference was extremely significantly **(Fig. 3.6A; Table 3.2)**. Between P3 and P12, there was an extremely significant increase of the VCN volume in both groups **(Fig. 3.6A; Table 3.2)**. In (-/-) animals, the VCN volume increased by a factor of 2.1. In (+/+) animals, the VCN volume increased by a factor of 2.7. Thus, in (-/-) animals, the developmental rate was decreased and the VCN volume reached smaller values at P12 compared to (+/+) animals at this age.

The *MNTB* volume was not significantly different between P3 (-/-) and P3 (+/+) animals **(Fig. 3.6B; Table 3.2)**. In contrast, the mean volume of the MNTB in P12 (-/-) animals was 77% of the value determined in P12 (+/+) animals and the difference was extremely significant **(Fig. 3.6B; Table 3.2).** Between P3 and P12, there was an extremely significant increase of the MNTB volume in both groups **(Fig. 3.6B)**. In (-/-)

animals, the MNTB volume increased by a factor of 1.7; in (+/+) animals the MNTB volume increased by a factor of 2.1. This shows that in the (-/-) animals, the developmental rate was also decreased and the MNTB volume reached smaller values at P12 than in the (+/+) animals.

In contrast, in the **MSO** neither at P3 nor at P12, statistical difference of the MSO mean volume between (-/-) and (+/+) animals occurred **(Fig. 3.6C; Table 3.2)**. In both groups, there was a significant or very significant increase in the MSO volume during development, respectively for (-/-) and (+/+) animals **(Fig. 3.6C; Table 3.2)**. The range of increase was 1.3-fold for both groups. Thus, the developmental rate of the MSO volume was preserved in (-/-) and in (+/+) animals.

The **LSO** absolute volume, as in the VCN and in the MNTB at P3 (-/-) animals, was not significantly different compare to P3 (+/+) animals **(Fig. 3.6D; Table3.2)**. However, the mean volume of the LSO in P12 (-/-) animals was 71% of the value determined in P12 (+/+) animals and the difference was extremely significantly **(Fig. 3.6D; Table 3.2).** During development, there was an extremely significant increase of the LSO volume in both groups **(Fig. 3.6D; Table 3.2)**. In (-/-) animals, the LSO volume increased by a factor of 1.4; in (+/+) animals, by a factor of 1.7. Thus, in (-/-) animals the developmental rate was decreased and the LSO volume reached smaller values at P12.

In summary, in all four nuclei no difference in the absolute volume occurred at P3. In the VCN, the MNTB, and the LSO there was an extremely significant difference in the absolute volume between (-/-) and (+/+) animals at P12. Only in the MSO the investigated parameter was not different between the two categories P12 (-/-) and P12 (+/+). During development in (-/-) animals, the developmental rate was decreased and in the VCN, the MNTB, and the LSO the absolute volume reached smaller values at P12 compared to P12 (+/+) animals, consistent with the smaller brains in P12 (-/-) animals **(Fig. 3.5B)**. However, the developmental rate of the MSO absolute volume between P3 and P12 was preserved in (-/-) and in (+/+) group.
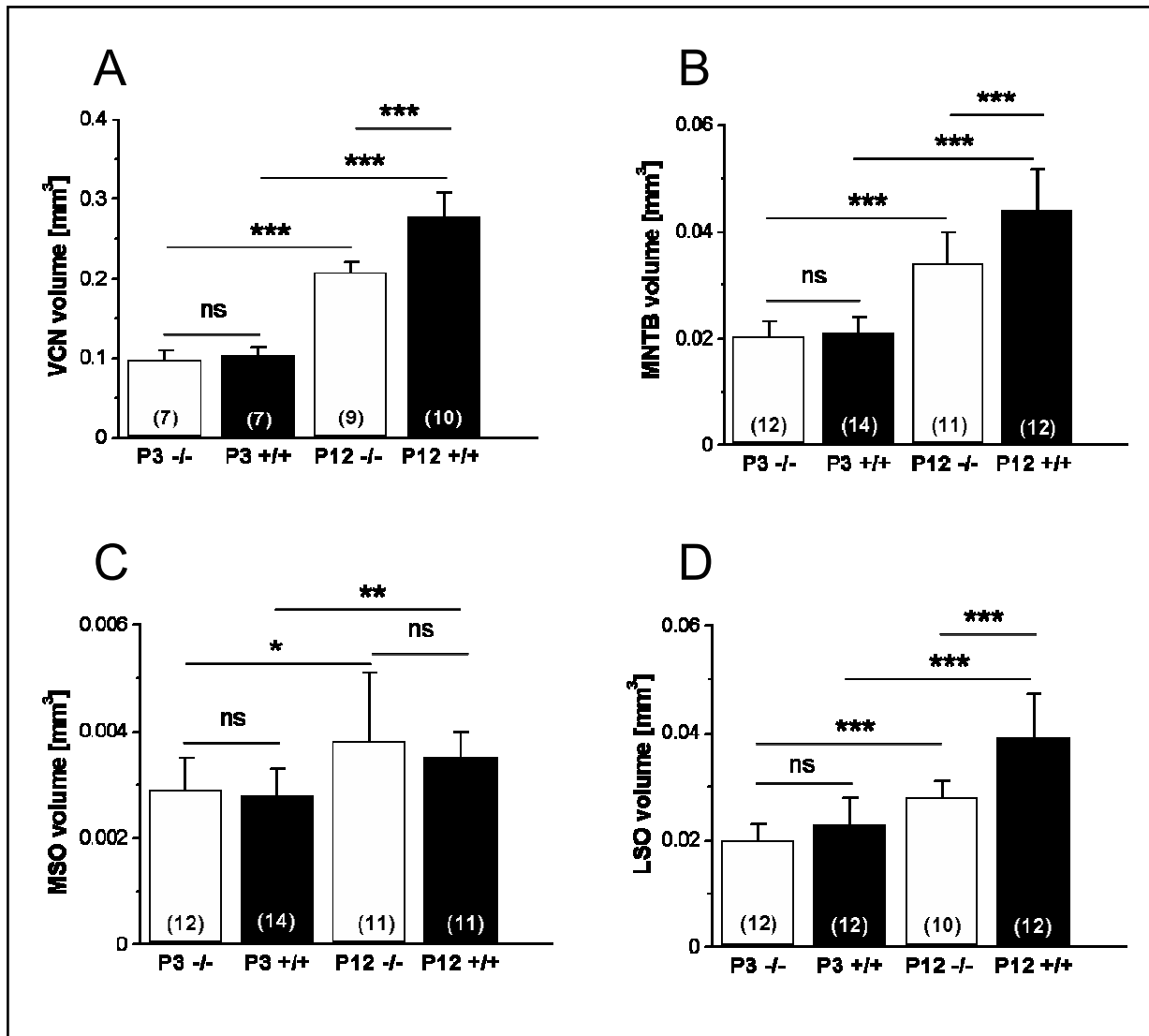
Figure 3.6: Volume calculation of the four nuclei (VCN, LSO, MNTB, and MSO) according to Cavalieri's principle

Statistical comparison was done between (-/-) and (+/+) mice at each age, as well as during development within each group. Note that the scaling of the Y axis is different between graphs.

(A) Mean volume (±SD) of the VCN for the four categories. The graph shows that at P3, the VCN volume was not significantly different between (-/-) and (+/+) animals (p>0.05). In contrast, the VCN volume was smaller in P12 (-/-) animals than in P12 (+/+) animals and the difference was extremely significant (p<0.001). In both groups, there was an extremely significant increase of the nucleus volume during development (p<0.001).
(B) Mean volume (±SD) of the MNTB for the four categories. The graph shows that at P3, the MNTB volume was not significantly different between (-/-) and (+/+) mice (p>0.05). In contrast, the MNTB volume was smaller in P12 (-/-) animals than in P12 (+/+) animals and the difference was extremely significant (p<0.001). In both groups, there was an extremely significant increase of the nucleus volume during development (p<0.001).
(C) Mean volume (±SD) of the MSO for the four categories. The graph shows that at P3, the MSO volume was not significantly different between (-/-) and (+/+) mice as well as at P12 between (-/-) and (+/+) mice (p>0.05). In both groups, there was very significant increase of the nucleus volume during development (p<0.01).

Table 3.2: Stereological volume data for the four nuclei: VCN, LSO, MNTB and MSO

	VCN volume [mm³]		p	MNTB volume [mm³]		p
	-/-	+/+	-/- vs. +/+	-/-	+/+	-/- vs. +/+
P3	0.098 ± 0.011	0.103 ± 0.011	p=0.4	0.020 ± 0.003	0.021 ± 0.003	p=0.6
P12	0.208 ± 0.012	0.279 ± 0.032	***p=0.000009	0.034 ± 0.006	0.045 ± 0.007	***p=0.0007
p P3 vs. P12	***p=0.00000000003	***p=0.0000000005		***p=0.0000002	***p=0.00000000001	

	MSO volume [mm³]		p	LSO volume [mm³]		p
	-/-	+/+	-/- vs. +/+	-/-	+/+	-/- vs. +/+
P3	0.0029 ± 0.0006	0.0028 ± 0.0005	p=0.8	0.020 ± 0.003	0.023 ± 0.005	p=0.05
P12	0.0038 ± 0.0013	0.0035 ± 0.0005	p=0.6	0.028 ± 0.003	0.039 ± 0.008	***p=0.0004
p P3 vs. P12	*p=0.04	**p=0.001		***p=0.000001	***p=0.000002	

3.2.3   Relative volume, neuron number, soma cross-sectional area and relative somata area of the nuclei

In order to minimize the error in the measurement of raw nuclear volumes in KCC2 null mice due to a retardation in development and the smaller brains in P12 (-/-) animals, I used for each comparison the ratio "nucleus volume/brain weight" (relative volume) instead of absolute volumes. In the following part, values for the relative volume, together with the other three investigated features (neuron number, soma cross-sectional area and relative somata area), will be presented separately for each nucleus. Two of them are values obtained from direct measurements (the soma cross-sectional area and the neuron number); the other two (the relative volume and the relative somata area) are relative calculations, based on absolute values (for definition, see 3.1.6 Morphometric analysis).

← *previous page*

(D) Mean volume (±SD) of the LSO for the four categories. The graph shows that at P3, the LSO volume was not significantly different between (-/-) and (+/+) mice (p=0.05). In contrast, the LSO volume was smaller in P12 (-/-) animals than in P12 (+/+) animals and the difference was extremely significant (p<0.001). In both groups, there was an extremely significant increase of the nucleus volume during development (p<0.001). The exact values of the mean (±SD) as well as the p values and the level of significance are shown in Table 3.2.

3.2.3.1   VCN

The data (mean ± SD) as well as the p values and the level of significance are presented in Table 3.3. Figures 3.7 and 3.8 provide relevant column diagrams.

P3. The nucleus volume/brain weight ratio was not significantly different between (-/-) and (+/+) animals **(Fig.3.7A; Table 3.3).** The VCN occupied approximately the same relative volume in the brain of both categories at this age. The number of VCN neurons was significantly lower in P3 (-/-) animals than in P3 (+/+) animals **(Fig. 3.7B; Table 3.3)** and differs by a factor of 1.3. There was no significant difference in the mean soma area between the two categories **(Fig. 3.7C; Table 3.3).** However, 1.1-fold smaller relative somata area was obtained in P3 (-/-) animals compare to P3 (+/+) animals; the difference was very significant **(Fig. 3.7D; Table 3.3).**

P12. The nucleus volume/brain weight ratio was not significantly different between (-/-) animals and (+/+) animals **(Fig. 3.8A; Table 3.3)**; i.e. the VCN occupied approximately the same relative volume in the brain of both categories at this age. The number of VCN neurons, however, was 1.3-fold lower in P12 (-/-) animals than in P12 (+/+) animals; the difference was very significant **(Fig. 3.8B; Table 3.3).** Note that the neuron number was statistically different also between P3 (-/-) and P3 (+/+) animals by the same factor (1.3-fold). There was no significant difference in the mean soma area **(Fig. 3.8C; Table 3.3)** and in the relative somata area **(Fig. 3.8D; Table 3.3)** between the two categories at this age.

Table 3.3: Morphometric characteristics of VCN

		Nucleus Volume/Brain Weight [mm³/g]		p	Neuron Number in Nucleus		p
		-/-	+/+	-/- vs. +/+	-/-	+/+	-/- vs. +/+
	P3	0.64±0.07	0.64±0.06	p=1	15 385±2 673	19 248±2 933	*p=0.02
	P12	0.77±0.04	0.85±0.07	p=0.06	21 645±2 168	27 582±4 859	**p=0.004
p	P3 vs. P12	**p=0.003	**p=0.004		***p=0.0001	**p=0.001	

		Soma Cross-sectional Area [µm²]		p	Relative Somata Area		p
		-/-	+/+	-/- vs. +/+	-/-	+/+	-/- vs. +/+
	P3	90±13	83±7	p=0.3	0.35±0.02	0.39±0.02	**p=0.003
	P12	136±7	148±17	p=0.06	0.36±0.04	0.37±0.02	p=0.3
p	P3 vs. P12	***p=0.0000003	***p=0.00000007		p=0.7	p=0.1	
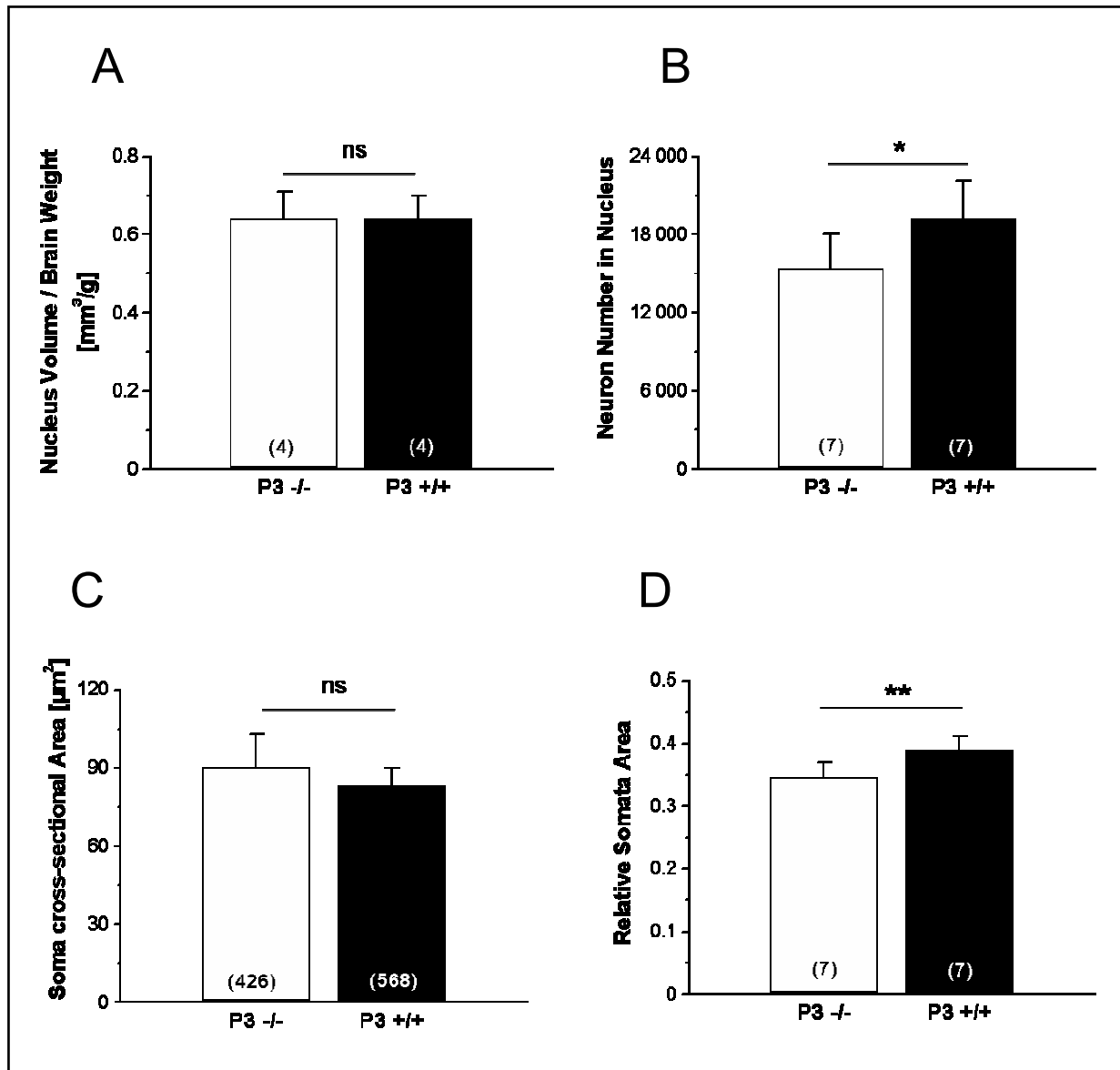
Figure 3.7: Comparison of four characteristic features (nucleus volume/brain weight, neuron numbers, soma cross-sectional area and relative somata area) determined in the VCN between P3 (-/-) and P3 (+/+)

(A) Nucleus volume/brain weight. There was no significant difference (p>0.05). The VCN occupied the same relative volume in the brain of both categories at this age.

(B) Neuron numbers. There was a significantly lower neuron number in P3 (-/-) animals than in P3 (+/+) animals (p<0.05). The values represent the calculation based on counting in a rectangular block with the size of 200 µm x 100 µm x 25 µm (see 3.1.6 Morphometric analysis).

(C) Soma cross-sectional area. There was no significant difference (p>0.05). The number of measured somata is shown in brackets; this is valid for panel C in Figures 3.8, 3.10, 3.11, 3.13, 3.14, 3.16, 3.17.

(D) Relative somata area. It appeared a significantly smaller relative somata area in P3 (-/-) animals (p<0.01). This is related to a lower neuron number in these animals compared to P3 (+/+) (panel B, same figure).

The exact values of the mean (±SD) as well as the p values and the level of significance are shown in Table 3.3.
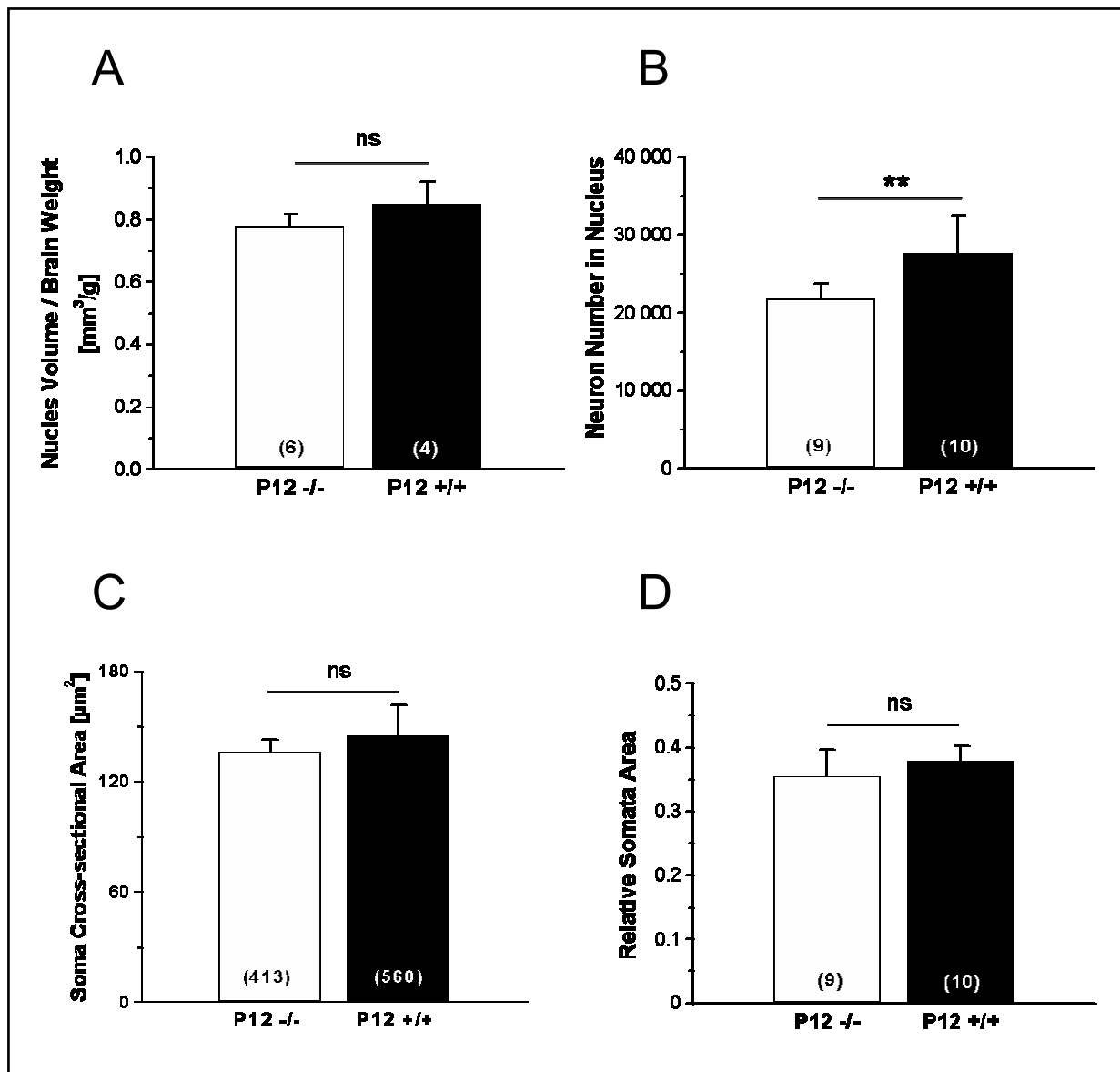
Figure 3.8: Comparison of the four characteristic features determined in the VCN between P12 (-/-) and P12 (+/+)

(A) Nucleus volume/brain weight. There was no significant difference (p>0.05). The VCN occupied the same relative volume in the brain of both categories at this age.

(B) Neuron numbers. There was lower neuron number in P12 (-/-) animals compare to P12 (+/+) animals and the difference was very significant (p<0.01). The counting block has the same size as in P3 animals (see 3.1.6 Morphometric analysis).

(C) Soma cross-sectional area. There was no significant difference (p>0.05).

(D) Relative somata area. There was no significant difference (p>0.05). This is related to lower neuron number in P12 (-/-) than in P12 (+/+), which occupy less volume (panel B, same figure).

The exact values of the mean (±SD) as well as the p values and the level of significance are shown in Table 3.3.

P3 vs. P12. The comparison in the groups during development revealed that the nucleus volume/brain weight ratio at P12 differed from the values obtained at P3 by a factor of 1.2 for the (-/-) group and by a factor of 1.3 for the (+/+) group **(Table 3.3)**; the difference was very significant. Thus, the VCN at P12 occupied more place in the brain compared to P3. In both groups, the VCN absolute volume increased by approximately the same factor and the nucleus occupied about the same place in the brain. In both groups, the neuron number increased 1.4-fold between P3 and P12; the difference was extremely significant for the (-/-) group and very significant for the (+/+) group. In both groups, the soma cross-sectional area increased with age by a factor of 1.5 in (-/-) animals and by a factor of 1.8 in (+/+) animals; the difference was extremely significant. The relative somata area did not change during development in both groups.

3.2.3.2   Summary for the VCN

P3. The relative somata area is determined by the neuron number and the soma cross-sectional area. As mentioned above, there was no difference in the soma cross-sectional area between the (-/-) animals and the (+/+) animals. Thus, the lower neuron number in the (-/-) group accounted for less relative somata area in these animals than in the (+/+) group **(Fig. 3.9)**.

P12. In (-/-) animals, the lower number of neurons (1.3-fold) and the lack of a difference in the soma cross-sectional area compared to (+/+) animals should account for smaller relative somata area **(Fig. 3.8)**. However, the absolute VCN volume of (-/-) animals was significantly smaller compared to (+/+) animals with the same factor (1.3-fold) **(Fig. 3.6A)** and this contributed to the result that the relative somata area was not significantly different between the categories **(Fig. 3.8, 3.9)**.

P3 vs. P12. In general, in both groups, the investigated parameters changed in the same direction within the similar range: nucleus volume/brain weight ratio demonstrated that VCN occupied more place in the brain at P12; the neuron number increased with the same factor (1.4-fold) with age; soma cross-sectional area increased with factor of 1.5-fold and 1.8-fold in (-/-) and (+/+) animals, respectively **(Table 3.3)**; absolute volume increased with factor of 2.1-fold and 2.8-fold in (-/-) and (+/+) animals, respectively **(Table 3.2)**, due to the observed grow retardation. Thus, no parameter in the VCN underwent a disproportional change due to null mutation **(Fig. 3.9)**.
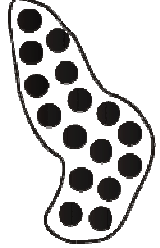
Figure 3.9: Summary drawing for the VCN after comparison between the four categories

No disproportional changes in the VCN were observed. Surprisingly, difference in the number of neurons between mutants and controls at P3 occur. The neurons increase during development, yet with the same factor in (-/-) and in (+/+) group.

3.2.3.3   MNTB

The data (mean ± SD) as well as the p values and the level of significance are presented in Table 3.4. Figures 3.10 and 3.11 provide relevant column diagrams.

P3. There was no significant difference in the nucleus volume/brain weight ratio **(Fig. 3.10A)**, the neuron number **(Fig. 3.10B)**, the soma cross-sectional area **(Fig. 3.10C)**, and the relative somata area **(Fig. 3.10D)** between (-/-) and (+/+) animals. These results indicate that the MNTB nucleus is not influenced by the KCC2 null mutation at this age in respect to the analysed morphometric parameters.

P12. There was no significant difference in the nucleus volume/brain weight ratio **(Fig. 3.11A)**, the neuron number **(Fig. 3.11B)**, and the soma cross-sectional area **(Fig. 3.11C).** The only parameter that displayed a significant difference was the relative somata area; it was 1.2-fold larger in (-/-) animals compared to (+/+) animals **(Fig. 3.11D)**.
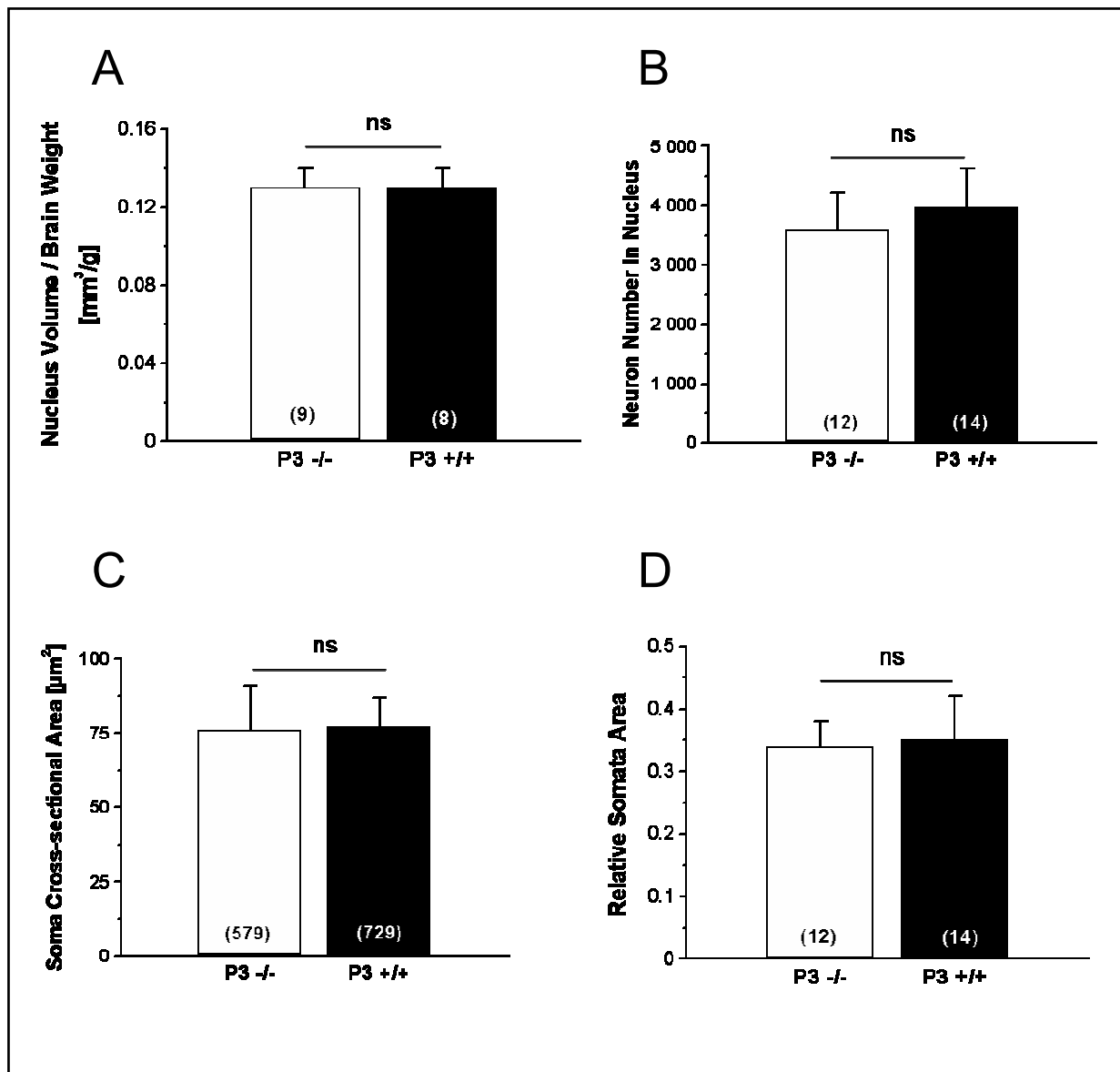
Figure 3.10: Comparison of the four characteristic features determined in the MNTB between P3 (-/-) and P3 (+/+)

(A) Nucleus volume/brain weight. There was no significant difference (p>0.05). The MNTB occupied the same relative volume in the brain of both categories at this age.

(B) Neuron numbers. There was no significant difference (p>0.05). The values represent calculation based on counting in a rectangular block with the size of 200 μm x 50 μm x 25 μm (see 3.1.6 Morphometric analysis).

(C) Soma cross-sectional area. There was no significant difference (p>0.05).

(D) Relative somata area. There was no significant difference (p>0.05). This is related to no significant change in the other parameters between (-/-) and (+/+) animals at this age.

The exact values of the mean (±SD) as well as the p values and the level of significance are shown in Table 3.4.
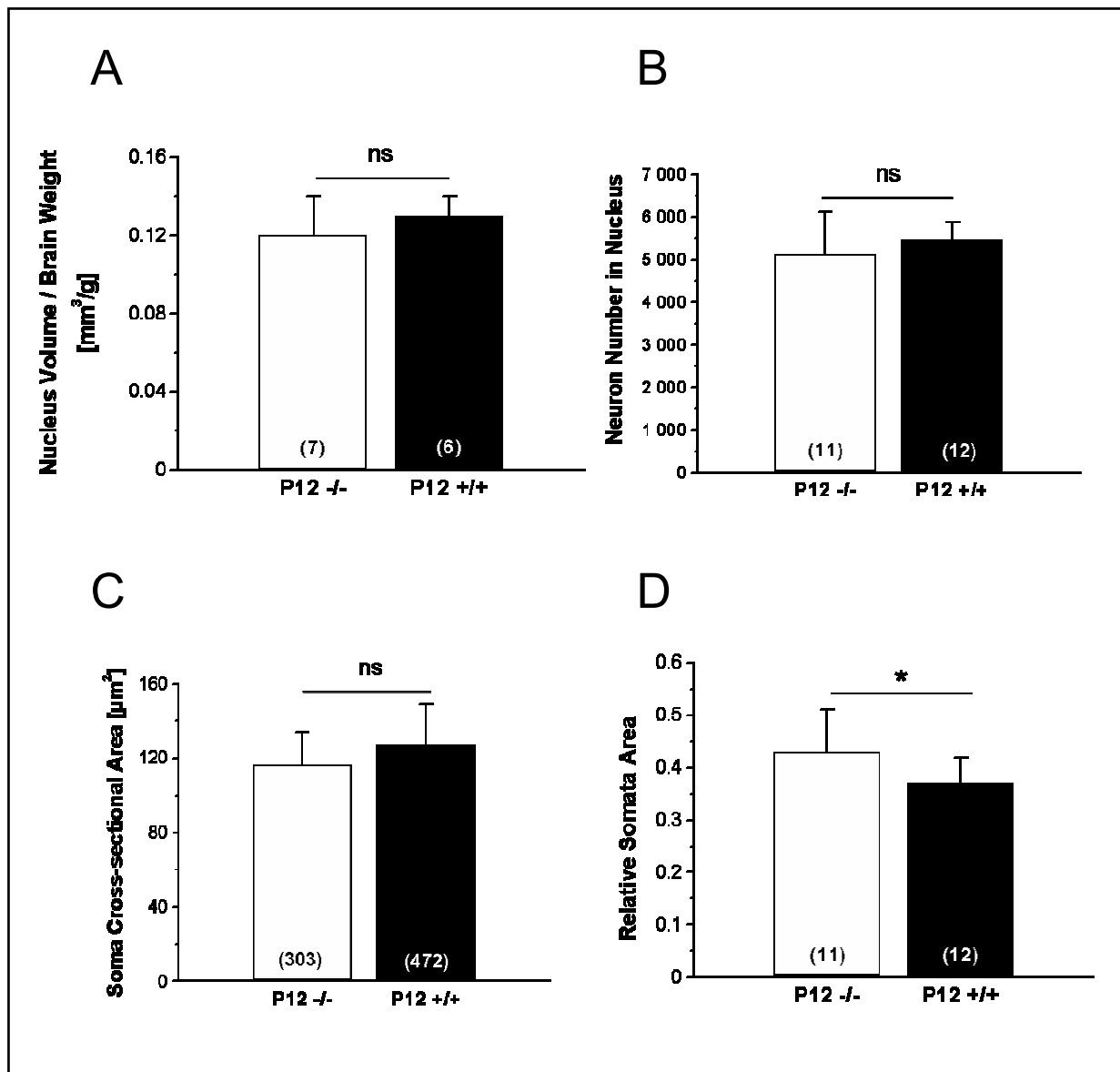
Figure 3.11: Comparison of the four characteristic features determined in the MNTB between P12 (-/-) and P12 (+/+)

(A) Nucleus volume/brain weight. There was no significant difference (p>0.05). The MNTB occupied the same relative volume in the brain of both categories at this age.
(B) Neuron numbers. There was no significant difference (p>0.05). The counting block has the same size as in P3 animals (see 3.1.6 Morphometric analysis).
(C) Soma cross-sectional area. There was no significant difference (p>0.05).
(D) Relative somata area. There was a significantly larger relative somata area in P12 (-/-) animals (p<0.05). It appeared that the smaller absolute volume in P12 (-/-) animals (Fig. 3.6C) is due to less neuropil.
The exact values of the mean (±SD) as well as the p values and the level of significance are shown in Table 3.4.

Table 3.4: Morphometric characteristics of MNTB

		Nucleus Volume/Brain Weight [mm³/g]		p	Neuron Number in Nucleus		p
		-/-	+/+	-/- vs. +/+	-/-	+/+	-/- vs. +/+
	P3	0.13±0.01	0.13±0.01	p=0.9	3 745±704	4 144±494	p=0.1
	P12	0.12±0.02	0.13±0.01	p=0.6	5 117±996	5 454±422	p=0.3
p	P3 vs. P12	p=0.05	p=0.3		**p=0.001	***p=0.0000002	

		Soma Cross-sectional Area [µm²]		p	Relative Somata Area		p
		-/-	+/+	-/- vs. +/+	-/-	+/+	-/- vs. +/+
	P3	76±15	76±10	p=1	0.34±0.04	0.35±0.07	p=0.7
	P12	116±18	127±22	p=0.2	0.43±0.08	0.37±0.05	*p=0.03
p	P3 vs. P12	***p=0.00001	***p=0.00000003		**p=0.001	p=0.3	

P3 vs. P12. The nucleus volume/brain weight ratio was significantly different in both groups during development. Thus, the MNTB grew proportionally to the brain growth and occupied the same place at both ages **(Table 3.4)**. With respect to neuron number, surprisingly, there was very significant increase in the (-/-) group by a factor of 1.4 and extremely significant increase in the (+/+) group by a factor of 1.3 **(Table 3.4)**. The soma cross-sectional area in both groups increased by a factor of 1.5 in the (-/-) animals and by a factor of 1.7 in the (+/+) animals; the difference was extremely significant **(Table 3.4)**. The relative somata area in the (-/-) group increased significantly with age by a factor of 1.3; in (+/+) animals, there was no significant change **(Table 3.4)**.

3.2.3.4   Summary for the MNTB

P3. The MNTB is not influenced by the KCC2 null mutation in respect to the parameters that have been analysed **(Fig. 3.12)**.

P12. The lack of difference in the neuron number and the soma cross-sectional area between the two groups could not account for the significantly bigger relative somata area in the (-/-) animals compared to (+/+) animals at this age (1.2-fold) **(Fig. 3.11)**. However, the absolute volume of MNTB in the (-/-) group was significantly smaller than in the (+/+) group (1.3-fold) **(Fig. 3.6B)**. In this case, the less neuropil part in the (-/-) animals is the feature that contributed to the difference in the nucleus volume and the relative somata area between the two groups at this age **(Fig. 3.12)**.

Figure 3.12: Summary drawing for the MNTB after comparison between the four categories

No difference in the investigated parameters occurs at P3. Less pronounced neuropil part in mutants in comparison to controls at P12 and increase numbers of neuron during development in both groups characterize the main changes in this nucleus.

P3 vs. P12. Surprisingly, but together with the results from the VCN, there was increase in the neuron number in both groups by a similar factor (1.4-fold in (-/-) group and 1.3-fold in (+/+) group) as well as in soma cross-sectional area (1.5-fold in (-/-) group and 1.7-fold in (+/+) group) **(Table. 3.4)**. In the (+/+) group, these changes were compensated with increase of the absolute volume between P3 and P12 (2.1-fold) **(Table 3.2)** i.e. the increase of the soma part correlated with increase in the neuropil part in a way that the relative somata area during development stayed unchanged **(Fig. 3.12; Table 3.4)**. However, in the (-/-) group the rate of increase in the absolute volume was smaller (1.7-fold) **(Table 3.2)** and the change in the neuropil part were less pronounced during development. This led to the increase in relative somata area in (-/-) animals with age **(Fig. 3.12; Table 3.4)**.

3.2.3.5   MSO

The data (mean ± SD) as well as the p values and the level of significance are presented in Table 3.5. Figures 3.13 and 3.14 provide relevant column diagrams.

P3. There was no significant difference in the nucleus volume/brain weight ratio **(Fig. 3.13A)**, the neuron number **(Fig. 3.13B)**, the soma cross-sectional area **(Fig. 3.13C)** and the relative somata area **(Fig. 3.13D)** between (-/-) and (+/+) animals. These results show that the MSO is not influenced by the KCC2 null mutation at this age in respect to the parameters that have been analysed.

P12. There was no significant difference in the nucleus volume/brain weight ratio **(Fig. 3.14A)** and the neuron number **(Fig. 3.14B)** between (-/-) and (+/+) animals. In contrast to the VCN and MNTB nuclei, a significantly smaller soma cross-sectional area was found in P12 (-/-) animals compared to P12 (+/+) animals **(Fig. 3.14C)**; the two values differed by a factor of 1.2. In P12 (-/-) 1.2-fold smaller relative somata area was obtained compared to P12 (+/+) animals and the difference was extremely significant **(Fig. 3.14D)**.

P3 vs. P12. The comparison in the groups revealed that the nucleus volume/brain weight ratio at P12 differed from the values at P3 by a factor of 0.7 for the (-/-) group and by a factor of 0.6 for the (+/+) group; the difference was significant for (-/-) animals and extremely significant for (+/+) animals **(Table 3.5)**. Thus, in contrast to the VCN that occupied more place in the brain at P12 then at P3 **(Table 3.3)** and to the MNTB which grew proportionally to the brain **(Table 3.4)**, the MSO occupied significantly less place in the brain in both groups at P12 then at P3. With respect to neuron numbers, no statistically significant change occurred in both groups. The soma cross-sectional area in the (+/+) group increased significantly by a factor of 1.2. In contrast, the soma cross-sectional area in the (-/-) group was not significantly altered during development. In both groups, there was no significant change in the relative somata area **(Table 3.5)**.

3.2.3.6   Summary for the MSO

P3. The MSO is not influenced by the KCC2 null mutation in respect to the parameters that have been analysed **(Fig. 3.15)**.

P12. The lack of difference in the neuron number and in the absolute volume between (-/-) and (+/+) animals **(Fig. 3.14)** but the smaller soma cross-sectional area in
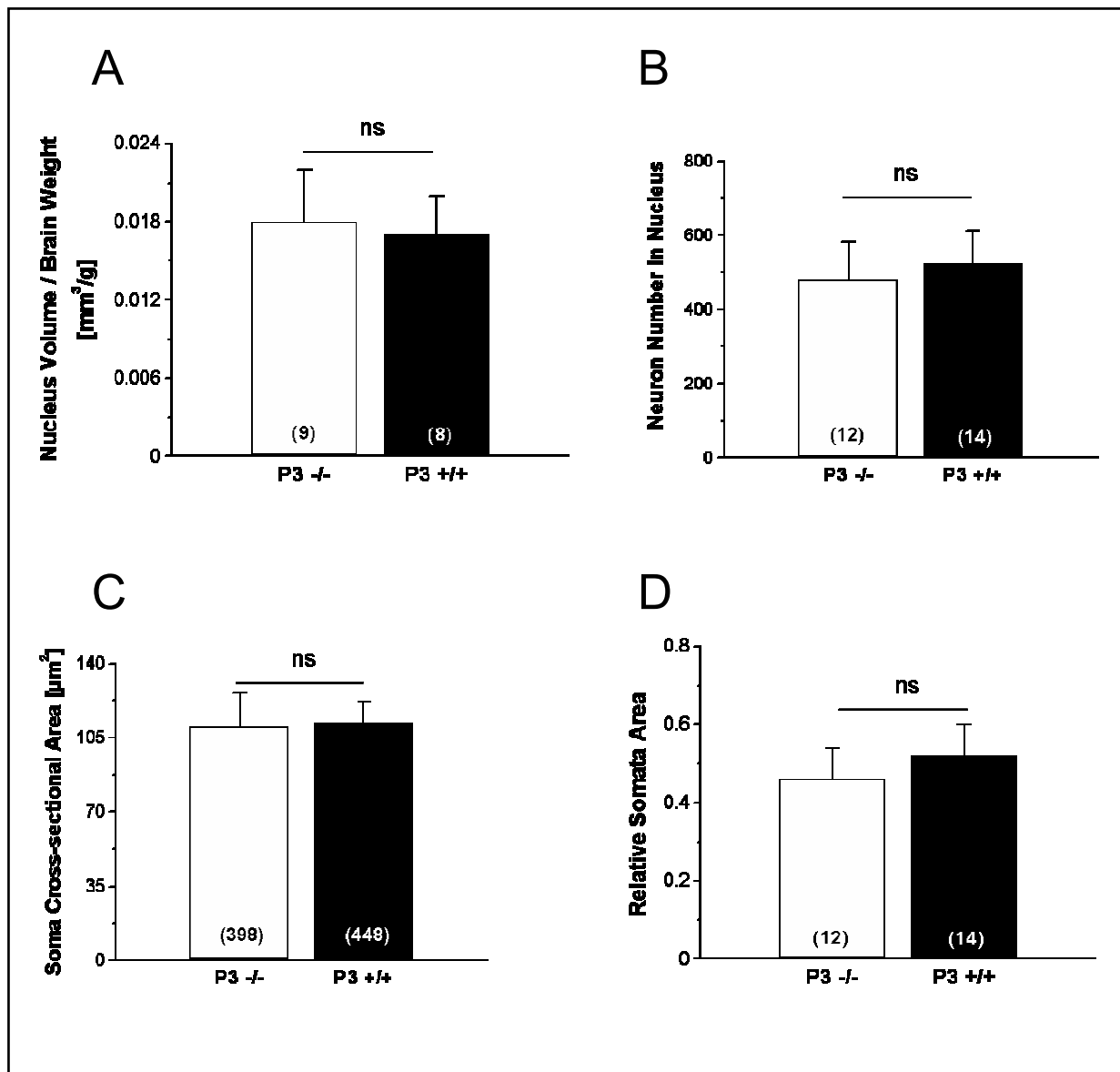
Figure 3.13: Comparison of the four characteristic features determined in the MSO between P3 (-/-) and P3 (+/+)

(A) Nucleus volume/brain weight. There was no significant difference (p>0.05). MSO occupied the same relative volume in the brain of both categories at this age.

(B) Neuron numbers. There was no significant difference (p>0.05). The values represent calculation based on counting in a block with the size of surface area of MSO in the current slice multiplied by 25 µm (see 3.1.6 Morphometric analysis).

(C) Soma cross-sectional area. There was no significant difference (p>0.05).

(D) Relative somata area. There was no significant difference (p>0.05). This is related to no significant change in the other parameters between (-/-) and (+/+) animals at P3.

The exact values of the mean (±SD) as well as the p values and the level of significance are shown in Table 3.5.
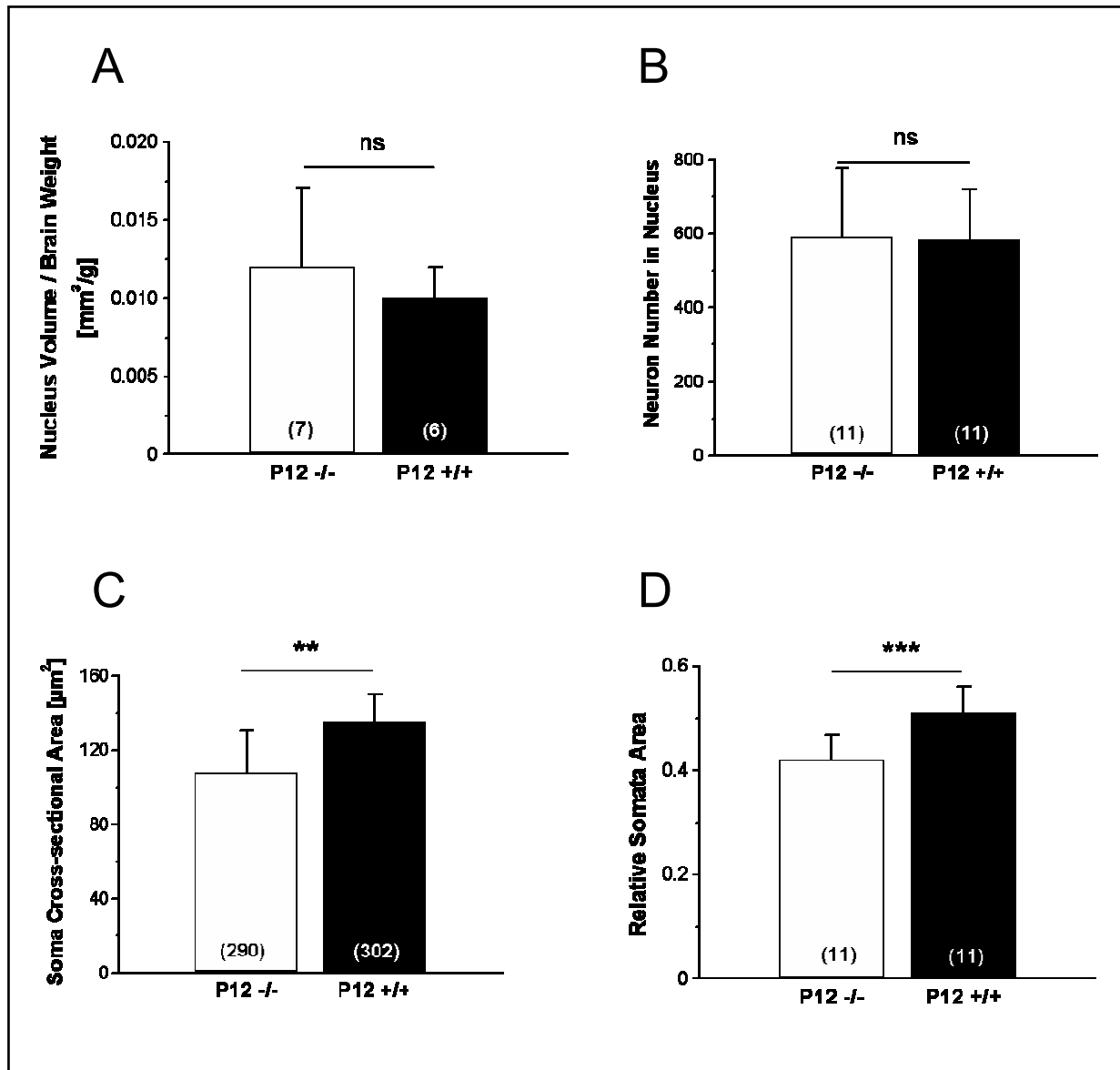
Figure 3.14: Comparison of the four characteristic features determined in the MSO between P12 (-/-) and P12 (+/+)

(A) Nucleus volume/brain weight. There was no significant difference (p>0.05). The MSO occupied the same relative volume in the brain of both categories at this age.

(B) Neuron numbers. There was no significant difference (p>0.05). The values represent calculation based on counting in a block with the size of surface area of MSO in the current slice multiplied by 25 µm (see 3.1.6 Morphometric analysis).

(C) Soma cross-sectional area. A significantly smaller mean soma area was present in P12 (-/-) animals compared to P12 (+/+) animals (p<0.001).

(D) Relative somata area. There was smaller relative somata area in P12 (-/-) animals compare to P12 (+/+) animals and the difference was extremely significant (p<0.001). This is due to the smaller soma cross-sectional area in these animals.

The exact values of the mean (±SD) as well as the p values and the level of significance are shown in Table 3.5.

**Table 3.5:** Morphometric characteristics of MSO

		Nucleus Volume/Brain Weight [mm³/g]		p	Neuron Number in Nucleus		p
		-/-	+/+	-/- vs. +/+	-/-	+/+	-/- vs. +/+
	P3	0.018±0.004	0.017±0.003	p=0.4	478±103	522±91	p=0.3
	P12	0.012±0.005	0.010±0.002	p=0.3	589±186	581±136	p=0.9
p	P3 vs. P12	*p=0.03	***p=0.0003		p=0.09	p=0.2	
		Soma Cross-sectional Area [µm²]		p	Relative Somata Area		p
		-/-	+/+	-/- vs. +/+	-/-	+/+	-/- vs. +/+
	P3	110±16	112±10	p=0.6	0.46±0.08	0.52±0.08	p=0.05
	P12	108±23	135±15	**p=0.006	0.42±0.05	0.52±0.05	***p=0.0003
p	P3 vs. P12	p=0.9	***p=0.0002		p=0.2	p=0.9	

 (-/-) animals (1.2-fold) accounted for their smaller relative somata area compared to (+/+) animals (again with the same factor 1.2-fold) **(Fig. 3.14, 3.15)**.

P3 vs. P12. In the MSO, as in the MNTB, no equal changes took place in the (-/-) and the (+/+) group. In (+/+) animals, there was a significant increase in the soma cross-sectional area with age (1.2-fold) but no change in the relative somata area **(Table 3.5)**. The increased absolute volume at P12 (1.3-fold) **(Table 3.2)** is a possible reason for this lack of difference in the relative somata area i.e. the development of the neuropil part followed the increasing of the somata part. In (-/-) animals, there was no difference in the relative somata area with age due to lack of difference in the neuron number and the soma cross-sectional area **(Table 3.5)**. However, there was a difference (1.3-fold) in the absolute volume between P3 (-/-) and P12 (-/-) animals. This result can be related only to increased neuropil part **(Fig. 3.15)**.
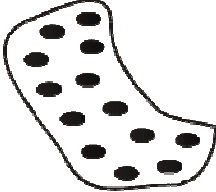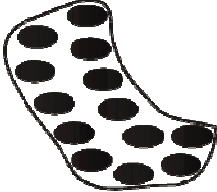
Figure 3.15: Summary drawing for the MSO after comparison between the four categories

No difference in the investigated parameters occurs at P3. No difference in the absolute volume and smaller soma cross-sectional area in mutants in comparison to controls at P12 characterizes the main changes in this nucleus.

3.2.3.7   LSO

The data (mean ± SD) as well as the p values and the level of significance are presented in Table 3.6. Figures 3.16 and 3.17 provide relevant column diagrams.

Note: in this nucleus one-way ANOVA test was applied for three-group comparison regarding the data from the medial, middle and lateral region. No significant regional difference was present in the values obtained from direct measurements: number of neurons, soma cross-sectional area and somata area occupation. Further calculation and comparison of the relative somata area in the three regions in the LSO was not made and the results for this nucleus are presented without differentiation between the medial, middle and the lateral part.

P3. The nucleus volume/brain weight ratio was not significantly different between (-/-) and (+/+) animals **(Fig. 3.16A)** i.e., the LSO occupied approximately the same relative volume in the brain of both categories at this age. There was no significant difference in the soma cross-sectional area **(Fig. 3.16C)** and in the relative somata area
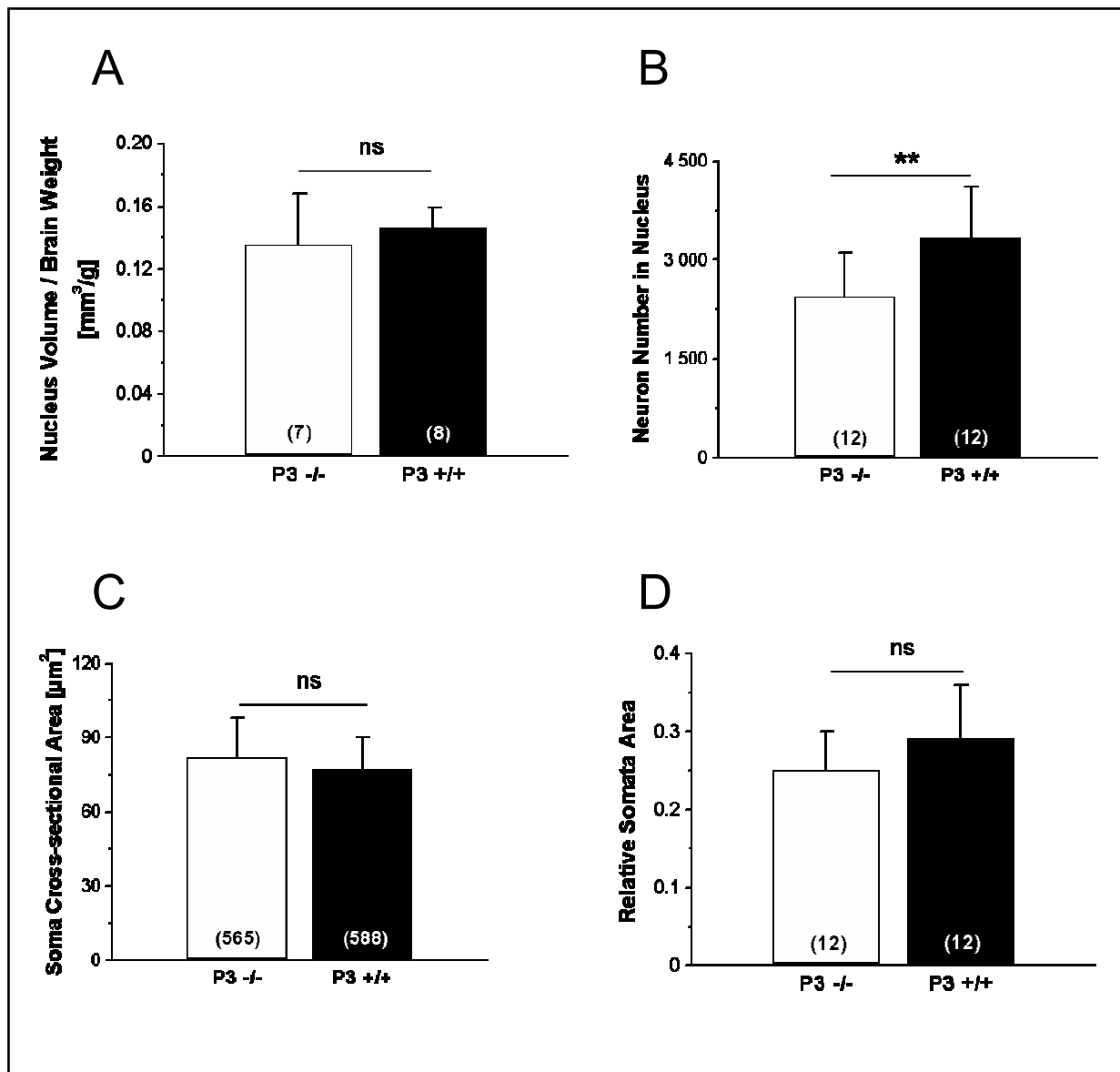
Figure 3.16: Comparison of the four characteristic features determined in the LSO between P3 (-/-) and P3 (+/+)

(A) Nucleus volume/brain weight. There was no significant difference (p>0.05). The LSO occupied the same relative volume in the brain of both categories at this age.

(B) Neuron numbers. There was a lower neuron number in P3 (-/-) animals and the difference was very significant (p<0.01). The values represent calculation based on counting in three rectangular blocks with the size of 100 µm x 50 µm x 25 µm each (see 3.1.6 Morphometric analysis).

(C) Soma cross-sectional area. There was no significant difference (p>0.05).

(D) Relative somata area. There was no significant difference (p>0.05).

The exact values of the mean (±SD) as well as the p values and the level of significance are shown in Table 3.6.
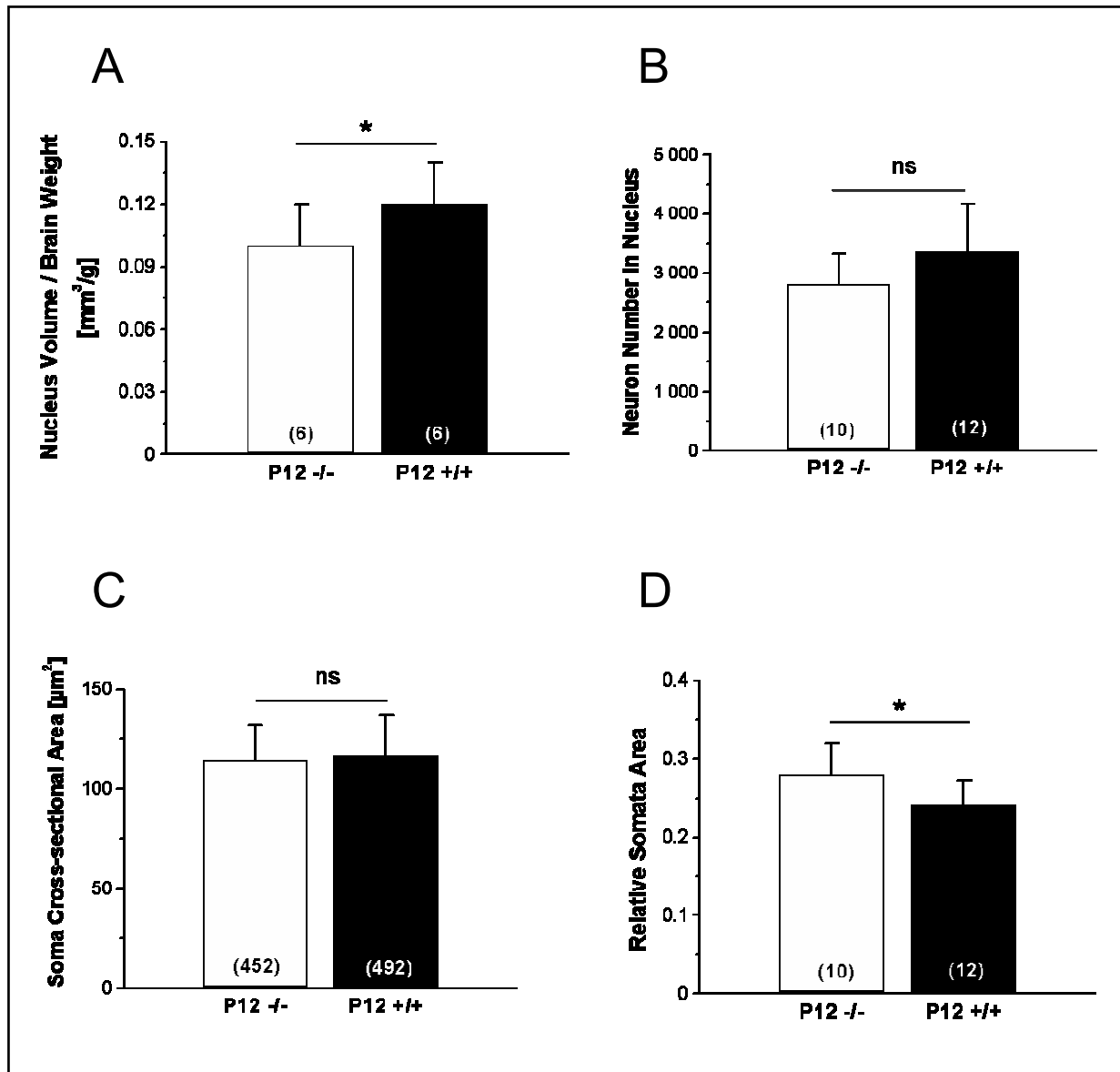
Figure 3.17: Comparison of the four characteristic features determined in the LSO between P12 (-/-) and P12 (+/+)

(A) Nucleus volume/brain weight. It appeared that the LSO in P12 (-/-) animals occupied significantly less relative volume in the brain compared to P12 +/+ animals (p<0.05).

(B) Neuron numbers. There was no significant difference (p>0.05). The counting blocks have the same size as in P3 animals (see 3.1.6 Morphometric analysis).

(C) Soma cross-sectional area. There was no significant difference (p>0.05).

(D) Relative somata area. There was a significantly larger relative somata area in P12 (-/-) animals compare to P12 (+/+) animals (p<0.05). It appeared that the smaller (unrelated to the brain) LSO in these animals (panel A, same figure) is due to less neuropil.

The exact values of the mean (±SD) as well as the p values and the level of significance are shown in Table 3.6

Table 3.6: Morphometric characteristics of LSO

		Nucleus Volume/Brain Weight [mm³/g]		p	Neuron Number in Nucleus		p
		-/-	+/+	-/- vs. +/+	-/-	+/+	-/- vs. +/+
	P3	0.13±0.02	0.15±0.01	p=0.1	2 439±680	3 322±790	**p=0.008
	P12	0.10±0.02	0.12±0.02	*p=0.02	2 814±508	3 355±810	p=0.08
p	P3 vs. P12	*p=0.02	*p=0.02		p=0.2	p=0.9	
		Soma Cross-sectional Area [µm²]		p	Relative Somata Area		p
		-/-	+/+	-/- vs. +/+	-/-	+/+	-/- vs. +/+
	P3	82±16	77±13	p=0.4	0.25±0.05	0.29±0.07	p=0.1
	P12	114±18	117±19	p=0.7	0.28±0.04	0.24±0.03	*p=0.02
p	P3 vs. P12	***p=0.0003	***p=0.000004		p=0.2	*p=0.02	

(Fig. 3.16D) between the two categories at this age. The number of LSO neurons in P3 (-/-) animals, however, was 1.4-fold lower compared to P3 (+/+) animals **(Fig. 3.6B)** and the difference was very significant (this result is discussed further).

P12. Like the absolute volume **(Fig. 3.6D)**, the nucleus volume/brain weight ratio was significantly smaller in (-/-) animals compared to (+/+) animals **(Fig. 3.17A)**. The factor of difference was 1.3. It seemed that the LSO in P12 (-/-) animals additionally remained smaller (not correlated to the smaller brains in these animals) compared to P12 (+/+) animals. The number of LSO neurons was not significantly different between the two categories **(Fig. 3.17B)**. There was also no significant difference in the soma cross-sectional area **(Fig. 3.17C)**. In contrast, the relative somata area was significantly larger in P12 (-/-) animals compared to the age-matched (+/+) group by a factor of 1.2 **(Fig. 3.17D)** which additionally manifested that the neuropil part developed with slower rate in P12 (-/-) animals.

P3 vs. P12. The comparison in the groups during development revealed that the nucleus volume/brain weight ratio at P12 differed from the values at P3 by a factor of 0.7 for the (-/-) group and by a factor of 0.8 for the (+/+) group; the difference was very significant for (-/-) animals and significant for (+/+) animals **(Table 3.6)**. Thus, the LSO at P12 occupied less place in the brain than at P3 in both (-/-) animals and (+/+) animals. With respect to neuron number, there was no significant change with age in both groups **(Table 3.6)**. The soma cross-sectional area increased by a factor of 1.4 in

(-/-) animals and by a factor of 1.5 in (+/+); the difference in both groups was extremely significant. The relative somata area did not change with the age in the (-/-) group. By contrast, in (+/+) animals the relative somata area decreased by a factor of 1.2 and the difference was very significant **(Table 3.6)**. Hence, in the (+/+) animals the rate of increase in the neuropil part with age prevailed over the somata part while in the (-/-) animals both part developed with equal rates.

3.2.3.8   Summary for the LSO

P3. The LSO is not influenced by the KCC2 null mutation in respect to the parameters that have been analysed **(Fig. 3.18)** and the difference in the number of neurons between P3 (-/-) and P3 (+/+) animals was taken as artefact.
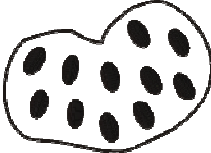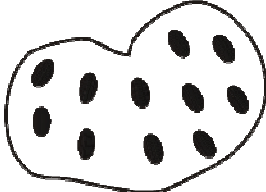
Figure 3.18: Summary drawing for the LSO after comparison between the four categories

No difference in the investigated parameters occurs at P3. In addition to the smaller absolute volume, the relative volume is also smaller in mutants in comparison to controls in respect to the less pronounced neuropil part at P12.

P12. There was no significant difference in the number of neurons and the soma cross-sectional area between the two groups but there was a significantly smaller relative (1.2-fold) **(Fig. 3.17)** and absolute volume (1.4-fold) **(Fig. 3.6)** in (-/-) animals

compared to (+/+) animals. Therefore, the relative somata area which appeared 1.2-fold more in (-/-) animals was due to less pronounced increase in the neuropil part than in (+/+) animals at P12 **(Fig. 3.17)**.

   P3 vs. P12. In the LSO, as in the MNTB and MSO, no equal changes took place in the (-/-) and the (+/+) group. There was a significant increase of the soma cross-sectional area **(Table 3.6)** and in the absolute volume **(Table 3.2)** in (-/-) as well as in (+/+) animals. A similar rate of in the neuropil and somata part led to no change in the relative somata area in (-/-) animals with age. In contrast to (+/+) animals which had prevalence increase of the neuropil over the somata and therefore the relative somata area decreased with age **(Fig. 3.18)**.

3.3   Discussion

By using animals in which the depolarizing phase of GABA/glycine signalling during development is prolonged due to a genetical knock-out of KCC2, I was able to analyse the effect of disturbed Cl⁻ regulation and, thus, the effect of disturbed GABA and glycine neurotransmission (lack of inhibition) on the maturation of neuron cytoarchitecture in the SOC and the VCN. The analyses were done using the Nissl staining technique and stereological methods.

The main results in Chapter 3 from the present study are: (1) the SOC nuclei were not influenced by the KCC2 null mutation at P3 considering the investigated morphometric parameters. However, a difference in the number of neurons occurred between mutants and controls in the VCN at P3; (2) at P12, the four nuclei behaved in a different way with respect to the null mutation: the MNTB and the LSO showed less pronounced neuropil in mutants in comparison to the age-matched controls; the MSO neurons in (-/-) animals had smaller soma cross-sectional area than the age-matched controls; no disproportional changes in the VCN were observed; (3) during development, the neuron number in the VCN and MNTB was increased in both mutants and controls.

It should be mentioned that in this morphometric analysis, the SPN was not investigated, yet the VCN was. The immunohistochemical study (Chapter 2) showed that the KCC2 in the main SOC nuclei was present in the soma surface before the onset of transporter function and the main quantitative and qualitative reorganization in the KCC2 immunofluorescent signal was observed in the neuropil. Therefore, here I analysed the VCN to test whether KCC2 influences the cytoarchitecture at lower stations of the auditory system.

3.3.1   Brain and body development of KCC2 mutants in comparison to control animals

The importance of KCC2 in the regulation of CNS excitability has been established by the characterization of mice with a targeted deletion of the KCC2 gene (Hübner et al., 2001; Woo et al., 2002). Complete deletion of KCC2 results in a severe motor deficit, leading to respiratory failure at birth and mortality (Hübner et al., 2001). A second mouse model was created with 95% reduction in the KCC2 expression. These

animals with a trace amount of KCC2 protein demonstrated handling-induced seizure behaviour that was evident as early as the day after birth (Woo et al., 2002). It was reported that seizures were naturally triggered by movement in the cage, and the frequent seizure activity produced significant injury in the brain (Woo et al., 2002). It is likely that the accumulated injury is responsible for the short life span of KCC2 homozygous (-/-) mice; by postnatal age P17, all homozygous KCC2 (-/-) mice had died. In the present investigation, in order to examine the influence of KCC2 during both the depolarizing and the hyperpolarizing stage of GABA/glycine signalling, the mice with a partial mutation and 5% amount of KCC2 were used. Probably due to my short experience, the reported distinct phenotype (Woo et al., 2002) of the (-/-) animals, in my hands, was barely visible even at P6-P7 and obvious only at P12 when animals were smaller than the age-matched controls, judged by eye. After analysing the data from brain weight and body weight, it appeared that the body weight in P12 (-/-) animals was more affected (58% from the controls) by the loss of KCC2 than the brain weight (81% from the controls). Moreover, this correlated with the statistically significant difference between the two categories in the body weight already at P3.

In general, the entire brain grows rapidly from birth until about the end of the second postnatal week in rats (Dobbing and Sands, 1971), mice (Kobayashi, 1963), and gerbils (Wilkinson, 1986). In the present study, both control and mutant animals showed extremely significant differences in body weight and brain weight between P3 and P12. In both groups, the rate of increase in body weight was bigger than the rate of increase in brain weight. It has previously been shown that differences in brain weight are proportional to total brain DNA content and to total CNS cell number (Zamenhof, 1976). For this reason, brain weight has been suggested to be a good surrogate measure for the total cell number, indicating a normal condition of the brain. The result for the impairment in body growth in KCC2 knock-out animals resembled the data obtained by Woo et al. (2002) who related it to the seizure activities which prevent normal feeding. Treatment with phenytoin, an agent believed to block type II A Na^+ channels and to prevent spread of seizure activity, had a positive effect on the growth of the null mutants (Woo et al., 2002). For this reason, a limitation of the present data has to be considered: the changes in the auditory brain stem nuclei could not be related for sure directly to the lack of the KCC2 protein. It might be necessary to generate conditional knock-out animals in which the defect is restricted to a given developmental stage and/or in a

given brain region or neuronal population. Nevertheless, the impairment of the body growth was not related to any disproportional changes in the brains. At first sight, the brain morphology in P12 (-/-) animals was similar to that of P12 (+/+), with the obvious exception that all structures were smaller. Further qualitative observation after Nissl staining revealed also a normal cytoarchitecture in P12 (-/-) animals. This is in agreement with results from spinal cord and brain stem nuclei in neonatal mutants with a complete deletion of KCC2 which also did not show obvious histological changes (Hübner et al., 2001). In the present study, only homozygous mutant animals were analyzed. However, in another study it was demonstrated that adult (six weeks old) heterozygous animals showed normal development, yet with increased susceptibility for epileptic seizures and resistance to anticonvulsant drugs (Woo et al., 2002). This indicates that KCC2 plays an important role in controlling CNS excitability during both postnatal development and adult life.

In summary, although body growth impairment in KCC2 knock-out animals, which was in part related to the seizure activity preventing normal feeding (Woo et al., 2002), their brains, in terms of brain weight, were less affected by the loss of the outward Cl⁻ transporter. Therefore, I conclude that Cl⁻ homeostasis per se is not essential to maintain brain weight development.

3.3.2　　Absolute and relative volume of the nuclei

Related to the body growth, the brain volume tends to increase gradually during maturation. The growth in volume of the auditory nuclei that occurs after birth (rat: Coleman et al., 1982; mouse: Webster, 1988a; gerbil: Rübsamen et al., 1994) is not due to an increase in the neuronal number but to neuronal growth, generation and growth of glial cells, myelination of fiber tracts and continuing angiogenesis (Cant, 1998). Certainly, one important contribution to this process is the continued growth of dendrites and the axon arbours that contact them.

Present results show that in all four nuclei (VCN, MNTB, MSO and LSO), no difference in their absolute volume occurred between P3 (-/-) and P3 (+/+) animals. At P12, however, in the VCN, MNTB, and the LSO the absolute volume in (-/-) animals was significantly smaller than in (+/+) animals. In the VCN and the MNTB, this result correlates with the smaller brains in mutants at this age and the relative volume of the

auditory nuclei was used to show if any disproportional changes in mutants occur in addition to the smaller brains in comparison to controls. Thus, no difference in the relative volume (presented as the ratio "nucleus volume/brain weight") in the VCN and the MNTB was found. In the LSO, however, I found a significant difference in the relative volume between P12 (-/-) and P12 (+/+) animals. Surprisingly, in the MSO the absolute volume as well as the relative volume did not differ between the P12 (-/-) and P12 (+/+) animals.

Indeed, possible artefact by the measurement of the MSO absolute volume could occur. Kulesza and co-workers (2002), which have used the same stereological method as myself to obtain the volume of different subcortical auditory nuclei in rats, mentioned a critical point that the correct definition of rostro-caudal borders of the nuclei could influence neuron number estimation. The authors observed the greatest discrepancy in the data for neuron number in those structures whose borders were the most difficult to identify in rostral coronal sections, namely, the MSO and two periolivary nuclei. I also found it difficult to define the rostral border of the MSO. It was due to the absence of the LSO (as a landmark) in these slices and a possible overlap of the dorso-ventrally expanded MSO with the lateral nucleus of trapezoid body which occupied the LSO's place in the more rostral slices (Kulesza et al., 2002). In addition, the biggest deviation from the mean absolute volume occurred for the MSO in P12 (-/-) animals (CV=SD/MEAN=0.34). This provides further evidence for the possible artefact in the measurement of the MSO absolute volume. Even if my estimations for the neuron number in this category (589 neurons) correlate with data from Irving and Harrison (1967) (690 neurons), other reports indicate considerably more MSO neurons and their estimation of 1,100 to 1,731 MSO cells is 2 to 3 times higher (Riemann and Reuss, 1999; Reuss et al., 1999; Kulesza et al., 2002). These discrepancies may be due, at least in part, to the manner in which the MSO structure was delineated, in addition to the different stereology tool and staining method. Another source of possibly incorrect volume definition in the MSO comes from the Nissl staining method. This technique allows the visualization of the neuronal body, but not of the processes. Therefore, the nucleus cross-sectional area in the MSO was delineated following the neuronal somata of the MSO primary bipolar neurons. The dendrites of these neurons extend both medially and laterally (Ramón y Cajal, 1907). Thus, with the Nissl staining method, one prevalent part of the neuropil is not included in the volume estimation and if there is a

change in the neuropil during development or between (-/-) and (+/+) animals, the change will be overlooked. This will affect all other relevant features with the exception of the soma cross-sectional area. In line with this opinion is the result about absolute and relative volume which do not differ between P12 (-/-) and P12 (+/+) animals although the brain weight is significantly different between the two categories. Therefore, I suggest that other staining techniques, for example silver method, allowing visualisation of both somata and dendrites in this nucleus, would give the final answer whether the MSO definition and volume estimation has been done correctly.

During development (between P3 and P12), a significant increase occurred in the absolute volume in the nuclei in both groups ((-/-) and (+/+)), yet with a decreased rate in (-/-) animals. An exception was found in the MSO where the increase was of the same magnitude in mutants and controls. In addition, between the nuclei in both mutants and controls, the VCN and the MNTB showed a higher rate than the LSO and MSO. The relative volume in both groups changed in the same direction during development in the different nuclei: the VCN almost doubled in size and occupied more space in the brain at P12; in contrast, the MSO and LSO occupied less space, and the MNTB stayed the same in the brain at P12. In a broad comparative morphometric study of the mammalian central auditory system, Glendenning and Masterton (1998) showed that the VCN in mice occupies around 30% of the total auditory system volume; among the SOC nuclei, the LSO has (around 20%) the biggest volume, followed by the MNTB (around 8%), followed by the MSO (around 3%). Therefore, the present results are consistent with the normal development of mice and normal relative size between the nuclei of the auditory system.

In summary, the KCC2 null mutation did not prevent the volume increase of the investigated auditory nuclei until P3, yet this parameter became impaired between P3 and P12. However, this is likely to be an epiphenomenon since brain weight increase related to brain volume is also impaired. Exception was found for the LSO. Therefore, I conclude that the Cl$^-$ homeostasis is not essential for the nucleus volume increase in the VCN, the MNTB and the MSO during development.

3.3.3   Possible role of KCC2 in neonates

KCC2 is the dominant neuronal Cl^- extrusion mechanism in adult animals that keeps the intracellular Cl^- concentration low to allow the hyperpolarization action of GABA and glycine (Rivera et al., 1999; Hübner et al., 2001; Balakrishnan et al., 2003). It was also shown that despite the early prenatal presence of KCC2 in the mouse brain stem (Stein et al., 2004), the functional switch occurs later on in different auditory nuclei (Srinivasan et al., 2004a), ranging from short before birth (in the SPN) to the third postnatal week (in the MNTB). Since the SPN was not included in this study, it was expected that KCC2 null mutation will have influence to the MNTB, MSO and the LSO and their morphometric parameters in comparison to controls, but only after P4, i.e. after KCC2 becomes functional (Chapter 2).

3.3.3.1   Neuron number differences in the VCN at P3

The neurons in the VCN were counted in the area of the bushy cells. These neurons are considered the most abundant type (Webster and Trune, 1982) and the main source of afferents from the VCN to the SOC (for review: Thompson and Schofield, 2000). A distinction between spherical and globular bushy cells in the AVCN and the posterior VCN, respectively, as well as between the two subregions of the VCN, was not make.

To my knowledge, electrophysiological data about whether/when the switch occurs from depolarizing to hyperpolarizing GABA/glycine signalling in the VCN (i.e. when KCC2 becomes functional) are not available. In vitro recordings from slices of the mouse CN at postnatal day 4 (i.e. about 1 week prior to the onset of hearing) have demonstrated inhibitory postsynaptic potentials in various cell types of the CN upon electrical stimulation of the auditory nerve (Wu and Oertel, 1987). Additionally, bath-applied GABA and glycine exert inhibitory actions. In general, it is proposed that inhibitory mechanisms appear to operate very early in the functional development of the CN (Gleich and Vater, 1998). Thus, it is not possible to predict when the absence of functional transporter would influence the morphometric parameters in this nucleus, if at all. Nevertheless, an immunohistochemical study (Vale et al., 2004) in the CN showed the presence of KCC2 protein at P3, without up-regulation during development.

About 30 years ago, it was believed that the AVCN serves primarily as a relay station responsible for the transmission of the activity of the auditory nerve to the next auditory neurons in the afferent auditory system in a high-fidelity fashion (Pfeiffer, 1966a,b; Rose et al., 1974). This was demonstrated by morphological data which show that the spherical bushy cells are innervated by only two to four auditory nerve fibers that form large synaptic end-bulbs on the somata (Ryugo and Sento, 1991). However, more recent anatomical and physiological results indicate that the AVCN receives not only excitatory auditory nerve fiber input, but also inhibitory inputs. The principle cells of the AVCN receive inhibitory projections from the dorsal and ventral cochlear nucleus (Wu and Oertel, 1986; Wickesberg and Oertel, 1990; Kolston et al., 1992; Ferragamo et al., 1998) and from higher order auditory brain stem nuclei [MNTB and SPN (Schofield, 1991, 1994); lateral and ventral nucleus of the trapezoid body (Covey et al., 1984; Warr and Beck, 1996)]. Pharmacological studies *in vivo* and *in vitro* confirmed that neurons in the AVCN are sensitive to GABA and glycine (Wu and Oertel, 1986; Wickesberg and Oertel, 1990; Caspary et al., 1994; Ebert and Ostwald, 1995). Electrophysiological results indicate that the inhibition in bushy cells of the AVCN is mediated primarily by glycine receptors, with only a minor contribution from $GABA_A$ receptors (mouse: Wu and Oertel, 1986; rat: Lim et al., 2000). Immunohistochemical studies in rats for glycine receptor and gephyrin showed many intense punctate clusters over the surface of AVCN bushy cells, compared with weak, diffuse labelling of postsynaptic $GABA_A$ receptors (Lim et al., 2000). These results provide strong evidence that inhibition in the AVCN alters the frequency tuning and the level-dependent responses and increases the precision of encoding of the signal onset (Kopp-Scheinpflug et al., 2002). Considering globular cells in the VCN, it appears that they also receive numerous afferents with GABA- or glycine-like immunoreactivity on their somata in rats (Osen et al., 1991). Thus, the neuronal activity is a result of excitation and inhibition already at the level of second-order neurons of the auditory system, and the KCC2 null mutation may, therefore, have influences on the VCN.

In the present study, the VCN was the only nucleus which displayed some differences at P3 between (-/-) and (+/+) animals. This difference considered the lower number of neurons in mutants than in controls. Two possible explanations can be given: first, due to the bad condition of KCC2 knock-out animals, the neurogenesis of the VCN neurons could be affected. Autoradiographic studies in rats and mice, however, have

indicated that only the production of the granule cells in the DCN occurs after birth (Altman and Das, 1966; Taber-Pierce, 1967). A peak of cell division occurring perinatally has been attributed to the production of glial cells (Martin and Ricketts, 1981), which were not included in my study. Neurogenesis and migration of nongranular VCN neurons occurs prenatally in the rodent. In the rhombic lip of the embryonic rat (Altman and Bayer, 1980c) and mouse (Taber-Pierce, 1967; Martin and Rickets, 1981), VCN neurons are born approximately 1 week before birth (E13 to E17, Altman and Bayer, 1980c) and migrate laterally to their characteristic location on the dorsal edge of the medulla until birth. Therefore, it could be speculated that there is a "critical period" in the brain stem during which the normal neurogenesis of the VCN neurons is impaired, but not the neurogenesis of the SOC nuclei which are generated earlier than the non-granular neurons of the VCN (mice: Taber-Pierce, 1973; rats: Altman and Bayer, 1980a; Cant, 1998). For example, a recently described KCC3 knock-out mouse model displayed a severe neurodegeneration in the peripheral nervous system and in several areas of the CNS at P13, in addition to the severely impaired cell volume regulation as assessed in renal tubules and neurons, and moderately raised intraneuronal Cl^- concentration (Boettger et al., 2003). The authors claim that the observed morphological changes in the spinal cord, the hippocampus and the cerebellum are not due to an impaired development since the degeneration occurred postnatally (no degeneration was found in corresponding tissues of P1 mice). I disagree with their definition that the period between P1 and P13 is not related to mouse development. In case of the KCC2 mutation, the lower number of neurons in the VCN in P3 (-/-) animals cannot be correlated directly with the loss of KCC2, because these animals have already a delay in the body growth at P3 i.e. body weight was smaller than it was in controls at P3. An open question is why such a difference is not present in the other nuclei.

Second, the fact that epileptic seizures can be observed at a very early age in animals which lack the KCC2 protein, before the development of GABA and glycine hyperpolarizing responses in most neurons studied, suggested that KCC2 may have additional functions (Woo et al., 2002). In the brain stem, KCC2 is expressed from E15.5 (Stein et al., 2004) but is functional later in development (Balakrishnan et al., 2003; Srinivasan et al., 2004a). It can be speculated that KCC2 is important for neuronal survival early on before performing its role in determining GABA/glycine signalling function. It is known that the survival of primary sensory neurons and retinal

ganglia cells is selectively supported by BDNF (review: Conover and Yancopoulos, 1997). In BDNF-overexpressing embryos, it was suggested that BDNF controls and coordinates network activity in part via up-regulation of KCC2 expression in rat hippocampal slices (Aguado et al., 2003). It is not known whether the lack of KCC2 in the brain stem at embryonic ages will influence the amount of BDNF which can manipulate, in turn, the neuronal survival. Moreover, no immunoreactivity for BDNF was detected on the day of birth in any auditory structure, although fibers comprising the spinal tract of the Vth cranial nerve were well labelled with antibodies against BDNF (Tierney et al., 2001). Diffuse immunoreactivity for BDNF was first detected at P3 in the cochlear nucleus and in several second order auditory nuclei in the SOC. A differential pattern of staining emerges at P6 in CN subdivisions, with more intense staining present in the ventral part (rat: Hafidi, 1999). Thus, an influence of BDNF on the neuronal survival in the animals with KCC2 null mutation before P3 is not likely to occur. Lower number of neurons in the AVCN was also observed after unilateral cochlear ablation (in gerbil: Hashisaki and Rubel, 1989; in mice: Mostafapour et al., 2000). The authors claim that this results from the presence of a "critical period" during development when afferent removal or changes in afferent activity have dramatic effects on neuronal structure and function maturation. In the present study, however, such a drastic functional deficit is not the case. In summary, I cannot give a clear explanation for the lower number of neurons in the VCN of P3 (-/-) compared to age-matched controls.

In the VCN, besides the significantly smaller number of neurons in P3 (-/-) animals compared to P3 (+/+) animals, I observed no difference in the soma cross-sectional area or in the absolute volume of the nucleus at this age. This can be related to an exuberance in the neuropil and is in accordance with my data on the relative somata area, which was significantly smaller in P3 (-/-) animals compared to P3 (+/+) animals. Therefore, it appears that in the VCN the neuropil in mutants compensates in a way the lower number of neurons. With the Nissl staining, it is not possible to relate the changes in the neuropil directly to dendritic growth. If the survival of VCN neurons is impaired, extensive glial cell production and growth can occur. Glia provides structural and functional support for the nervous system and is involved in restoring damaged neurons (Jessell, 1991). Certain types of brain injury as well as several pathological conditions are accompanied by astroglial proliferation, called astrogliosis, or more simply gliosis. Astrocytes are ubiquitous in the brain and have multiple functions. It is believed that

reactive astrogliosis observed in most neurological disorders may regulate the removal of toxic compounds produced by damaged neurons and support neuronal growth by releasing trophic factors (Banker, 1980; Rudge et al., 1992; Schmalenbach and Muller, 1993; review: Tacconi, 1998).

In summary, no clear answer about the influence of KCC2 null mutation in the VCN at P3 can be given. Probably additional immunohistochemical investigation of glial presence in KCC2 knock-out mice in this nucleus would be helpful, as well as electrophysiology data for the time of switch of GABA/glycine transmission. After P3 until P12, no other investigated parameter in the VCN underwent a disproportional change due to impaired Cl⁻ homeostasis.

3.3.3.2   Significant increase of neuron number with age in the VCN and the MNTB

In spite of the significantly lower number of neurons in P3 (-/-) animals compared to P3 (+/+) animals in the VCN, I observed no further age-related changes in the nucleus due to the KCC2 null mutation. The investigated morphometric parameters changed in the same direction and within a similar range in both the (-/-) and the (+/+) group. Surprisingly, in both groups the neuron number increased by the same factor (1.4-fold) between P3 and P12. As mentioned above, only granule cells in the DCN are generated after birth (Altman and Das, 1966; Taber-Pierce, 1967). A possible explanation derives from the presence of undifferentiated neurons in the VCN. Webster (1988a) showed that in normal CBA/J mice, the number of VCN neurons which contained Nissl substance remained constant during the first 6 days of postnatal life. Then this number almost doubled until P12. Webster claimed that this great increase of neurons does not necessarily mean that either cell division or migration occurs. He supposed that it is rather caused by differentiation of neuroblasts into neurons, not by mitoses. In the MNTB, no difference in the neuron number between P3 (-/-) and P3 (+/+) occurred. However, as well as in the VCN, I observed an age-related increase in the number of neurons in both mutants and controls within a similar range. In fact, many somata in the VCN and the MNTB in P3 animals contained a darkly stained nucleolus but poorly stained plasma membrane and less Nissl substance within the cytoplasm which hampered neuron identification and precluded the analysis of either number or neuron size at this age. At P12, there was no such methodological difficulty and the

neurons were easily identified. Thus, I suspect that underestimation of neuron number at P3 could occur in both (-/-) and (+/+) group and this to explain the difference in the neuron number between P3 and P12. Moreover, this is consistent with previous observations in gerbil (Tierney and Moore, 1997). Therefore, I suppose it is likely that a major reason for the increase in the neuron number in both VCN and MNTB during development is the presence of undifferentiated neurons.

An open question is why such undifferentiated neurons are present only in the VCN and the MNTB, but not in the MSO and the LSO? One possibility derives from the similarities in the anatomical organization and synaptic inputs in the VCN and the MNTB. Auditory nerve fibres make large excitatory synaptic contacts, the end-bulbs of Held, with bushy cells in the AVCN (Neises et al., 1982). The bushy cells, in turn, provide large somatic terminals, known as calyces of Held, and form synapses with the cell bodies of principal neurons of the MNTB (Held, 1893). Approximately half of the available synaptic space on the surface area of the soma is taken up by these specialized excitatory inputs which provide a potent excitatory drive to the VCN and to the MNTB, respectively. The end-bulb of Held and the calyx of Held undergo marked morphological and physiological changes during development (in rats CN: Kandler and Friauf, 1993; in gerbils MNTB: Kil et al., 1995; in mice VCN: Limb and Ryugo, 2000). The changes take place not only presynaptically but postsynaptically as well, and allow this type of synaptic contact to become extraordinarily fast and reliable. The elaborate pattern of terminal branching of these endings continues to develop during the first two postnatal weeks and it is likely to underlie the late maturation of the postsynaptic neurons. Thus, the presence of the similar excitatory input in the VCN and the MNTB is likely to be responsible for the extended differentiation period of the VCN and the MNTB neurons. In addition, neurons of the different nuclei of the SOC are generated in a specific order (mice: Taber-Pierce, 1973; rats: Altman and Bayer, 1980a) and in general earlier than neurons from the VCN (Cant, 1998). The generation of neurons in the MNTB begins several days later than in the other nuclei (Cant, 1998). Hence, the subsequent migration and differentiation of the VCN and the MNTB neurons is likely to occur later than in the LSO and the MSO. This may also explain the underestimation of neuron number in the VCN and the MNTB at P3.

In summary, in the VCN and the MNTB, the presence of undifferentiated neurons at P3 is possible reason for the increased neuron number between P3 and P12. In

addition, the lack of KCC2 did not prevent the process of neuronal differentiation in both nuclei with age.

3.3.4   The significant difference of the neuron number in the LSO at P3 is considered an artefact

I found that the number of LSO neurons in P3 (-/-) animals was 1.4-fold lower than in P3 (+/+) animals and the difference was very significant. The number of LSO neurons was not significantly different between the two categories at P12. Moreover, there was no significant change in this parameter with age in both groups.

Considering the mathematical and biological logic behind the statistical analysis, this difference in the number of neurons at P3 in the LSO was taken as an artefact. Note that the immunohistochemical study (Chapter 2) presented also a special case for the LSO at an early age (P0): the labelling for KCC2 revealed intensely stained neuropil that tightly surrounded the cell bodies. In the present morphometric investigation, the staining method did not allow the direct observation of the neuropil. Still, the abundance of neuropil at this age is possible to impair the identification of the somata in the P3 (-/-) and P3 (+/+) animals.

3.3.5   Effects of excitatory and inhibitory inputs on neuronal integrity

3.3.5.1   The neuropil is affected in the MNTB and the LSO in P12 (-/-) animals

The present study revealed that in the MNTB as well as in the LSO, the less pronounced neuropil part in the P12 (-/-) animals in comparison to the age-matched controls contributed to the smaller absolute volume of these nuclei and the bigger relative somata area. Furthermore, the LSO in P12 (-/-) animals remained even smaller, due to less neuropil, and did not correlate to the smaller brain in comparison to P12 (+/+) animals.

The dendrites of the neurons are like antennae, picking up signals from many neurons and passing the signal down to the soma and the axon. The amount of dendrites is important, because it will affect the quantity and quality of signals the

neuron receives. During normal development, one change that occurs is an increase in size and complexity of the neurons' dendritic trees, i.e. the maturation is accomplished via overproduction of dendrites (Jacobson, 1991; Cant, 1998). In rats and mice, a rapid increase in cell size and dendritic proliferation occurs within the first two postnatal weeks (Ollo and Schwartz, 1979; Cant, 1998). This process typically begins once the neurons have completed their migration and are in their final position. During further development, the complex dendritic arbour with an exuberant number of end branches is reduced via a pruning mechanism (Sanes et al., 1992a; Rietzel and Friauf, 1998). Dendrite development, however, is one property of the neurons that can be influenced by the environment during development. For example, the dendritic arbour generally decreases in size when its excitatory synapses are blocked or eliminated (Deitch and Rubel, 1984; Russell and Moore, 1999). Previous in vivo studies in the gerbil LSO (Sanes et al., 1992a; Sanes and Chokshi, 1992) suggest that inhibitory transmission can also regulate the growth of neuronal processes and, thus, contribute to the maturation of neurons. Different manipulation of the animals to depress glycinergic transmission during development (deafferentation or strychnine-containing continuous release pellets) produced nearly identical results, namely a hypertrophy in the dendritic arbour during the third postnatal week (Sanes et al., 1992b). A more direct proof of the idea that the inhibitory transmission influences dendrite growth was provided in organotypic cultures of the MNTB and the LSO (Sanes and Hafidi, 1996). However, in the present study, the investigated age (P12) does not overlap with the normal period of regressive events (pruning). Thus, in the case of KCC2 P12 (-/-) animals, I suppose that the normal overproduction of neuropil in the MNTB and the LSO during the first postnatal week is somehow impaired. The reason for this is not clear. Electrophysiology data from KCC2 knock-out animals show that KCC2 is not functional at P12 and the glycine application on the neurons has depolarizing effects, instead of the typical hyperpolarizing ones (Balakrishnan et al., 2003). Thus, it is possible that the lack of "normal" inhibitory transmission in P12 (-/-) animals results in excessive depolarization of the neurons (sum of the depolarizing inhibitory inputs plus the usual depolarizing excitatory inputs) and hyperexcitation. Moreover, diverse types of dendritic injury associated with excitotoxicity have been described (Ramón y Cajal, 1907; Olney, 1971; Ikonomidou et al., 1989; Ikegaya et al., 2001; Monnerie et al., 2003). Dendrites serve as crucial input devices of a neuron, depending on their specialized, unique geometry –

they form an anatomical framework for the spatiotemporal integration of signals from hundreds or thousands of synapses arranged on its complex arbour (Midtgaard, 1994). For this reason, the dendrites may also be a major input site of stressful disturbance under pathological conditions, such as excessive excitatory signals, and thus have been considered more susceptible to neuronal injury than the axon or the soma (Ikegaya et al., 2001). Excitotoxicity is referred to the ability of glutamate or related excitatory amino acids to mediate the death of neurons in the CNS, for example, after intense stimulation. Such excitotoxic neuronal death may contribute to the pathogenesis of brain or spinal cord injury associated with several human disease states, e.g. ischemia and stroke (Martin et al., 1998; Arundine and Tymianski, 2004). This excitotoxicity has a concrete cellular basis and, in most cases, it is mediated by glutamate receptors. NMDA receptor activation may be able to trigger lethal injury more rapidly than AMPA or kainate receptor activation, perhaps reflecting a greater ability to induce calcium influx and subsequent calcium overload (Choi, 1992; Gagliardi, 2000). In addition, it was suggested that dendrites may be selectively vulnerable to neuronal injury because the receptors for excitatory amino acids that mediate the excitotoxicity are localized predominantly in the dendrites (Racca et al., 2000). It was also shown that inhibitory transmission may cause changes at excitatory synapses via the depolarisation mediated by $GABA_A$ receptors that diminishes the voltage-dependent block of the NMDA receptor by Mg^{2+}, sufficient to account for frequency modulation of synaptic NMDA receptor activation (Staley et al., 1995) and, indirectly, to excitotoxicity. For example, alcoholic brain damage arises in regions where GABA-mediated inhibition is deficient, and fails to limit the excitation (Dodd, 2002). During normal development, GABA and glycine are excitatory in immature neurons and can produce Ca^{2+} influx through voltage-gated channels or via activated NMDA receptors (Ben-Ari et al., 1997; Kullmann et al., 2002). It is believed that particularly during early development, Ca^{2+} is a key component that plays a crucial role for many processes: as a second messenger, Ca^{2+} appears to be necessary for synapse stabilization (Sanes and Friauf, 2000); changes in intracellular Ca^{2+} have long been known to influence neuronal differentiation, as well as axon outgrowth and pathfinding (Spitzer, 2002); dendritic spine development and synaptic plasticity has been investigated exclusively in respect to intracellular Ca^{2+} (Rose and Konnerth, 2001; Sabatini et al., 2001); recent studies indicate the role of calcium signalling in dendritic growth and patterning (Lohmann et al., 2002; Redmond et

al., 2002). A study in organotypic cultures of the rat auditory brain stem (Piechotta and Friauf, 1999) proposed that Ca^{2+} influx into LSO neurons may no longer be essential at the time when the hyperpolarizing stage has been reached. Hence, the Ca^{2+} needs to be within an optimal range to be beneficial and especially regarding the neurite outgrowth which can only proceed when intracellular calcium levels lie within a specific outgrowth-permissive range (Kater et al., 1999). Kater and co-workers claim that if the intracellular calcium levels are not regulated within normal limits, neurodegeneration occurs. Therefore, in the case of GABA and glycine, being depolarizing, the increased activation of NMDA receptors and voltage-dependent Ca^{2+} channels might initiate toxic conditions by increasing intracellular calcium and promoting dendrite damage and degeneration (Siman et al., 1989; Choi, 1992). This is also the case after neuronal trauma (van den Pol et al., 1996). In my investigation under the described "unusual" conditions of an extended period of GABA/glycine depolarization, the excessive excitation and overstimulation of NMDA receptors is a possible scenario. One way to test if the neurons in P12 KCC2 knock-out animals are overloaded with intracellular Ca^{2+} will be to show the expression of calbindin-D28k. A strong transient expression of this calcium-binding protein was shown in the rat LSO during the first postnatal week (Friauf, 1993) i.e. exactly during the time of GABA- and glycine-induced Ca^{2+} influx in immature neurons. If there is an abnormal Ca^{2+} load in P12 (-/-) animals, I would suppose an extended and increased expression of calbindin-D28k in relation to its role as a buffer, protecting cells against toxic levels of calcium (Friauf, 1994; Forster and Illing, 2000).

Another possibility, apart from the alteration in GABA/glycine transmission, is that in the KCC2 null mutation animals, because of their body growth impairment, some trophic factors may be influenced. For example, an impaired dendritic morphology of LSO neurons is demonstrated in somatostatin-depleted animals during early development (Kungel et al., 1997).

In summary, I propose two reasons for the impaired neuropil development in the MNTB and the LSO in P12 (-/-) animals: 1) the depolarizing GABA/glycine transmission in mutants may contribute to excessive Ca^{2+} load, excitotoxicity and dendrite damage; 2) decrease of some trophic factors, thus preventing normal body growth and dendrite development.

3.3.5.2   Smaller soma cross-sectional area in the MSO neurons at P12 (-/-) animals

Unlike the neurons in the other three nuclei, MSO neurons displayed a significantly smaller soma cross-sectional area in P12 (-/-) animals compared to P12 (+/+) animals. This result cannot be explained by the possibly incorrect volume determination of the nucleus.

During normal development, the somatic growth in all nuclei is completed by the onset of hearing (P12) (mouse: Webster and Webster, 1980). No further growth in this parameter occurs during further development (gerbil: Tierney and Moore, 1997). Soma size tends to be associated with both the dendritic and axonal architecture. For example, in some neuronal populations, soma size correlates with the extent of a neuron's dendritic (Hayes and Lewis, 1993; Jacobs et al., 1997) and axonal arbour (Gilbert and Kelly, 1975; Lund et al., 1975). In the present study, however, due to reasons mentioned above, no exact estimation of changes in the MSO neuropil can be made. A possibility for decreased soma size can be an alteration in the neuron metabolism and its capacity to form and maintain appropriate afferent and efferent connections. Reduced soma size in auditory brain stem nuclei is shown after decreased connectivity (auditory deprivation, conductive hearing loss or alteration in the sensory experience) (Webster and Webster, 1977, 1979; Born and Rubel, 1988; Pasic and Rubel, 1989). However, in the present study this is not the case.

The open question is why the smaller soma cross-sectional area is found only in the MSO neurons but not in the neurons of other nuclei. One possibility comes from the source of input in the MSO. In contrast to the MNTB and LSO, the MSO receives inhibitory input from both the ipsi- and the contralateral side via the lateral nucleus of trapezoid body and the MNTB, respectively (Cant and Hyson, 1992; Kuwabara and Zook, 1992; Grothe and Sanes, 1993; Smith et al., 2000). Therefore, I suppose that the lack of "normal" inhibition in the MSO, due to lack of KCC2, is probably related to more profound changes in this nucleus in comparison to the other auditory nuclei.

In summary, I do not have a clear explanation for the smaller soma size of MSO neurons in the KCC2 mutants at P12. The result, however, shows that the Cl^- homeostasis is likely to be required at some older ages to maintain and achieve a proper soma size.

3.3   Summary of chapter 3

1.   Despite the body growth impairment in KCC2 knock-out animals, the brains of these animals (in terms of brain weight) were less affected by the loss of outward Cl^- transporter. Therefore, I conclude that Cl^- homeostasis is not essential to maintain brain weight development.

2.   The lack of KCC2 did not prevent the volume increase of the investigated auditory nuclei until P3, yet this parameter was impaired between P3 and P12. However, this is likely to be an epiphenomenon since brain weight increase is also impaired with the same magnitude. Hence, I suppose that the Cl^- homeostasis is not crucial to maintain nucleus volume increase in the VCN, MNTB and the MSO during development. An exception was found for the LSO.

3.   The lack of KCC2 also did not have drastic effects on the number of neurons in the investigated auditory nuclei, with one exception being the VCN at P3. The reason for this is not clear. In addition, the lack of KCC2 did not prevent the process of neuronal differentiation in the VCN and the MNTB between P3 and P12.

4.   I present two possible reasons which may explain the impaired production of neuropil in the MNTB and the LSO in P12 (-/-) animals due to the lack of KCC2: first, the depolarizing GABA/glycine transmission in mutants may contribute to excessive Ca^{2+} load, excitotoxicity and dendrite damage; second, decrease of some trophic factors may prevent dendrite development in addition to impaired normal body growth.

5.   The KCC2 expression and normal Cl^- homeostasis is likely to be required in the MSO at older ages (P12) to achieve and maintain a proper soma size.

4   General summary

In my doctoral thesis, I present new information about the developmental expression pattern of the potassium chloride cotransporter KCC2 in the rat auditory brain stem and the morphometrical effects caused by KCC2 gene silencing in mice. The thesis is divided into 3 Chapters.

Chapter 1 is a general introduction which gives a brief outline of the primary ascending auditory pathway in mammals. Also, it provides information about the presence of a large number of inhibitory inputs in the auditory system and how these inputs develop; the involvement of inhibition in the acoustic processing is mentioned. In addition, the role of the KCC2 cotransporter in the shift of GABA/glycine transmission, and thus, in maintaining the normal level of inhibition in the mature brain, is described.

The focus of Chapter 2 was to investigate the KCC2 immunofluorescent signal from postnatal day (P) 0 to P60 in four major nuclei of the rat's superior olivary complex (SOC), namely the medial nucleus of the trapezoid body (MNTB), the medial superior olive (MSO), the lateral superior olive (LSO), and the superior paraolivary nucleus (SPN). The lack of a correlation between the continuous presence of KCC2 mRNA/protein in the postnatal rat brain stem on one side, and the shift in GABA/glycinergic polarity (i.e. KCC2 functionality) on the other side, prompted me to search for a specific cellular expression pattern of the KCC2 protein that might correlate with the switch in GABA/glycine signalling. To do so, the KCC2 immunoreactivity was analysed using high-resolution confocal microscopy in three cellular regions of interest: the soma surface, the soma interior, and the neuropil. In the soma surface, I observed an increase of the KCC2 immunofluorescent signal intensity, yet with a moderate magnitude (1.1 to 1.6-fold). Therefore, I conclude that the change in the soma surface signal is only of minor importance and does not explain the change in KCC2 functionality. The KCC2 signal intensity in the soma interior decreased in all nuclei (1.4 to 2-fold) with the exception of the MNTB where no statistically significant change was found. The decrease in the soma interior was probably related to the increase in the soma surface immunoreactivity and the proposed (weak) intracellular trafficking process of the KCC2 protein. The main developmental reorganization (in qualitative as well as in quantitative aspects) of the KCC2 immunofluorescence in the SOC nuclei was observed in the neuropil. The signal changed its pattern from a diffusely stained neuropil early in

development (P0-P4) to a crisp and membrane-confined signal later on (P8-P60), with single dendrites becoming apparent. The exception was found in the MNTB, where the neuropil became almost unlabeled. Quantification revealed a statistically significant decrease (2.2 to 3.8-fold) in the neuropil immunoreactivity in all four nuclei, although the remaining KCC2-stained dendrites became thicker and the signal became stronger. I suppose that, at least in part, the neuropil reorganization can be explained by an age-related reduction of dendritic branches via a pruning mechanism and with the absence of an abnormal Cl^- load via extrasynaptic $GABA_A$ receptors. This is consistent with the proposed additional role of KCC2, namely to maintain the cellular ionic homeostasis and to prevent dendritic swelling (Gulyás et al., 2001).

In conclusion, neither the increase in the KCC2 soma surface signal intensity, nor the reorganization in the neuropil can be strictly related to the developmental switch in the GABA/glycine polarity and the onset of KCC2 function, although some correlation (the appearance of a specific membrane-confined *dendritic* pattern) between structure and function was found. Further implication of different molecular methods, regarding the proposed posttranslational modification of KCC2, will shed light upon the question of what leads to the functional activation of the cotransporter.

In Chapter 3, the advantage of loss-of-function KCC2 mice made it possible, via manipulating the duration of the depolarizing phase of GABA/glycine transmission, to analyse the effect of disturbed Cl^- regulation and, thus, the effect of disrupted GABA/glycine neurotransmission (lack of inhibition). I asked the following question: how important is the Cl^- homeostasis to maintain general aspects (brain weight) and specific aspects (nucleus volume, neuron number, and soma cross-sectional area) of brain development?

Brain stem slices from KCC2 knock-out animals (-/-), with a trace amount of transporter (~5%), as well as from wild type animals (+/+) at P3 and P12 were stained for Nissl substance and the analyses were performed with the help of basic morphometrical and stereological methods. In KCC2 (-/-) animals, body growth impairment was observed, in part related to the seizure activity preventing normal feeding (Woo et al., 2002). However, their brains, in terms of brain weight, were less affected. Therefore, I conclude that Cl^- homeostasis is not essential per se to maintain the brain weight. Four auditory nuclei (MNTB, MSO, LSO, and ventral cochlear nucleus (VCN)), were compared with respect to the KCC2 null mutation. The SOC nuclei were

not influenced by the lack of KCC2 at P3 considering the morphometric parameters. A difference in the number of neurons occurred in the VCN at P3. I suggest to perform additional immunohistochemical studies of glial presence related to its involvement in the structural and functional support of the neurons and their survival. At P12, the volume of the auditory nuclei in KCC2 (-/-) animals was smaller than in (+/+) animals. However, this is likely to be an epiphenomenon since the brain weight increase was also impaired with the same magnitude. Therefore, I suppose that the Cl⁻ homeostasis is not crucial for the nucleus volume increase in the VCN, the MNTB and the MSO during development. An exception was found for the LSO. Regarding the other morphometric parameters at P12, the four nuclei behaved in a different way: (1) in the VCN, after P3, no parameter underwent a disproportional change due to impaired Cl⁻ homeostasis; (2) the MNTB and the LSO showed less pronounced neuropil in mutants in comparison to age-matched controls and two reasons were proposed: first, the depolarizing GABA/glycine transmission in mutants may contribute to excessive Ca^{2+} load, excitotoxicity and dendrite damage; second, a decrease of some trophic factors may prevent dendrite development in addition to impaired normal body growth; (3) the MSO neurons in P12 (-/-) animals had smaller soma cross-sectional area than in P12 (+/+) animals. I conclude that the normal Cl⁻ homeostasis is required in the MSO at older ages (P12) to achieve and maintain a proper soma size; (4) the lack of KCC2 did not prevent the process of neuronal differentiation in the VCN and the MNTB during development in both mutant and control animals.

In conclusion, the various auditory nuclei have to be discussed independently regarding the influence of Cl⁻ homeostasis on some morphometric parameters. Presumably, this is related to the different time of the shift in the GABA/glycine polarity i.e., the onset of KCC2 function (Srinivasan et al., 2004a).

Taken together, my thesis accumulated data about the immunohistological expression pattern of KCC2 in various auditory brain stem nuclei and the influence of impaired Cl⁻ homeostasis on some morphometric features in these nuclei. This information will be helpful for further investigations involved to discover the mechanisms and the events that govern the inhibition and the inhibitory pathway in the central auditory system.

5 Bibliography

Abercrombie M (1946) Estimation of nuclear population from microtome sections. *Anat Rec* 94: 239-247.

Adams JC, Mugnaini E (1990) Immunocytochemical evidence for inhibitory and disinhibitory circuits in the superior olive. Hear Res. Nov;49(1-3):281-98.

Aguado F, Carmona MA, Pozas E, Aguilo A, Martinez-Guijarro FJ, Alcantara S, Borrell V, Yuste R, Ibanez CF, Soriano E (2003) BDNF regulates spontaneous correlated activity at early developmental stages by increasing synaptogenesis and expression of the K^+/Cl^- co-transporter KCC2. Development. Apr;130(7):1267-80.

Altman J, Bayer SA (1980a) Development of the brain stem in the rat. I. Thymidine-radiographic study of the time of origin of neurons of the lower medulla. J Comp Neurol. Nov 1;194(1):1-35.

Altman J, Bayer SA (1980c) Development of the brain stem in the rat. III. Thymidine-radiographic study of the time of origin of neurons of the vestibular and auditory nuclei of the upper medulla. J Comp Neurol. Dec 15;194(4):877-904.

Altman J, Das GD (1966) Autoradiographic and histological studies of postnatal neurogenesis. I. A longitudinal investigation of the kinetics, migration and transformation of cells incorporating tritiated thymidine in neonate rats, with special reference to postnatal neurogenesis in some brain regions. J Comp Neurol. Mar;126(3):337-89.

Alvarez-Bolado G., Swanson LW (1996) Developmental Brain Maps: Structure of the Embryonic Rat Brain. Elsevier Science Ltd

Alvarez-Leefmans FJ (2001) Intracellular chloride regulation. In: Cell physiology sourcebook: A molecular approach (Sperelakis N, ed), pp 301-318. San Diego: Academic Press.

Anderson GW, Schoonover CM, Jones SA (2003) Control of thyroid hormone action in the developing rat brain. Thyroid 13: 1039-1056.

Arundine M, Tymianski M (2004) Molecular mechanisms of glutamate-dependent neurodegeneration in ischemia and traumatic brain injury. Cell Mol Life Sci. Mar;61(6):657-68. Review.

Backus KH, Deitmer JW, Friauf E (1998) Glycine-activated currents are changed by coincident membrane depolarization in developing rat auditory brainstem neurones. J Physiol (Lond) 507: 783-794.

Baddeley AJ (2001) Is stereology 'unbiased'? Trends Neurosci 24: 375-376; author reply 378-380.

Balakrishnan V (2004) The role of plasma membrane transporters in chloride homeostasis of developing auditory brainstem neurons. April, TU Kaiserslautern, Department of Biology, Doctoral thesis.

Balakrishnan V, Becker M, Lohrke S, Nothwang HG, Guresir E, Friauf E (2003) Expression and function of chloride transporters during development of inhibitory neurotransmission in the auditory brainstem. J Neurosci 23: 4134-4145.

Baldwin SA, Gibson T, Callihan CT, Sullivan PG, Palmer E, Scheff SW (1997) Neuronal cell loss in the CA3 subfield of the hippocampus following cortical contusion utilizing the optical disector method for cell counting. J Neurotrauma. Jun;14(6):385-98.

Banker GA (1980) Trophic interactions between astroglial cells and hippocampal neurons in culture. Science. Aug 15;209 (4458):809-10.

Banks MI, Pearce RA (2000) Kinetic differences between synaptic and extrasynaptic $GABA_A$ receptors in CA1 pyramidal cells. J Neurosci. Feb 1;20(3):937-48.

Banks MI, Smith PH (1992) Intracellular recordings from neurobiotin-labeled cells in brain slices of the rat medial nucleus of the trapezoid body. J Neurosci 12: 2819-2837.

Barker JL, Behar T, Li YX, Liu QY, Ma W, Maric D, Maric I, Schaffner AE, Serafini R, Smith SV, Somogyi R, Vautrin JY, Wen XL, Xian H (1998) GABAergic cells and signals in CNS development. Perspect Dev Neurobiol 5: 305-322.

Basavappa S, Ellory JC (1996) The role of swelling-induced anion channels during neuronal volume regulation. Mol Neurobiol. Oct;13(2):137-53. Review.

Behrend O, Brand A, Kapfer C, Grothe B (2002) Auditory response properties in the superior paraolivary nucleus of the gerbil. J Neurophysiol 87: 2915-2928.

Ben-Ari Y (2002) Excitatory actions of GABA during development: the nature of the nurture. Nat Rev Neurosci 3: 728-739.

Ben-Ari Y, Cherubini E, Corradetti R, Gaiarsa JL (1989) Giant synaptic potentials in immature rat CA3 hippocampal neurones. J Physiol (Lond) 416: 303-325.

Ben-Ari Y, Khazipov R, Leinekugel X, Caillard O, Gaiarsa JL (1997) $GABA_A$, NMDA and AMPA receptors: a developmentally regulated 'menage a trois'. Trends Neurosci. Nov;20(11):523-9. Review.

Ben-Ari Y, Tseeb V, Raggozzino D, Khazipov R, Gaiarsa JL (1994) Gammaaminobutyric acid (GABA): a fast excitatory transmitter which may regulate the development of hippocampal neurones in early postnatal life. Prog Brain Res 102:261–273.

Bendtsen TF, Nyengaard JR (1989) Unbiased estimation of particle number using sections--an historical perspective with special reference to the stereology of glomeruli. J Microsc. Jan;153 (Pt 1):93-102.

Bibel M, Barde YA (2000) Neurotrophins: key regulators of cell fate and cell shape in the vertebrate nervous system. Genes Dev. Dec 1;14(23):2919-37. Review.

Bize I, Guvenc B, Buchbinder G, Brugnara C (2000) Stimulation of human erythrocyte K-Cl cotransport and protein phosphatase type 2A by n-ethylmaleimide: role of intracellular Mg^{2+}. J Membr Biol. Sep 15;177(2):159-68.

Blaesse P (2003) Untersuchung des K^+-Cl^- - Kotransporters KCC2 auf Spleißvarianten und Etablierung eines Einzelzell-Systems zur Analyse seines Plasmamembraneinbaus. März, TU Kaiserslautern, Fachbereich Biologie, Diplomarbeit.

Blaesse P, Nothwang HG, Lohr C, Friauf E (2004) Subcellular localization of KCC2 in immature neurons in the rat lateral superior olive. 3rd Symposium for Molecular Mechanisms in Central Auditory Function, Plasticity, and Disorders. Jackson Hole, Wyoming, Aug 25-27th

Boettger T, Rust MB, Maier H, Seidenbecher T, Schweizer M, Keating DJ, Faulhaber J, Ehmke H, Pfeffer C, Scheel O, Lemcke B, Horst J, Leuwer R, Pape HC, Volkl H, Hubner CA, Jentsch TJ (2003) Loss of K-Cl co-transporter KCC3 causes deafness, neurodegeneration and reduced seizure threshold. EMBO J. Oct 15;22(20):5422-34.

Born DE, Rubel EW (1988) Afferent influences on brain stem auditory nuclei of the chicken: presynaptic action potentials regulate protein synthesis in nucleus magnocellularis neurons. J Neurosci. Mar;8(3):901-19.

Brand A, Behrend O, Marquardt T, Mcalpine D, Grothe B (2002) Precise inhibition is essential for microsecond interaural time difference coding. Nature 417: 543-547.

Brickley SG, Cull-Candy SG, Farrant M (1996) Development of a tonic form of synaptic inhibition in rat cerebellar granule cells resulting from persistent activation of GABA$_A$ receptors. J Physiol. Dec 15;497 (Pt 3):753-9.

Brickley SG, Revilla V, Cull-Candy SG, Wisden W, Farrant M (2001) Adaptive regulation of neuronal excitability by a voltage-independent potassium conductance. Nature. Jan 4;409(6816):88-92.

Brines ML, Tabuteau H, Sundaresan S, Kim J, Spencer DD, de Lanerolle N (1995) Regional distributions of hippocampal Na+,K(+)-ATPase, cytochrome oxidase, and total protein in temporal lobe epilepsy. Epilepsia. Apr;36(4):371-83.

Busch C, Bohl J, Ohm TG (1997) Spatial, temporal and numeric analysis of Alzheimer changes in the nucleus coeruleus. Neurobiol Aging. Jul-Aug;18(4):401-6.

Caicedo A, Eybalin M (1999) Glutamate receptor phenotypes in the auditory brainstem and mid-brain of the developing rat. Eur J Neurosci. Jan;11(1):51-74.

Caird D, Klinke R (1983) Processing of binaural stimuli by cat superior olivary complex neurons. Exp Brain Res 52: 385-399.

Cant NB (1997) Neuroscience: The auditory system (Purves D, Augustine GJ, Fitzpatrick D, Katz LC, Lamantia AS, Mcnamara JO, eds), pp 238. Massachusetts: Sinauer Publishers.

Cant NB (1998) Structural development of the mammalian auditory pathway. In: Development of the auditory system. Edited by Edwin W Rubel, Arthur N. Popper and Richard R. Fay, Spinger-Verlag, New York, chapter 7

Cant NB, Hyson RL (1992) Projections from the lateral nucleus of the trapezoid body to the medial superior olivary nucleus in the gerbil. Hear Res. Feb;58(1):26-34.

Caspary DM, Backoff PM, Finlayson PG, Palombi PS (1994) Inhibitory nputs modulate discharge rate within frequency receptive fields of anteroventral cochlear nucleus eurons. J. Neurophysiol. 72:2124–2133.

Chalkley HW (1943) Methods for quantitative morphological analysis of tissue. J Natl Cancer Inst 4: 47-53.

Chan S, Kilby MD (2000) Thyroid hormone and central nervous system development. J Endocrinol 165: 1-8.

Chao MV (2003) Neurotrophins and their receptors: a convergence point for many signalling pathways. Nat Rev Neurosci. Apr;4(4):299-309. Review.

Chen Q, Moulder K, Tenkova T, Hardy K, Olney JW, Romano C (1999) Excitotoxic cell death dependent on inhibitory receptor activation. Exp Neurol. Nov;160(1):215-25.

Cherubini E, Gaiarsa JL, Ben-Ari Y (1991) GABA: an excitatory transmitter in early postnatal life. Trends Neurosci. Dec;14(12):515-9. Review.

Cherubini E, Martina M, Sciancalepore M, Strata F (1998) GABA excites immature CA3 pyramidal cells through bicuculline-sensitive and –insensitive chloride-dependent receptors. Perspect Dev Neurobiol 5:289–304.

Choi DW (1992) Excitotoxic cell death. J Neurobiol. Nov;23(9):1261-76. Review.

Chung C, Payne JA (2001) Glutamate excitotoxity causes rapid degradation of the neuronal K-Cl cotransporter (KCC2) via a calcium-activated neutral protease (calpain). *Soc. Neurosci. Abstr. 27, 710.1*

Clayton GH, Owens GC, Wolf JS, Smith RL (1998) Ontogeny of cation-Cl cotransporter expression in rat neocortex. Dev Brain Res 109: 281-292.

Coggeshall RE, Lekan HA (1996) Methods for determining number of cells and synapses: a case for more uniform standars of reviews. J Comp Neurol 364:6–15.

Cohen I, Navarro V, Clemenceau S, Baulac M, Miles R (2002) On the origin of interictal activity in human temporal lobe epilepsy in vitro. Science. Nov 15;298(5597):1418-21.

Coleman J, Blatchley BJ, Williams JE (1982) Development of the dorsal and ventral cochlear nuclei in rat and effects of acoustic deprivation. Brain Res. May;256(1):119-23.

Conover JC, Yancopoulos GD (1997) Neurotrophin regulation of the developing nervous system: analyses of knockout mice. Rev Neurosci. Jan-Mar;8(1):13-27. Review.

Covey E, Jones DR, Casseday JH (1984) Projections from the superior olivary complex to the cochlear nucleus in the tree shrew. J Comp Neurol. Jun 20;226(2):289-305.

DeFazio RA, Keros S, Quick MW, Hablitz JJ. (2000) Potassium-coupled chloride cotransport controls intracellular chloride in rat neocortical pyramidal neurons. J Neurosci 20: 8069-8076.

Dehmel S, Kopp-Scheinpflug C, Dörrscheidt GJ, Rübsamen R (2002) Electrophysiological characterization of the superior paraolivary nucleus in the mongolian gerbil. Hearing Res 172: 18-36.

Deitch JS, Rubel EW (1984) Afferent influences on brain stem auditory nuclei of the chicken: time course and specificity of dendritic atrophy following deafferentation. J Comp Neurol. Oct 10;229(1):66-79.

Deleu D, Bamanikar SA, Muirhead D, Louon A (1997) Familial progressive sensorimotor neuropathy with agenesis of the corpus callosum (Andermann syndrome): a clinical, neuroradiological and histopathological study. Eur Neurol. 37(2):104-9.

Delpire E, Mount DB (2002) Human and murine phenotypes associated with defects in cation-chloride cotransport. Annu Rev Physiol. 64:803-43. Review.

Destexhe A, Pare D (1999) Impact of network activity on the integrative properties of neocortical pyramidal neurons in vivo. J Neurophysiol. Apr;81(4):1531-47.

Dietzel I, Heinemann U, Hofmeier G, Lux HD (1980) Transient changes in the size of the extracellular space in the sensorimotor cortex of cats in relation to stimulus-induced changes in potassium concentration. Exp Brain Res.;40(4):432-9.

Dobbing J, Sands J (1971) Vulnerability of developing brain. IX. The effect of nutritional growth retardation on the timing of the brain growth-spurt. Biol Neonate.;19(4):363-78.

Dodd PR (2002) Excited to death: different ways to lose your neurones. Biogerontology. 3(1-2):51-6. Review.

Ebert U, Ostwald J (1995) GABA can improve acoustic contrast in the rat ventral cochlear nucleus. Exp Brain Res.104(2):310-22.

Ehrlich I, Löhrke S, Friauf E (1999) Shift from depolarizing to hyperpolarizing glycine action in rat auditory neurons is due to age-dependent Cl regulation. J Physiol (Lond) 520: 121-137.

Ferragamo MJ, Golding NL, Oertel D (1998) Synaptic inputs to stellate cells in the ventral cochlear nucleus. J Neurophysiol. Jan;79(1):51-63.

Ferragamo MJ, Golding NL, Oertel D (1998) Synaptic inputs to stellate cells in the ventral cochlear nucleus. J Neurophysiol. Jan;79(1):51-63.

Fiala JC, Harris KM (2001) Extending unbiased stereology of brain ultrastructure to three-dimensional volumes. J Am Med Inform Assoc. Jan-Feb;8(1):1-16.

Forster CR, Illing RB (2000) Plasticity of the auditory brainstem: cochleotomy-induced changes of calbindin-D28k expression in the rat. J Comp Neurol. Jan 10;416(2):173-87.

Friauf E (1993) Transient appearance of calbindin-D28k-positive neurons in the superior olivary complex of developing rats. J Comp Neurol. Aug 1;334(1):59-74.

Friauf E (1994) Distribution of calcium-binding protein calbindin-D28k in the auditory system of adult and developing rats. J Comp Neurol. Nov 8;349(2):193-211.

Friauf E, Aragon C, Lohrke S, Westenfelder B, Zafra F (1999) Developmental expression of the glycine transporter GLYT2 in the auditory system of rats suggests involvement in synapse maturation. J Comp Neurol. 1999 Sep 13;412(1):17-37.

Friauf E, Hammerschmidt B, Kirsch J (1997) Development of adult-type inhibitory glycine receptors in the central auditory system of rats. J Comp Neurol. Aug 18;385(1):117-34.

Friauf E, Ostwald J (1988) Divergent projections of physiologically characterized rat ventral cochlear nucleus neurons as shown by intraaxonal injection of horseradish peroxidase. Exp Brain Res 73: 263-284.

Gagliardi RJ (2000) Neuroprotection, excitotoxicity and NMDA antagonists. Arq Neuropsiquiatr. Jun;58(2B):583-8. Review.

Ganguly K, Schinder AF, Wong ST, and Poo M-m (2001) GABA itself promotes the developmental switch of neuronal GABAergic responses from excitation to inhibition. Cell 105: 521-532.

Gao BX, Stricker C, Ziskind-Conhaim L (2001) Transition from GABAergic to glycinergic synaptic transmission in newly formed spinal networks. J Neurophysiol. Jul;86(1):492-502.

Gauck V, Jaeger D (2000) The control of rate and timing of spikes in the deep cerebellar nuclei by inhibition. J Neurosci. Apr 15;20(8):3006-16.

Gilbert CD, Kelly JP (1975) The projections of cells in different layers of the cat's visual cortex. J Comp Neurol. Sep;163(1):81-105.

Gimenez I, Forbush B (2003) Short-term stimulation of the renal Na-K-Cl cotransporter (NKCC2) by vasopressin involves phosphorylation and membrane translocation of the protein. J Biol Chem. Jul 18;278(29):26946-51.

Gleich O, Vater M (1998) Postnatal development of GABA- and glycine-like immunoreactivity in the cochlear nucleus of the Mongolian gerbil (Meriones unguiculatus). Cell Tissue Res. 1998 Aug;293(2):207-25.

Glendenning KK, Hutson KA, Nudo RJ, Masterton RB (1985) Acoustic chiasm II: Anatomical basis of binaurality in the lateral superior olive of the cat. J Comp Neurol 232: 261-285.

Glendenning KK, Masterton RB (1998) Comparative morphometry of mammalian central auditory systems: variation in nuclei and form of the ascending system. Brain Behav Evol. 51(2):59-89.

Goldberg JM, Brown PB (1969) Response of binaural neurons of dog superior olivary complex to dichotic tonal stimuli: Some physiological mechanism of sound localization. J Neurophysiol 32: 613-636.

Goodman CS, Shatz CJ (1993) Developmental mechanisms that generate precise patterns of neuronal connectivity. Cell.Jan;72 Suppl:77-98. Review.

Grothe B (2000) The evolution of temporal processing in the medial superior olive, an auditory brainstem structure. Prog Neurobiol. Aug;61(6):581-610.

Grothe B (2003) New roles for synaptic inhibition in sound localization. Nat Rev Neurosci 4: 540-550.

Grothe B, Park TJ (2000) Structure and function of the bat superior olivary complex. Microsc Res Tech. Nov 15;51(4):382-402. Review.

Grothe B, Sanes DH (1993) Bilateral inhibition by glycinergic afferents in the medial superior olive. J Neurophysiol 69: 1192-1196.

Grundersen HJ, Jensen EB (1987) The efficiency of systematic sampling in stereology and its prediction. J Microsc 147:229-63.

Guillery RW, Herrup K (1997) Quantification without pontification: choosing a method for counting objects in sectioned tissues. J Comp Neurol. Sep 15;386(1):2-7.

Guinan JJ Jr, Li RY (1990) Signal processing in brainstem auditory neurons which receive giant endings (calyces of Held) in the medial nucleus of the trapezoid body of the cat. Hearing Res 49: 321-334.

Gulyás AI, Sík A, Payne JA, Kaila K, Freund TF (2001) The KCl cotransporter, KCC2, is highly expressed in the vicinity of excitatory synapses in the rat hippocampus. Eur J Neurosci 13: 2205-2217.

Gundersen HJ, Bagger P, Bendtsen TF, Evans SM, Korbo L, Marcussen N, Moller A, Nielsen K, Nyengaard JR, Pakkenberg B (1988) The new stereological tools: disector, fractionator, nucleator and point sampled intercepts and their use in pathological research and diagnosis. APMIS. Oct;96(10):857-81. Review.

Gundersen HJG (1986) Stereology of arbitrary particles. A review of unbiased number and size estimators and the presentation of some new ones, in memory of William R. Thompsen, *J. Microsc.* 143: 3-45.

Hafidi A (1999) Distribution of BDNF, NT-3 and NT-4 in the developing auditory brainstem. Int J Dev Neurosci. Jul;17(4):285-94.

Hafidi A, Moore T, Sanes DH (1996) Regional distribution of neurotrophin receptors in the developing auditory brainstem. J Comp Neurol. Apr 8;367(3):454-64.

Harrison JM, Irving R (1966) Ascending connections of the anterior ventral cochlear nucleus in the rat. J Comp Neurol Jan;126(1):51-63.

Hashisaki GT, Rubel EW (1989) Effects of unilateral cochlea removal on anteroventral cochlear nucleus neurons in developing gerbils. J Comp Neurol. May 22;283(4):5-73.

Hayes TL, Lewis DA (1993) Hemispheric differences in layer III pyramidal neurons of the anterior language area. Arch Neurol. May;50(5):501-5.

Hedreen JC (1999) Unbiased stereology? Trends Neurosci 22: 346-347.

Held H (1893) Die centrale Gehörleitung. Arch Anat Physiol, Anat Abt 201–248.

Helfert RH, Bonneau JM, Wenthold RJ, Altschuler RA (1990) GABA and glycine immunoreactivity in the guinea pig superior olivary complex. Brain Res. 1989 Nov 6;501(2):269-86.Erratum in: Brain Res Feb 12;509(1):180.

Hiki K, D'Andrea RJ, Furze J, Crawford J, Woollatt E, Sutherland GR, Vadas MA, Gamble JR (1999) Cloning, characterization, and chromosomal location of a novel human K^+-Cl^- cotransporter. J Biol Chem 274: 10661-10667.

Howard CV, Reed MG (1998) Unbiased Stereology: 3D Measurements in Microscopy, Bios Scientific Publishers.

Huang BO, Redburn DA (1996) GABA-induced increases in $[Ca^{2+}]_i$ in retinal neurons of postnatal rabbits. Vis Neurosci 13: 441-447.

Hübner CA, Stein V, Hermans-Borgmeyer I, Meyer T, Ballanyi K, Jentsch TJ (2001) Disruption of KCC2 reveals an essential role of K-Cl cotransport already in early synaptic inhibition. Neuron 30: 515-524.

Ikegaya Y, Kim JA, Baba M, Iwatsubo T, Nishiyama N, Matsuki N (2001) Rapid and reversible changes in dendrite morphology and synaptic efficacy following NMDA receptor activation: implication for a cellular defense against excitotoxicity. J Cell Sci. Nov;114(Pt 22):4083-93.

Ikonomidou C, Mosinger JL, Salles KS, Labruyere J, Olney JW (1989) Sensitivity of the developing rat brain to hypobaric/ischemic damage parallels sensitivity to N-methyl-aspartate neurotoxicity. J Neurosci. Aug;9(8):2809-18.

Illing RB, Kraus KS, Michler SA (2000) Plasticity of the superior olivary complex. Microsc Res Tech 51: 364-381.

Irvine DRF (1986) Progress in sensory physiology 7. The auditory brainstem. Berlin, Heidelberg, New York: Springer Press, Ltd.

Irvine DRF (1992) Physiology of the auditory brainstem. In: The mammalian auditory pathway: Neurophysiolgy (Popper AN, Fay RR, eds), pp 153-231. New York: Springer Press, Ltd.

Irving R, Harrison JM (1967) The superior olivary complex and audition: a comparative study. J Comp Neurol. May;130(1):77-86.

Ishihara H, Ozaki H, Sato K, Hori M, Karaki H, Watabe S, Kato Y, Fusetani N, Hashimoto K, Uemura D (1989) Calcium-independent activation of contractile apparatus in smooth muscle by calyculin-A. J Pharmacol Exp Ther 250: 388-396.

Jacobs B, Driscoll L, Schall M (1997) Life-span dendritic and spine changes in areas 10 and 18 of human cortex: a quantitative Golgi study. J Comp Neurol. Oct 6;386(4):661-80.

Jacobson M (1991) Developmental neurobiology (3rd Ed). New York: Plenum Press.

Janson AM, Moller A (1993) Chronic nicotine treatment counteracts nigral cell loss induced by a partial mesodiencephalic hemitransection: an analysis of the total number and mean volume of neurons and glia in substantia nigra of the male rat. Neuroscience. Dec;57(4):931-41.

Jarolimek W, Lewen A, Misgeld U (1999) A furosemide-sensitive K^+-Cl^- cotransporter counteracts intracellular Cl^- accumulation and depletion in cultured rat midbrain neurons. J Neurosci 19: 4695-4704.

Jarvis CR, Lilge L, Vipond GJ, Andrew RD (1999) Interpretation of intrinsic optical signals and calcein fluorescence during acute excitotoxic insult in the hippocampal slice. Neuroimage. Oct;10(4):357-72.

Jeffress LA (1948) A place theory of sound localization. J Comp Psychol 41: 35-39.

Jessell TM (1991) Reactions of neurons to injury. In: Principles of Neural Science. E.R. Kandel, J.H. Schwartz, and T.M. Jessell, eds. Elsevier, New York, pp. 258–269.

Joris PX, Smith PH, Yin TCT (1998) Coincidence detection in the auditory system: 50 years after Jeffress. Neuron 21: 1235-1238.

Kaila K (1994) Ionic basis of $GABA_A$ receptor channel function in the nervous system. Prog Neurobiol 42: 489-537.

Kandler K, Friauf E (1993) Pre- and postnatal development of efferent connections of the cochlear nucleus in the rat. J Comp Neurol. Feb 8;328(2):161-84.

Kandler K, Friauf E (1995) Development of glycinergic and glutamatergic synaptic transmission in the auditory brainstem of perinatal rats. J Neurosci 15: 6890- 6904.

Kandler K, Kullmann PH, Ene FA, Kim G (2002) Excitatory action of an immature glycinergic/GABAergic sound localization pathway. Physiol Behav. Dec;77(4-5):583-7. Review.

Kandler K (2004) Activity-dependent organization of inhibitory circuits: lessons from the auditory system. Curr Opin Neurobiol. Feb;14(1):96-104. Review.

Kater SB, Mattson MP, Guthrie PB (1989) Calcium-induced neuronal degeneration: a normal growth cone regulating signal gone awry (?). Ann N Y Acad Sci. 568:252-61. Review.

Kelsch W, Hormuzdi S, Straube E, Lewen A, Monyer H, Misgeld U (2001) Insulinlike growth factor 1 and a cytosolic tyrosine kinase activate chloride outward transport during maturation of hippocampal neurons. J Neurosci 21: 8339- 8347.

Kernie SG, Liebl DJ, Parada LF (2000) BDNF regulates eating behavior and locomotor activity in mice. EMBO J. Mar 15;19(6):1290-300.

Kil J, Kageyama GH, Semple MN, Kitzes LM (1995) Development of ventral cochlear nucleus projections to the superior olivary complex in gerbil. J Comp Neurol. Mar 13;353(3):317-40.

Kirsch J, Betz H (1998) Glycine-receptor activation is required for receptor clustering in spinal neurons. Nature 392:717–720.

Klug A, Park TJ, Pollak GD (1995) Glycine and GABA influence binaural processing in the inferior colliculus of the mustache bat. J. Neurophysiol. 74:1701–1713.

Kneussel M, Betz H (2000) Receptors, gephyrin and gephyrin-associated proteins: novel insights into the assembly of inhibitory postsynaptic membrane specializations. J Physiol. 2000 May 15;525 Pt 1:1-9. Review.

Kobayashi T (1963) Brain-to-body ratios and time of maturation of the mouse brain. Am J Physiol. Feb;204:343-6.

Koch U, Grathe B (1998) GABAergic and glycinergic inhibition sharpens tuning for frequency modulations in the inferior colliculus of the big brown bat. J. Neurophysiol. 80:71–82.

Kolston J, Osen KK, Hackney CM, Ottersen OP, Storm-Mathisen J (1992) An atlas of glycine- and GABA-like immunoreactivity and colocalization in the cochlear nuclear complex of the guinea pig. Anat Embryol (Berl). 1992 Oct;186(5):443-65.

Kopp-Scheinpflug C, Dehmel S, Dorrscheidt GJ, Rubsamen R (2002) Interaction of excitation and inhibition in anteroventral cochlear nucleus neurons that receive large endbulb synaptic endings. J Neurosci. Dec 15;22(24):11004-18.

Kopp-Scheinpflug C, Lippe WR, Dorrscheidt GJ, Rubsamen R (2003) The medial nucleus of the trapezoid body in the gerbil is more than a relay: comparison of pre- and postsynaptic activity. J Assoc Res Otolaryngol. Mar;4(1):1-23.

Korada S, Schwartz IR (1999) Development of GABA, glycine, and their receptors in the auditory brainstem of gerbil: a light and electron microscopic study. J Comp Neurol. Jul 12;409(4):664-81.

Kotak VC, Korada S, Schwartz IR, Sanes DH (1998) A developmental shift from GABAergic to glycinergic transmission in the central auditory system. J Neurosci. Jun 15;18(12):4646-55.

Kotak VC, Sanes DH (1996) Developmental influence of glycinergic transmission: regulation of NMDA receptor-mediated EPSPs. J Neurosci. Mar 1;16(5):1836-43.

Koulen P, Sassoe-Pognetto M, Grunert U, Wassle H (1996) Selective clustering of $GABA_A$ and glycine receptors in the mammalian retina. J Neurosci. Mar 15;16(6):2127-40.

Kriegstein AR, Owens DF (2001) GABA may act as a self-limiting trophic factor at developing synapses. Sci STKE 2001: E1.

Kulesza R, Holt A, Spirou G, Berrebi AS (2000) Intracellular labeling of axonal collaterals of SPON neurons. Assoc. Res. Otolaryngol. 3:132.

Kulesza RJ Jr, Berrebi AS (2000) Superior paraolivary nucleus of the rat is a GABAergic nucleus. J Assoc Res Otolaryngol. Dec;1(4):255-69.

Kulesza RJ Jr, Vinuela A, Saldana E, Berrebi A (2002) Unbiased stereological estimates of neuron number in subcortical auditory nuclei of the rat. Hearing Research 168:12-24.

Kulesza RJ, Spirou GA, Berrebi AS (2003) Physiological response properties of neurons in the superior paraolivary nucleus of the rat. J Neurophysiol 89, 2299-2312.

Kullmann PH, Ene FA, Kandler K (2002) Glycinergic and GABAergic calcium responses in the developing lateral superior olive. Eur J Neurosci 15:1093–1104.

Kungel M, Piechotta K, Rietzel HJ, Friauf E (1997) Influence of the neuropeptide somatostatin on the development of dendritic morphology: a cysteamine-depletion study in the rat auditory brainstem. Brain Res Dev Brain Res. Jul 18;101(1-2):107-14.

Kurtz I (1998) Molecular pathogenesis of Bartter's and Gitelman's syndromes. Kidney Int. Oct;54(4):1396-410. Review.

Kuwabara N, Zook JM (1991) Classification of the principal cells of the medial nucleus of the trapezoid body. J Comp Neurol. 1991 Dec 22;314(4):707-20.

Kuwabara N, Zook JM (1992) Projections to the medial superior olive from the medial and lateral nuclei of the trapezoid body in rodents and bats. J Comp Neurol 324: 522-538.

Lang F, Busch GL, Ritter M, Volkl H, Waldegger S, Gulbins E, Haussinger D (1998) Functional significance of cell volume regulatory mechanisms. Physiol Rev. Jan;78(1):247-306. Review.

Lim R, Alvarez FJ, Walmsley B (2000) GABA mediates presynaptic inhibition at glycinergic synapses in a rat auditory brainstem nucleus. J Physiol. Jun 1;525 Pt 2:447-59.

Limb CJ, Ryugo DK (2000) Development of primary axosomatic endings in the anteroventral cochlear nucleus of mice. J Assoc Res Otolaryngol. Sep;1(2):103-19.

Linnarsson S, Bjorklund A, Ernfors P (1997) Learning deficit in BDNF mutant mice. Eur J Neurosci. Dec;9(12):2581-7.

Lohmann C, Myhr KL, Wong RO (2002) Transmitter-evoked local calcium release stabilizes developing dendrites. Nature. Jul 11;418(6894):177-81.

Lu J, Karadsheh M, Delpire E (1999) Developmental regulation of the neuronalspecific isoform of K-Cl cotransporter KCC2 in postnatal rat brains. J Neurobiol 39: 558-568.

Luhmann HJ, Prince DA (1991) Postnatal maturation of the GABAergic system in rat neocortex. J Neurophysiol 65: 247-263.

Lund JS, Lund RD, Hendrickson AE, Bunt AH, Fuchs AF (1975) The origin of efferent pathways from the primary visual cortex, area 17, of the macaque monkey as shown by retrograde transport of horseradish peroxidase. J Comp Neurol. Dec 1;164(3):287-303.

Lyons WE, Mamounas LA, Ricaurte GA, Coppola V, Reid SW, Bora SH, Wihler C, Koliatsos VE, Tessarollo L (1999) Brain-derived neurotrophic factor-deficient mice develop aggressiveness and hyperphagia in conjunction with brain serotonergic abnormalities. Proc Natl Acad Sci U S A. Dec 21;96(26):15239-44.

Maric D, Liu QY, Maric I, Chaudry S, Chang YH, Smith SV, Sieghart W, Fritschy JM, Barker JL (2001) GABA expression dominates neuronal lineage progression in the embryonic rat neocortex and facilitates neurite outgrowth via GABA$_A$ autoreceptor/Cl$^-$ channels. J Neurosci 21:2343–2360.

Martin LJ, Al-Abdulla NA, Brambrink AM, Kirsch JR, Sieber FE, Portera-Cailliau C (1998) Neurodegeneration in excitotoxicity, global cerebral ischemia, and target deprivation: A perspective on the contributions of apoptosis and necrosis. Brain Res Bull. Jul 1;46(4):281-309. Review.

Martin MR, Rickets C (1981) Histogenesis of the cochlear nucleus of the mouse. J Comp Neurol. Mar 20;197(1):169-84.

Marty S, Berninger B, Carroll P, Thoenen H (1996) GABAergic stimulation regulates the phenotype of hippocampal interneurons through the regulation of brain-derived neurotrophic factor. Neuron 16:565–570.

Mayhew TM, Gundersen HJG (1996) 'If you assume, you can make an ass out of u and me": a decade of the disector for stereological counting of particles in 3D space. J Anat 188:1–15.

McBain CJ, Traynelis SF, Dingledine R (1990) Regional variation of extracellular space in the hippocampus. Science. Aug 10;249(4969):674-7.

Midtgaard J (1994) Processing of information from different sources: spatial synaptic integration in the dendrites of vertebrate CNS neurons. Trends Neurosci. Apr;17(4):166-73. Review.

Mody I (2001) Distinguishing between GABA$_A$ receptors responsible for tonic and phasic conductances. Neurochem Res. Sep;26(8-9):907-13. Review.

Monnerie H, Shashidhara S, Le Roux PD (2003) Decreased dendrite growth from cultured mouse cortical neurons surviving excitotoxic activation of alpha-amino-3-hydroxy-5-methyl-4-isoxazole propionate/kainate receptors. Neurosci Lett. Jul 24;345(3):182-6.

Mostafapour SP, Cochran SL, Del Puerto NM, Rubel EW (2000) Patterns of cell death in mouse anteroventral cochlear nucleus neurons after unilateral cochlea removal. J Comp Neurol. Oct 30;426(4):561-71.

Motulsky, H (1995) Intuitive Biostatistics. Oxford University Press, New York, ISBN: 0-19-50-8607-4

Mount DB, Delpire E, Gamba G, Hall AE, Poch E, Hoover RS, Hebert SC (1998) The electroneutral cation-chloride cotransporters. J Exp Biol. Jul;201 (Pt 14):2091-102. Review.

Mount DB, Gamba G (2001) Renal potassium-chloride cotransporters. Curr Opin Nephrol Hypertens 10: 685-691.

Nabekura J, Ueno T, Okabe A, Furuta A, Iwaki T, Shimizu-Okabe C, Fukuda A, Akaike N (2002) Reduction of KCC2 expression and GABA$_A$ receptor-mediated excitation after in vivo axonal injury. J Neurosci. Jun 1;22(11):4412-7.

Needham K, Paolini AG (2003) Fast inhibition underlies the transmission of auditory information between cochlear nuclei. J Neurosci. Jul 16;23(15):6357-61.

Neises GR, Mattox DE, Gulley RL (1982) The maturation of the end bulb of Held in the rat anteroventral cochlear nucleus. Anat Rec. Nov;204(3):271-9.

Nusser Z, Lujan R, Laube G, Roberts JD, Molnar E, Somogyi P (1998) Cell type and pathway dependence of synaptic AMPA receptor number and variability in the hippocampus. Neuron. Sep;21(3):545-59.

Nusser Z, Mody I (2002) Selective modulation of tonic and phasic inhibitions in dentate gyrus granule cells. J Neurophysiol. May;87(5):2624-8.

Nusser Z, Roberts JD, Baude A, Richards JG, Somogyi P (1995b) Relative densities of synaptic and extrasynaptic GABA$_A$ receptors on cerebellar granule cells as determined by a quantitative immunogold method. J Neurosci. Apr;15(4):2948-60.

Nusser Z, Sieghart W, Stephenson FA, Somogyi P (1996) The alpha 6 subunit of the GABA$_A$ receptor is concentrated in both inhibitory and excitatory synapses on cerebellar granule cells. J Neurosci. Jan;16(1):103-14.

Nusser Z (1999) Subcellular distribution of amino acid neurotransmitter receptors and voltage-gated channels. In Dendrites. Stuart, G., Spruston, N., and Hausser, M. (eds), Oxford University Press, Oxford, 85-113.

Oliver DL (2000) Ascending efferent projections of the superior olivary complex. Microsc Res Tech 51: 355-363.

Ollo C, Schwartz IR (1979) The superior olivary complex in C57BL/6 mice. Am J Anat. Jul;155(3):349-73.

Olney JW (1971) Glutamate-induced neuronal necrosis in the infant mouse hypothalamus. An electron microscopic study. J Neuropathol Exp Neurol. Jan;30(1):75-90.

Osen KK (1988) Anatomy of the mammalian cochlear nuclei: A review. In: Syka, J., Masterton, R.B. (Eds.), Auditory Pathway Structure and Function. Plenum Press, New York, pp. 65-75.

Osen KK, Lopez DE, Slyngstad TA, Ottersen OP, Storm-Mathisen J (1991) GABA-like and glycine-like immunoreactivities of the cochlear root nucleus in rat. J Neurocytol. Jan;20(1):17-25.

Ostapoff EM, Benson CG, Saint Marie RL (1997) GABA- and glycine-immunoreactive projections from the superior olivary complex to the cochlear nucleus in guinea pig. J Comp Neurol. May 19;381(4):500-12.

Overstreet LS, Westbrook GL (2001) Paradoxical reduction of synaptic inhibition by vigabatrin. J Neurophysiol. Aug;86(2):596-603.

Owens DF, Boyce LH, Davis MB, Kriegstein AR (1996) Excitatory GABA responses in embryonic and neonatal cortical slices demonstrated by gramicidin perforated-patch recordings and calcium imaging. J Neurosci 16: 6414-6423.

Pakkenberg B, Gundersen HJ (1988) Total number of neurons and glial cells in human brain nuclei estimated by the disector and the fractionator. J Microsc. Apr;150 (Pt 1):1-20.

Pakkenberg B, Gundersen HJ (1997) Neocortical neuron number in humans: effect of sex and age. J Comp Neurol. 1997 Jul 28;384(2):312-20.

Pasic TR, Rubel EW (1989) Rapid changes in cochlear nucleus cell size following blockade of auditory nerve electrical activity in gerbils. J Comp Neurol. May 22;283(4):474-80.

Payne JA (1997) Functional characterization of the neuronal-specific K-Cl cotransporter: implications for $[K^+]_o$ regulation. Am J Physiol 273: 1515-1525.

Payne JA, Rivera C, Voipio J, Kaila K (2003) Cation-chloride co-transporters in neuronal communication, development and trauma. Trends Neurosci 26: 199-206.

Payne JA, Stevenson TJ, Donaldson LF (1996) Molecular characterization of a putative K-Cl cotransporter in rat brain. A neuronal-specific isoform. J Biol Chem. Jul 5;271(27):16245-52.

Pfeiffer RR (1966a) Anteroventral cochlear nucleus: wave forms of extracellularly recorded spike potentials. Science 154:667–668.

Pfeiffer RR (1966b) Classification of response patterns of spike discharges for units in the cochlear nucleus: tone-burst stimulation. Exp Brain Res 1:220–235

Piechotta K, Friauf E (1999) Glutamate agonists promote organotypicity in slice cultures of the rat auditory brainstem. Proc. Göttingen Neurobiol. Conference 1, 287.

Piechotta K, Weth F, Harvey RJ, Friauf E (2001) Localization of rat glycine receptor alpha1 and alpha2 subunit transcripts in the developing auditory brainstem. J Comp Neurol. Sep 24;438(3):336-52.

Pollak GD, Burger RM, Park TJ, Klug A, Bauer EE (2002) Roles of inhibition for transforming binaural properties in the brainstem auditory system. Hear Res. Jun;168(1-2):60-78. Review.

Poo MM (2001) Neurotrophins as synaptic modulators. Nat Rev Neurosci. Jan;2(1):24-32. Review.

Racca C, Stephenson FA, Streit P, Roberts JD, Somogyi P (2000) NMDA receptor content of synapses in stratum radiatum of the hippocampal CA1 area. J Neurosci. Apr 1;20(7):2512-22.

Ramirez V, Ulfhake B (1991) Postnatal development of cat hind limb motoneurons supplying the intrinsic muscles of the foot sole. Brain Res Dev Brain Res. Oct 21;62(2):189-202.

Ramón y Cajal S (1907) Histologie du systeme nerveux de l'homme et des vertebrates. Paris: Malonie.

Redmond L, Kashani AH, Ghosh A (2002) Calcium regulation of dendritic growth via CaM kinase IV and CREB-mediated transcription. Neuron. Jun 13;34(6):999-1010.

Reimer RJ, Fremeau RT, Jr., Bellocchio EE, Edwards RH (2001) The essence of excitation. Curr Opin Cell Biol 13: 417-421.

Reuss S, Disque-Kaiser U, De Liz S, Ruffer M, Riemann R (1999) Immunfluorescence study of neuropeptides in identified neurons of the rat auditory superior olivary complex. Cell Tissue Res. Jul;297(1):13-21.

Riemann R, Reuss S (1999) Nitric oxide synthase in identified olivocochlear projection neurons in rat and guinea pig. Hear Res. Sep;135(1-2):181-9.

Rietzel HJ, Friauf E (1998) Neuron types in the rat lateral superior olive and developmental changes in the complexity of their dendritic arbors. J Comp Neurol. Jan 5;390(1):20-40.

Rivera C, Li H, Thomas-Crusells J, Lahtinen H, Viitanen T, Nanobashvili A, Kokaia Z, Airaksinen MS, Voipio J, Kaila K, Saarma M (2002) BDNF-induced TrkB activation down-regulates the K^+/Cl^- cotransporter KCC2 and impairs neuronal Cl^- extrusion. J Cell Biol. Dec 9;159(5):747-52. Epub 2002 Dec 09.

Rivera C, Voipio J, Payne JA, Ruusuvuori E, Lahtinen H, Lamsa K, Pirvola U, Saarma M, Kaila K (1999) The K^+/Cl^- co-transporter KCC2 renders GABA hyperpolarizing during neuronal maturation. Nature 397: 251-255.

Roberts RC, Ribak CE (1987) GABAergic neurons and axon terminals in the brainstem auditory nuclei of the gerbil. J Comp Neurol. Apr 8;258(2):267-80.

Rose CR, Konnerth A (2001) Stores not just for storage. intracellular calcium release and synaptic plasticity. Neuron. Aug 30;31(4):519-22. Review.

Rose CR, Kovalchuk Y, Eilers J, Konnerth A (1999) Two-photon Na^+ imaging in spines and fine dendrites of central neurons. Pflugers Arch. Dec;439(1-2):201-7.

Rose JE, Kitzes LM, Gibson MM, Hind JE (1974) Observations on phase-sensitive neurons of anteroventral cochlear nucleus of the cat: nonlinearity of cochlear output. J Neurophysiol 37:218–253.

Rossi DJ, Hamann M (1998) Spillover-mediated transmission at inhibitory synapses promoted by high affinity alpha6 subunit $GABA_A$ receptors and glomerular geometry. Neuron. Apr;20(4):783-95.Erratum in: Neuron 1998 Jul;21(1):527.

Rothman SM (1985) The neurotoxicity of excitatory amino acids is produced by passive chloride influx. J Neurosci. Jun;5(6):1483-9.

Rübsamen R, Gutowski M, Langkau J, Dorrscheidt GJ (1994) Growth of central nervous system auditory and visual nuclei in the postnatal gerbil (Meriones unguiculatus). J Comp Neurol. Aug 8;346(2):289-305.

Rudge JS, Alderson RF, Pasnikowski E, McClain J, Ip NY, Lindsay RM (1992) Expression of Ciliary Neurotrophic Factor and the Neurotrophins-Nerve Growth Factor, Brain-Derived Neurotrophic Factor and Neurotrophin 3-in Cultured Rat Hippocampal Astrocytes. Eur J Neurosci. 4(6):459-471.

Russell FA, Moore DR (1999) Effects of unilateral cochlear removal on dendrites in the gerbil medial superior olivary nucleus. Eur J Neurosci. Apr;11(4):1379-90.

Russell JM (2000) Sodium-potassium-chloride cotransport. Physiol Rev 80: 211- 276.

Russell JM, Boron WF (1976) Role of choloride transport in regulation of intracellular pH. Nature 264: 73-74.

Ryugo DK, Sento S (1991) Synaptic connections of the auditory nerve in cats: relationship between endbulbs of Held and spherical bushy cells. J Comp Neurol 305:35–48.

Sabatini BL, Maravall M, Svoboda K (2001) Ca^{2+} signaling in dendritic spines. Curr Opin Neurobiol. Jun;11(3):349-56. Review.

Saldana E, Berrebi AS (2000) Anisotropic organization of the rat superior paraolivary nucleus. Anat Embryol (Berl). Oct;202(4):265-79.

Sanes D, Wooten G (1987) Development of Glycine Receptor Distribution in the Lateral Superior Olive of the Gerbil. J. Neurosci, November 7(11): 3803-3811

Sanes DH (1993) The development of synaptic function and integration in the central auditory system. J Neurosci 13: 2627-2637.

Sanes DH, Chokshi P (1992) Glycinergic transmission influences the development of dendrite shape. Neuroreport. Apr;3(4):323-6.

Sanes DH, Friauf E (2000) Development and influence of inhibition in the lateral superior olivary nucleus. Hear Res. 2000 Sep;147(1-2):46-58. Review.

Sanes DH, Geary WA, Wooten GF, Rubel EW (1987) Quantitative distribution of the glycine receptor in the auditory brain stem of the gerbil. J Neurosci. Nov;7(11):3793-802.

Sanes DH, Hafidi A (1996) Glycinergic transmission regulates dendrite size in organotypic culture. J Neurobiol. Dec;31(4):503-11.

Sanes DH, Markowitz S, Bernstein J, Wardlow J (1992b) The influence of inhibitory afferents on the development of postsynaptic dendritic arbors. J Comp Neurol. Jul 22;321(4):637-44.

Sanes DH, Rubel EW (1988) The ontogeny of inhibition and excitation in the gerbil lateral superior olive. J Neurosci 8: 682-700.

Sanes DH, Siverls V (1991) Development and specificity of inhibitory terminal arborizations in the central nervous system. J Neurobiol. Nov;22(8):837-54.

Sanes DH, Song J, Tyson J (1992a) Refinement of dendritic arbors along the tonotopic axis of the gerbil lateral superior olive. Brain Res Dev Brain Res. May 22;67(1):47-55.

Sanna PP, Berton F, Cammalleri M, Tallent MK, Siggins GR, Bloom FE, Francesconi W (2000) A role for Src kinase in spontaneous epileptiform activity in the CA3 region of the hippocampus. Proc Natl Acad Sci U S A. Jul 18;97(15):8653-7.

Sassoe-Pognetto M, Wassle H, Grunert U (1994) Glycinergic synapses in the rod pathway of the rat retina: cone bipolar cells express the alpha 1 subunit of the glycine receptor. J Neurosci. Aug;14(8):5131-46.

Schmalenbach C, Muller HW (1993) Astroglia-neuron interactions that promote long-term neuronal survival. J Chem Neuroanat. Jul-Aug;6(4):229-37.

Schofield BR (1991) Superior paraolivary nucleus in the pigmented guinea pig: separate classes of neurons project to the inferior colliculus and the cochlear nucleus. J Comp Neurol. 1991 Oct 1;312(1):68-76.

Schofield BR (1994) Projections to the cochlear nuclei from principal cells in the medial nucleus of the trapezoid body in guinea pigs. J Comp Neurol. Jun 1;344(1):83-100.

Schwarz DW (1992) Sound delay lines in the nucleus laminaris of the chicken. J Otolaryngol 21: 202-208.

Shatz CJ (1996) Emergence of order in visual system development. Proc Natl Acad Sci U S A. Jan 23;93(2):602-8. Review.

Shibata S, Kakazu Y, Okabe A, Fukuda A, Nabekura J (2004) Experience-dependent changes in intracellular Cl⁻ regulation in developing auditory neurons. Neurosci Res 48: 211-220.

Shore SE, Helfert RH, Bledsoe SC Jr, Altschuler RA, Godfrey DA (1991) Descending projections to the dorsal and ventral divisions of the cochlear nucleus in guinea pig. Hear Res. 1991 Mar;52(1):255-68.

Shore SE. Influence of centrifugal pathways on forward masking of ventral cochlear nucleus neurons (1998) J Acoust Soc Am. Jul;104(1):378-89.

Siman R, Noszek JC, Kegerise C (1989) Calpain I activation is specifically related to excitatory amino acid induction of hippocampal damage. J Neurosci. May;9(5):1579-90.

Singer JH, Talley EM, Bayliss DA, Berger AJ (1998) Development of glycinergic synaptic transmission to rat brain stem motoneurons. J Neurophysiol 80: 2608-2620.

Smith AJ, Owens S, Forsythe ID (2000) Characterisation of inhibitory and excitatory postsynaptic currents of the rat medial superior olive. J Physiol. Dec 15;529 Pt 3:681-98.

Smith PH, Joris PX, Yin TCT (1993) Projections of physiologically characterized spherical bushy cell axons from the cochlear nucleus of the cat: evidence for delay lines to the medial superior olive. J Comp Neurol 331: 245-260.

Smith PH, Joris PX, Yin TCT (1998) Anatomy and physiology of principal cells of the medial nucleus of the trapezoid body (MNTB) of the cat. J Neurophysiol 79: 3127-3142.

Sommer I, Lingenhohl K, Friauf E (1993) Principal cells of the rat medial nucleus of the trapezoid body: an intracellular in vivo study of their physiology and morphology. Exp Brain Res. 95(2):223-39.

Somogyi P, Takagi H (1982) A note on the use of picric acid-paraformaldehyde glutaraldehyde fixative for correlated light and electron microscopic immunocytochemistry. Neuroscience. Jul;7(7):1779-83.

Spitzer NC (2002) Activity-dependent neuronal differentiation prior to synapse formation: the functions of calcium transients. J Physiol Paris. Jan-Mar;96(1-2):73-80. Review.

Srinivasan G, Friauf E, Löhrke S (2004a) Differential timing of the development of inhibition within the superior olivary complex revealed by optical imaging. Assn Res Otolaryngol Abstr 27: 917.

Staley KJ, Soldo BL, Proctor WR (1995) Ionic mechanisms of neuronal excitation by inhibitory $GABA_A$ receptors. Science. Aug 18;269(5226):977-81.

Stein V, Hermans-Borgmeyer I, Jentsch TJ, Hübner CA (2004) Expression of the KCl cotransporter KCC2 parallels neuronal maturation and the emergence of low intracellular chloride. J Comp Neurol 468: 57-64.

Sterio DC (1984) The unbiased estimation of number and size of arbitrary particles using the disector. *J. Microsc.* 134: 127-136.

Strange K, Singer TD, Morrison R, Delpire E (2000) Dependence of KCC2 K-Cl cotransporter activity on a conserved carboxy terminus tyrosine residue. Am J Physiol Cell Physiol. Sep;279(3):C860-7.

Taber-Pierce E (1967) Histogenesis of the dorsal and ventral cochlear nuclei in the mouse. An autoradiographic study. J Comp Neurol 131:27–54

Taber-Pierce E (1973) Time of origin of neurons in the brain stem of the mouse. Prog Brain Res 40:53–65

Tacconi MT (1998) Neuronal death: is there a role for astrocytes? Neurochem Res. May;23(5):759-65. Review.Erratum in: Neurochem Res 1999 Mar;24(3):459.

Thompson AM, Schofield BR (2000) Afferent projections of the superior olivary complex. Microsc Res Tech 51: 330-354.

Tierney TS, Moore DR (1997) Naturally occurring neuron death during postnatal development of the gerbil ventral cochlear nucleus begins at the onset of hearing. J Comp Neurol. Oct 27;387(3):421-9.

Tierney TS, P Doubell T, Xia G, Moore DR (2001) Development of brain-derived neurotrophic factor and neurotrophin-3 immunoreactivity in the lower auditory brainstem of the postnatal gerbil. Eur J Neurosci. Sep;14(5):785-93.

Trettel J, Morest KD (2001) In: Handbook of Mouse Auditory Research. From behavior to molecular biology. Edited by James F. Willott, CRC Press LLC, chapter 19

Trussell LO (2002) Modulation of transmitter release at giant synapses of the auditory system. Curr Opin Neurobiol. Aug;12(4):400-4. Review.

Ulfhake B, Kellerth JO (1981) A quantitative light microscopic study of the dendrites of cat spinal alpha-motoneurons after intracellular staining with horseradish peroxidase. J Comp Neurol. Nov 10;202(4):571-83.

Vale C, Caminos E, Martinez-Galan JR, Juiz JM (2004) Developmental expression of the K-Cl transporter (KCC2) in the central auditory system of the rat. Assn Res Otolaryngol Abstr 27:734

Vale C, Sanes DH (2000) Afferent regulation of inhibitory synaptic transmission in the developing auditory midbrain. J Neurosci. Mar 1;20(5):1912-21.

Vale C, Sanes DH (2002) The effect of bilateral deafness on excitatory and inhibitory synaptic strength in the inferior colliculus. Eur J Neurosci. Dec;16(12):2394-404.

Vale C, Schoorlemmer J, Sanes DH (2003) Deafness disrupts chloride transporter function and inhibitory synaptic transmission. J Neurosci 23: 7516-7524.

van den Pol AN, Obrietan K, Chen G (1996) Excitatory actions of GABA after neuronal trauma. J Neurosci. Jul 1;16(13):4283-92.

Vara H, Munoz-Cuevas J, Colino A (2003) Age-dependent alterations of long-term synaptic plasticity in thyroid-deficient rats. Hippocampus 13: 816-825.

Vardi N, Masarachia P, Sterling P (1992) Immunoreactivity to $GABA_A$ receptor in the outer plexiform layer of the cat retina. J Comp Neurol. Jun 15;320(3):394-7.

Vardi N, Zhang LL, Payne JA, Sterling P (2000) Evidence that different cation chloride cotransporters in retinal neurons allow opposite responses to GABA. J Neurosci. Oct 15;20(20):7657-63.

Vitten H, Reusch M, Friauf E, Lohrke S (2004) Expression of functional kainate and AMPA receptors in developing lateral superior olive neurons of the rat. J Neurobiol. Jun;59(3):272-88.

Von Bartheld C (2002) Counting particles in tissue sections: choices of methods and importance of calibration to minimize biases. Histol Histopathol 17: 639-648.

Vu TQ, Payne JA, Copenhagen DR (2000) Localization and developmental expression patterns of the neuronal K-Cl cotransporter (KCC2) in the rat retina. J Neurosci 20: 1414-1423.

Warr WB (1966) Fiber degeneration following lesions in the anterior ventral cochlear nucleus of the cat. Exp Neurol 14: 453-474.

Warr WB (1972) Fiber degeneration following lesions in the multipolar and globular cell areas in the ventral cochlear nucleus of the cat. Brain Res 40: 247-270.

Warr WB, Beck JE (1996) Multiple projections from the ventral nucleus of the trapezoid body in the rat. Hear Res. Apr;93(1-2):83-101.

Webster DB (1988a) Conductive hearing loss affects the growth of the cochlear nuclei over an extended period of time. Hear Res. Feb-Mar;32(2-3):185-92.

Webster DB, Popper AN, Fay RR (Editors) (1992) The mammalian auditory pathway: Neuroanatomy. New York: Springer-Verlag

Webster DB, Trune DR (1982) Cochlear nuclear complex of mice. Am J Anat. Feb;163(2):103-30.

Webster DB, Webster M (1977) Neonatal sound deprivation affects brain stem auditory nuclei. Arch Otolaryngol. Jul;103(7):392-6.

Webster DB, Webster M (1979) Effects of neonatal conductive hearing loss on brain stem auditory nuclei. Ann Otol Rhinol Laryngol. Sep-Oct;88(5 Pt 1):684-8.

Webster DB, Webster M (1980) Mouse brain auditory nuclei development Ann Oto-Rhinol-Laryngol 89 (Suppl 68):254-256

Wenthold RJ (1991) Neurotransmitters of brainstem auditory nuclei. In: Neurobiology of Hearing: The Central Auditory System (Altschuler RA, Bobbin RP, Clopton BM, Hoffman DW, eds), pp 121-139. New York: Raven Press Ltd.

West MJ (1993) New stereological methods for counting neurons. Neurobiol Aging 14:275–285.

West MJ (1999) Stereological methods for estimating the total number of neurons and synapses: issues of precision and bias. Trends Neurosci. Feb;22(2):51-61. Review.

West MJ (2001) Design based stereological methods for estimating the total number of objects in histological material. Folia Morphol (Warsz); 60(1):11-9. Review.

West MJ, Ostergaard K, Andreassen OA, Finsen B (1996) Estimation of the number of somatostatin neurons in the striatum: an in situ hybridization study using the optical fractionator method J Comp Neurol. Jun 17;370(1):11-22.

West MJ, Slomianka L (1998) Total number of neurons in the layers of the human entorhinal cortex. Hippocampus; 8(1):69-82

West MJ, Slomianka L, Gundersen HJ (1991) Unbiased stereological estimation of the total number of neurons in thesubdivisions of the rat hippocampus using the optical fractionator. Anat Rec. 1991 Dec;231(4):482-97.

Wickesberg RE, Oertel D (1988) Tonotopic projection from the dorsal to the anteroventral cochlear nucleus of mice. J Comp Neurol. 1988 Feb 15;268(3):389-99.

Wickesberg RE, Oertel D (1990) Delayed, frequency-specific inhibition in the cochlear nuclei of mice: a mechanism for monaural echo suppression. J Neurosci. Jun;10(6):1762-8.

Wilkinson F (1986) Eye and brain growth in the Mongolian gerbil (Meriones unguiculatus). Behav Brain Res. Jan;19(1):59-69.

Williams JR, Sharp JW, Kumari VG, Wilson M, Payne JA (1999) The neuron-specific K-Cl cotransporter, KCC2. Antibody development and initial characterization of the protein. J Biol Chem. Apr 30;274(18):12656-64.

Williams RW, Rakic P (1988) Three-dimensional counting: an accurate and direct method to estimate numbers of cells in sectioned material. J Comp Neurol. Dec 15;278(3):344-52.

Woo NS, Lu J, England R, McClellan R, Dufour S, Mount DB, Deutch AY, Lovinger DM, Delpire E (2002) Hyperexcitability and epilepsy associated with disruption of the mouse neuronal-specific K-Cl cotransporter gene. Hippocampus 12(2):258-68

Woodin MA, Ganguly K, Poo MM (2003) Coincident pre- and postsynaptic activity modifies GABAergic synapses by postsynaptic changes in Cl- transporter activity. Neuron. Aug 28;39(5):807-20.

Wu SH, Kelly JB (1992a) NMDA, non-NMDA and glycine receptors mediate binaural interaction in the lateral superior olive: physiological evidence from mouse brain slice. Neurosci Lett 134: 257-260.

Wu SH, Kelly JB (1992b) Synaptic pharmacology of the superior olivary complex studied in mouse brain slice. J Neurosci 12: 3084-3097.

Wu SH, Oertel D (1986) Inhibitory circuitry in the ventral cochlear nucleus is probably mediated by glycine. J Neurosci. Sep;6(9):2691-706.

Yamasaki EN, Ramoa AS (1993) Dendritic remodelling of retinal ganglion cells during development of the rat. J Comp Neurol. Mar 8;329(2):277-89.

Yang L, Pollak GD, Resler C (1992) GABAergic circuits sharpen tuning curves and modify response properties in the mustache bat inferior colliculus. J. Neurophysiol. 68:1760–1774.

Yeung JY, Canning KJ, Zhu G, Pennefather P, MacDonald JF, Orser BA (2003) Tonically activated $GABA_A$ receptors in hippocampal neurons are high-affinity, low-conductance sensors for extracellular GABA. Mol Pharmacol. Jan;63(1):2-8.

Yuste R, Katz LC (1991) Control of postsynaptic Ca^{2+} influx in developing neocortex by excitatory and inhibitory neurotransmitters. Neuron. Mar;6(3):333-44.

Zamboni L, De Martino C (1967) Buffered picric acid-formaldehyde: a new, rapid fixative for electron microscopy J. Cell Biol. 35 : 145A

Zamenhof S (1976) Final number of Purkinje and other large cells in the chick cerebellum influenced by incubation temperatures during their proliferation. Brain Res. Jun 11;109(2):392-4.

Zhang LI, Poo MM (2001) Electrical activity and development of neural circuits. Nat Neurosci. Nov;4 Suppl:1207-14. Review.

6.   Appendix

Abbreviations

(-/-)	Knockout mice
(+/-)	Heterozygous mice
(+/+)	Wild type mice
AGV_s	Absolute gray values
AMPA	-amino-3-hydroxy-5-methyl-4-isoxazolepropionic acid
AVCN	Anteroventral cochlear nucleus
BDNF	Brain derived neurotrophic factor
CN	Cochlear nucleus
CNS	Central nervous system
CV	Coefficient of variance
GABA	-amino-butyric acid
GlyR	Glycine receptor
IGF	Insulin-like growth factor
IgG	Immunoglobulin G
IID	Interaural intensity difference
ITD	Interaural time difference
KCC2	Potassium chloride cotransporter isoform 2
LNTB	lateral nucleus of trapezoid body
LSO	Lateral superior olive
MAP2	Microtubule-associated protein
MGV	Mean gray value
MNTB	Medial nucleus of trapezoid body
MSO	Medial superior olive

NKCC2	Na^+-dependent, potassium chloride cotransporter isoform 2
NMDA	N-methyl-D-aspartate
P	Postnatal day
PBS	Phosphate buffer saline
PFA	Paraformaldehyde
RT-PCR	Reverse transcription – polymerase chain reaction
SD	Standard deviation
SDS	Sodium dodecyl sulphate
SOC	Superior olivary complex
SPN	Superior paraolivary nucleus
TrkB	Tyrosine kinase receptor of BDNF
VCN	Ventral cochlear nucleus

Curriculum Vitae

Ekaterina Doncheva

Born in Sofia (12.11.1974), Bulgaria.

2001 - present   PhD student in the Sensory and Developmental   Neurobiology
laboratory of Prof. Eckhard Friauf, University of Kaiserslautern,
Kaiserslautern, Germany

1995 - 2000   Graduate Education, University of Sofia "St. Kliment Ohridski",
Department Biology

September 2000   Awarded with qualification of MSc as Molecular biologist with
specialty Microbiology
Title of MSc Thesis: "Biosynthesis of Galacto-oligosaccharides
of Lactic Acid Bacteria, isolated from kefir grains"

January 2000   MSc thesis at the Department Microbiology

January 1999   Graduate study at the Department Microbiology

October 1995   After entrance examinations admitted as a graduate student
of Molecular Biology in University of Sofia, Department Biology

October 1993   After entrance examinations, admitted as a graduate student
of Chemistry and Physics in University of Sofia,
Department Chemistry
(not finished)

1988 - 1993   Secondary Education, National Educational Complex of Culture
with Lyceum for Studying of Italian Language and Culture, Sofia

May 1993   Accomplished the National Educational Complex of Culture with
speciality Nature and Culture

September 1991-1993 Attended the National Educational Complex of Culture

1988 - 1991   Attended the 1st Secondary School, Sofia

1981 - 1988   Primary Education

Acknowledgments

I am very grateful to Prof. Dr. Eckhard Friauf, Leader of the Laboratory of Sensory and Developmental Neurobiology and my direct supervisor, for the given opportunity to do my PhD thesis in this laboratory under his valuable guidance. He has taught me most of what I know about neurobiology and readily spent his time to discuss my studies. I appreciate his helpful comments on the draft of my thesis which enabled me to complete and submit this work. The errors, idiocies and inconsistencies remain my own. I am indebted to Prof. Dr. Joachim W. Deitmer for the permission to use the confocal microscope setup, for his constructive criticisms during the neurobiology seminar and agreeing to review my thesis.

I would like to express my gratitude to Dr. Stefan Löhrke for his support and useful advices on my work, for the friendly informal atmosphere apart from the scientific discussions and for the improvement of my knowledge in German language. I also thank Dr. Hans Gerd Nothwang for his concern in my study, for his helpful comments and discussions during the lab meetings.

I acknowledge the help of Dr. Christian Lohr and Robin Zur Nieden taking their time to introduce me to the confocal microscopy technique and their assistance in enhancing the quality of my images. My special thanks go to Obi and Geeta, whose data helped me and were a contribution to part of the discussion in my thesis.

I wish to thank Kornelia and Sascha, for their excellent technical assistance and for their help. Many thanks go to Petra doing the administrative work for me and her warm attitude. Special thanks to Isa for her friendship, support and cheery atmosphere in the lab and outside, making my adaptation in Kaiserslautern easier, getting to know German (and French) culture as well as practicing the German language. I am thankful to my other colleagues, Alex, Anne, Jens, Michael, Mirko, Peter and Veera, whose comments and ideas I often took into consideration and for the good times in the lab. Thanks to Dennis for his help in solving the computer problems.

Above all I wish to thank to my parents and my sister for their intellectual and emotional support during my stay in Germany and for giving me the confidence to cope with my task. It would not have been possible without them. Last but not least, thanks to my boyfriend Stefan for his love, patience and encouragement moving me toward my goal.